Spatiotemporal modeling of actin cytoskeletal mechanics linked to morphology and mechanotransduction

John Kang

July 2013

CMU-CB-13-103

Publisher:

Lane Center for Computational Biology

School of Computer Science

Carnegie Mellon University

Pittsburgh, PA 15213

Committee:

Michael Grabe

Philip LeDuc

Russell Schwartz

Alan Wells

This document is submitted in partial fulfillment
of the requirements for the degree of Doctor of Philosophy.

This work was partially supported by NIH T32 training grant T32 EB009403 as part of the HHMI-NIBIB Interfaces Initiative, NIH grant #1R01AI076318, and NIH grant #1R01CA140214.

Keywords: cell mechanics, multiscale modeling, mechanobiology, mixture model, cyclic stretch, pulsatile shear

Acknowledgements

I would like to sincerely thank my two advisors, Philip LeDuc and Russell Schwartz, for their support and belief in me throughout my PhD. I could not have found two more complementary advisors.

I would like to thank my collaborator Kathleen Puskar for being an invaluable source of information especially at the genesis of my research.

Lastly, I would like to thank my mother, Liya, for her love and always having my best interests at heart throughout the years.

Abstract

Cells are complex, dynamic systems that actively adapt to various stimuli including mechanical alterations. Central to understanding cellular response to mechanical stimulation is the organization of the cytoskeleton and its actin filament network. While there is extensive research on the downstream signaling effects of mechanical forces, there is a lack of understanding of how physical forces are converted into biochemical signals that are classically understood to control cellular behavior. Here, we approach this problem by utilizing coarse-grained multiscale models of cell mechanics. We begin with a minimalistic network Monte Carlo approach to model cytoskeletal actin filament organization under cyclic stretching-based energy minimization. After we establish that our cytoskeleton model can recapitulate experimental results under single-mode mechanical stimulation, we apply this model to emulate the response of an *in vitro* network of actin filaments and associated signaling molecules undergoing stretch-based mechanotransduction in order to answer fundamental questions about the physical-biochemical basis of mechanically-induced signaling. Lastly, we upgrade our initial model to also incorporate fluid shear stress such that our model can experience both cyclic stretch and cyclic shear while still maintaining an overall 2D structure.

Table of Contents

Chapter 1 : Introduction

1.1 Introduction to Cell Biomechanics

Biomechanics is the study of how biology integrates with mechanical forces. Cells experience mechanical forces from a variety of sources, including intracellular forces such as those generated by myosin motors and extracellular forces from sources such as blood flow. Micromechanics is implicated in a wide variety of pathologic processes ranging from cardiac failure and pulmonary injury to cell fate and cancer. Many of these processes were initially thought to be defects in cellular signaling, a complex system of communications that is commonly thought of as being driven by biochemical networks. In truth, many diseases ranging from arterial stiffening to extracellular matrix metastases are defects in mechanics as well. More specifically, micromechanics has been tied to key cell functions and responses to other influences, such as external forces, cytoskeletal tension, cell deformation, and cell shape changes, factors known to control cell signal transduction, gene expression, and differentiation [1] (**Figure 1-1**).

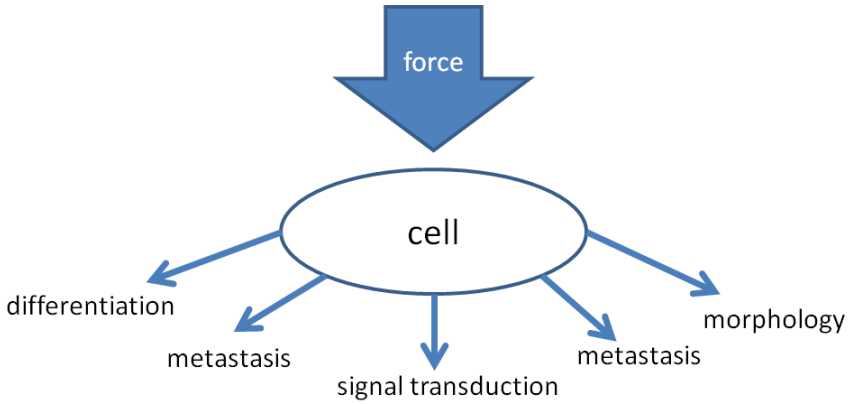

Figure 1-1: Example responses of cells to mechanical stimulation

Key in all cell mechanics interactions is the cytoskeleton, which provides both a structural and signaling backbone for the cell. The cytoskeleton is directly linked to the mechanical environment of cells through multiple sites of interaction, including focal adhesions, integrins, cellular junctions and the extracellular matrix [2]. The cytoskeleton is a dynamic structure capable of rearranging to adapt to changing environments, even though the specifics of these active adaptations are not well understood. Among the major components of the cytoskeleton is its network of actin filaments, which assemble into specialized bundles, arrays and complex branching structures to influence cell functions such as cell motility, spreading, and adhesion. From a physiological perspective, the mechanical stimulation experienced by individual cells is often comprised of multiple mechanical modes (e.g., stretching and shear), thus presenting a challenge to characterize their influence on cell structure. Endothelial cells comprise the endothelium, which is a single layer of squamous epithelial cells that line the inside wall of blood vessels. Mechanotransduction—the study of how mechanical forces effect cell signaling responses—has been a topic of significant recent interest, particularly in endothelial cells [3].

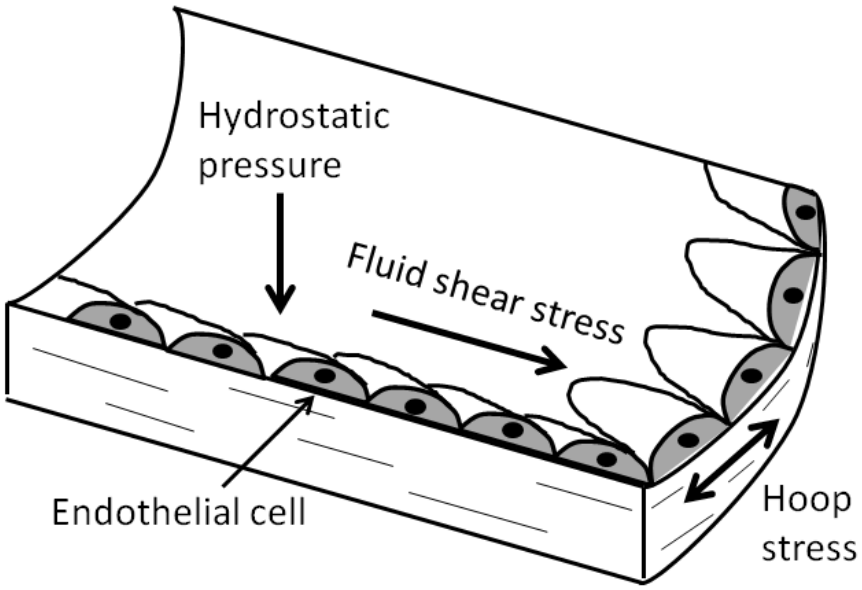

Figure 1-2: Direction of action for the three primary forces (hydrostatic pressure, fluid shear stress, and hoop stress) on endothelial cells relative to the blood vessel wall

Endothelial cells are classically considered to undergo three mechanical stresses: shear from blood flow, hydrostatic pressure from blood pressure, and cyclic hoop stress due to repeated vessel deformation [4] **(Figure 1-2).** In addition, fibroblasts form a major component (tunica externa) of the vasculature in a layer surrounding the endothelial cells (tunica intima) and thus experience similar forces to the endothelium. The cellular response to mechanical stimuli is often directly linked to its actin cytoskeleton. For example, *in vivo* experiments performed in flow-regulating chambers using cultured endothelial cells revealed that cells and their stress fibers dynamically reorient themselves parallel to the direction of flow, which is perpendicular to the direction of hoop stress [5]. In vertebrate tissues, endothelial cells are similarly found to align themselves parallel to the direction of flow and perpendicular to the direction of hoop stress [6]. Fibroblasts have also been shown to align perpendicular to the direction of cyclic stretch *in vivo* [7-10], suggesting that a biomechanical similarity could cause comparable behavior in both cell types under cyclic stretching. This pattern of cyclic stretch alignment has been shown to

occur in the absence of microtubules in cultured cells [11] and in the absence of shear flow in intact rat arteries [12].

Computational models can provide a valuable complement to experimental work in understanding the intricate responses of cellular systems to heterogeneous mechanical environments. For example, they provide a basis for rationalizing complex experimental observations and a platform to test the sufficiency of theories and minimal models of the experimental system. They are therefore in principal well suited to understanding how mechanical stimulation influences actin cytoskeleton structure and dynamics. Actin in particular has attracted considerable interest in the modeling and simulation area due to its relative simplicity and the wealth of experimental data available for it. Specifically, mechanical modeling of the actin cytoskeleton has contributed much to understanding the interplay between these polymer networks and mechanics. Properties at many scales have been examined, from atomic-scale models of small numbers of actin monomers [13], through models of properties of single filaments [14], through coarse-grained models of the overall mechanical properties of full actin networks [15-19]. A key observation of the field is that multiscale modeling approaches make it possible to translate detailed mechanical properties of filaments at the atomic scale into coarse-grained models of large filaments or filament networks [13, 20]. One can thus use insights from the more computationally expensive models, as well as experimental studies of the mechanical properties of filaments and filament bundles, to set parameters for simplified but far more tractable models of the macroscopic behaviors of full actin networks.

The goal of this research is to increase our understanding of spatial and temporal characteristics of cytoskeletal morphology and associated signaling under mechanical stimulation. We will test the hypothesis that observed spatial and temporal patterns of

cytoskeletal alignment can be explained by the effect of mechanical forces on the cytoskeleton. Additionally, we hypothesize that we can recapitulate experimental behavior of mechanically-induced signal factor release at actin crosslinkers by linking our cytoskeletal mechanics model to a geometric crosslinking-angle-based release model. To meet this goal, we will develop novel computational approaches to examine the structural and mechanical responses of cells stimulated with both single and dual forces designed to mimic physiology. We will attempt to validate these models with existing empirical data.

1.1.1 Micromechanics at the Cellular Level

Mechanical stimulation of mammalian cells has been shown to affect a diversity of cell functions through the cytoskeleton and the extracellular matrix (ECM), including cell motility, apoptosis, differentiation, and proliferation [21-25]. Mechanical stimulation comes in many different forms, including shear, tension, and compression. While cells may experience only one type of mechanical stimulus in controlled situations, they frequently experience multiple modes of mechanical stimulation *in vivo*.

The mechanics at the level of the cell, which consist of both external forces (i.e., shear, stretch) and internal forces (i.e., motor proteins) are critical for the health of the cell. Endothelial cells are a prime model system to study the effects of multiple modes of force stimulation. These epithelial cells line the surface of all blood vessels and provide the direct interface to the blood itself. Endothelial cells are classically considered to be exposed to three different mechanical forces simultaneously: shear from blood flow, hydrostatic pressure from blood pressure, and cyclic radial stress due to pulsatile flow [3, 4, 26-28]. Interestingly, cellular response to similar modes of stimulation is often cell-type specific. For example, both the whole cells and the actin filaments in vascular smooth muscle cells and endothelial cells grown in a co-culture system were shown to orient themselves perpendicular or parallel, respectively, to the direction of fluid flow [29-33].

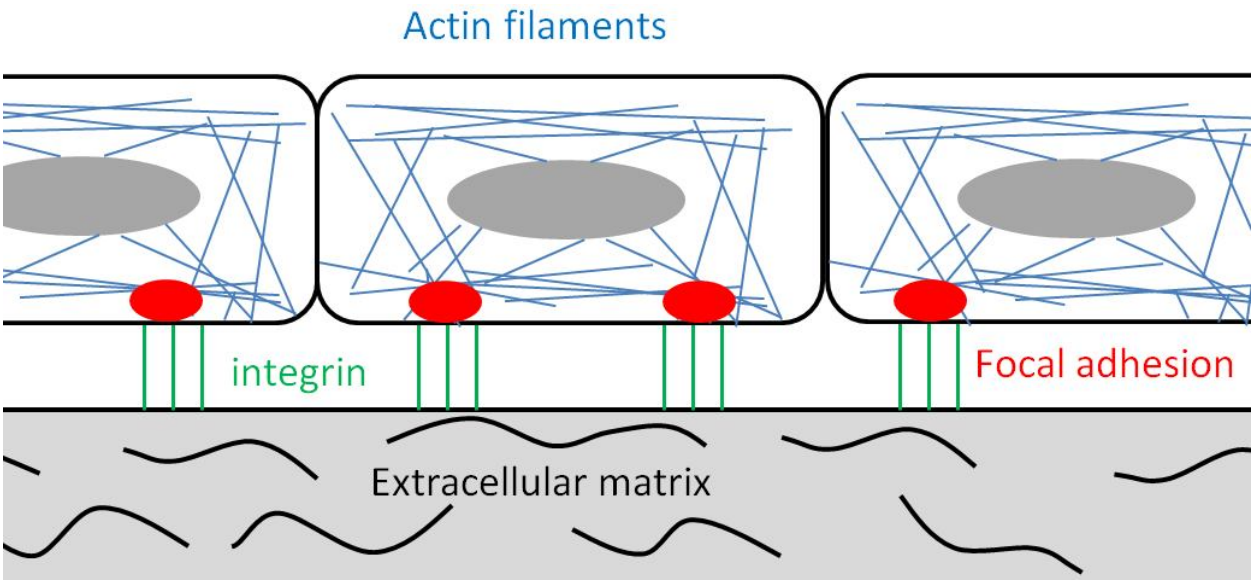

Figure 1-3: Endothelial cells lying on substrate with highlights on integrins (green), focal adhesions (red), and actin filaments (blue)

The endothelial cell is linked to the substrate it rests on via transmembrane integrins (**Figure 1-3**). These integrins are linked to the cytoskeleton of the cell via focal adhesion complexes. These complexes can be large and their size and turnover rate is related to the amount of stress they experience [34]. Additionally, the numerous proteins contained within these complexes have intricate 3D spatial architecture [35].

Recently, there has been a high amount of interest in the mechanotransduction of cryptic binding sites, which are binding sites for proteins that can either be opened or closed by mechanical forces. Del Rio et al. investigated two focal adhesion proteins talin and vinculin, showing that force on talin results in progressive uncovering of vinculin cryptic binding sites [36]. A recent paper by Ehrlich et al. focused on an actin filament crosslinker filamin A (FLNa), showing that angle opening at orthogonal junctions between crosslinker and filament led to release of certain proteins and binding of other proteins [37].

1.1.2 Experimental Stretching and Shear on Fibroblasts

In order to develop a model for mechanical stimulation, we developed a device that could collect necessary experimental data. Many studies involving mechanical forces on cells involve tensile forces via cyclic or static loading modes [31, 32, 38-40]. We developed a device to impose two separate mechanical stimuli (fluid shear stress and uniaxial stretch) on living cells (**Figure 1-4**) [41]. We stretch the elastomeric membrane with an air pressurization system to generate nearly-uniaxial tensile stresses on adhered cells to the membrane [42, 43]. For the shearing experiments, single cells were cultured on polydimethylsiloxane (PDMS) surfaces and then exposed to fluid shear flow from a variable-flow peristaltic pump (Fisher Scientific, Pittsburgh, PA; No.13-867-2), in a fluid chamber in an incubator.

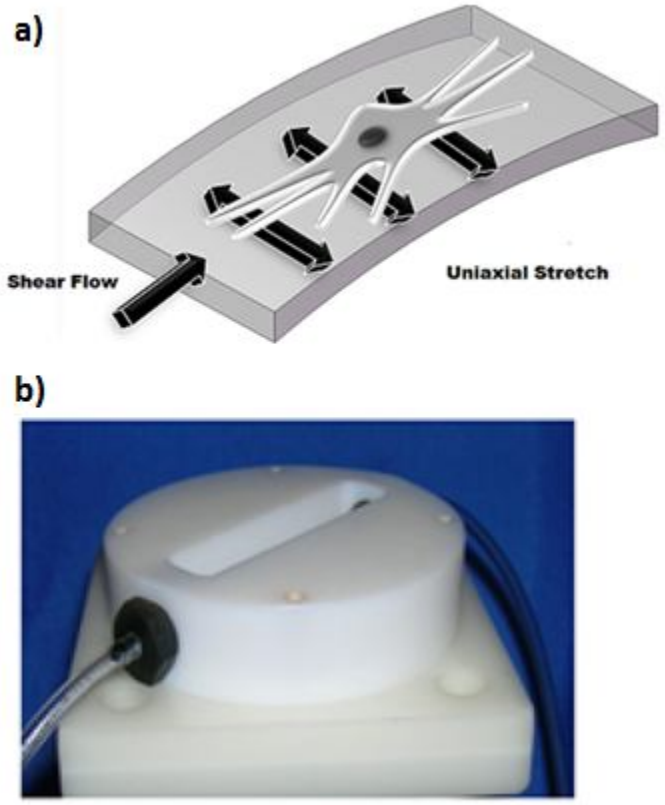

Figure 1-4: a) Schematic of a single cell in our experimental system under dual stimulation. (b) An image of the device developed to impose dual stimulation

Following the application of mechanical stimulation, the cells were immediately fixed and visualized for actin filament orientation and cell shape. NIH 3T3 fibroblasts were used to observe changes in morphology and cell alignment that occurred as a result of exposure to static tension or shear flow.

1.1.3 Computational Modeling of Cell Structure Background

Computational models provide a basis for rationalizing complex experimental observations and providing a platform to test the sufficiency of theories and minimal models of the experimental system. The capability to isolate and test the sufficiency of a defined set of components is critical to understanding complex biological systems; modeling billions of molecules in single cells in realistic spatial and temporal detail is far beyond our computational resources. Minimal, or coarse-grained, models are in principal suited to understanding how mechanical stimulation influences actin cytoskeleton structure and dynamics. In addition to extensive mathematical modeling of general actin assembly dynamics, there is a significant amount of literature on mechanical modeling of the actin cytoskeleton from which novel methods can draw. This literature has examined properties at many scales, from atomistic-scale models of small numbers of actin monomers [13], through models of properties of single filaments [14], to coarse-grained models of the bulk mechanical properties of full actin networks [15-19]. A key observation of the field is that multiscale modeling makes it possible to infer detailed mechanical properties of filaments at the atomic scale and translate these into simplified, coarse-grained models of large filaments or filament networks [13, 20].

The coupling of actin assembly to mechanics has also been previously addressed through simulation methods of polymerization as a force-generating mechanism for cell shape changes [44-46] or motility [47-50]. While there has been extensive empirical study of the actin

network's function as a force-responsive (rather than force-producing) structure, computational work on that direction has been limited. Hsu et al. [51] recently showed that a continuum filament model of polymerization under stretch can reorient in a manner consistent with experimental observations of endothelial cells. To our knowledge, no model has yet attempted to integrate distinct mechanical stimulus types on discrete filaments, but the prior work and our own preliminary studies provide a conceptual basis for such an approach.

1.2 Thesis contributions

This dissertation document has three main, novel contributions. In Chapter 2, we present a minimalistic discrete element model of the actin cytoskeleton which can undergo cyclic uniaxial stretch. This model is able to recapitulate analogous experimental results and suggest a parsimonious mechanism for cytoskeletal morphological changes. In 0, we apply our model to tackle the question of how cells can convert mechanical signals to biochemical signaling changes. We postulate three geometrically-driven mechanisms by which mechanosensitive proteins may control signal release and validate our models using recently published data. Lastly, in Chapter 4, we upgrade our model to simulate both shearing and stretching forces simultaneously and present our initial findings.

Chapter 2 : A cellular model for single-mode stretching mechanics[1]

2.1 Abstract

Cells are complex, dynamic systems that actively adapt to various stimuli including mechanical alterations. Central to understanding cellular response to mechanical stimulation is the organization of the cytoskeleton and its actin filament network. In this chapter, we present a minimalistic network Monte Carlo based approach to model actin filament organization under cyclic stretching. Utilizing a coarse-grained model, a filament network is prescribed within a two-dimensional circular space through nodal connections. When cyclically stretched, the model demonstrates that a perpendicular alignment of the filaments to the direction of stretch emerges in response to nodal repositioning to minimize net nodal forces from filament stress states. In addition, the filaments in the network rearrange and redistribute themselves to reduce the overall stress by decreasing their individual stresses. In parallel, we cyclically stretch NIH 3T3 fibroblasts and find a similar cytoskeletal response. Robert Steward (a previous PhD student in the LeDuc lab) performed the wet lab experiments in this chapter. With this work, we test the hypothesis that a first-principles mechanical model of filament assembly in a confined space is by itself capable of yielding the remodeling behavior observed experimentally. Identifying minimal mechanisms sufficient to reproduce mechanical influences on cellular structure has important implications in a diversity of fields, including biology, physics, medicine, computer science, and engineering.

[1] Chapter 2 adapted from Reference 52. Kang, J., et al., *Response of an actin filament network model under cyclic stretching through a coarse grained Monte Carlo approach.* Journal of theoretical biology, 2011. **274**(1): p. 109-19.

2.2 Introduction

The cytoskeleton is directly linked to the mechanical environment of cells through multiple sites of interaction, including focal adhesions, integrins, cellular junctions and the extracellular matrix. The cytoskeleton is a dynamic structure capable of rearranging to adapt to changing environments, even though the specifics of these active adaptations are not well understood. Among the major components of the cytoskeleton is its network of actin filaments, which assemble into specialized bundles, arrays and complex branching structures to influence cell functions such as cell motility, spreading, and adhesion. For example, stress fibers, which are cross-linked bundles of actin filaments, maintain tensile forces in the cell to assist in cell adhesion and cytokinesis. From a physiological perspective, the mechanical stimulation experienced by individual cells is often comprised of multiple mechanical modes (e.g., stretching and shear), thus presenting a challenge to characterize their influence on cell structure. Endothelial mechanotransduction has been a topic of significant interest [3]. Endothelial cells are classically considered to undergo three mechanical stresses: shear from blood flow, hydrostatic pressure from blood pressure, and cyclic hoop stress due to repeated vessel deformation [4] (**Figure 1-2**). In addition, fibroblasts form a major component (tunica externa) of the vasculature in a layer surrounding the endothelial cells (tunica intima) and thus experience similar forces to the endothelium. Cellular response to mechanical stimuli is often directly linked to its actin cytoskeleton. For example, *in vivo* experiments performed in flow-regulating chambers using cultured endothelial cells revealed that cells and their stress fibers dynamically reorient themselves parallel to the direction of flow, which is perpendicular to the direction of hoop stress [5]. Physiologically, endothelial cells are similarly found to align themselves parallel to the direction of flow and perpendicular to the direction of hoop stress [6]. Fibroblasts have

also been shown to align perpendicular to the direction of cyclic strain ranging from 2% to 20% amplitude *in vivo* [7-9], suggesting that a biomechanical similarity could cause comparable behavior in both cell types under cyclic stretching. This pattern of cyclic stretch alignment has been shown to occur in the absence of microtubules in cultured cells [11] and in the absence of shear flow in intact rat arteries [12].

Computational models can provide a valuable complement to experimental work in understanding the complex responses of cellular systems to heterogeneous mechanical environments. For example, they provide a basis for rationalizing complex experimental observations and a platform to test the sufficiency of theories and minimal models of the experimental system. They are therefore in principal well suited to understanding how mechanical stimulation influences actin cytoskeleton structure and dynamics. Actin in particular has attracted considerable interest in the modeling and simulation area due to its relative simplicity and the wealth of experimental data available for it. Specifically, mechanical modeling of the actin cytoskeleton has contributed much to understanding the interplay between these polymer networks and mechanics. Properties at many scales have been examined, from atomic-scale models of small numbers of actin monomers [13], through models of properties of single filaments [14], through coarse-grained models of the overall mechanical properties of full actin networks [15-19]. A key observation of the field is that multiscale modeling approaches make it possible to infer detailed mechanical properties of filaments at the atomic scale and translate these into coarse-grained models of large filaments or filament networks [13, 20]. One can thus use insights from the more computationally expensive models, as well as experimental studies of the mechanical properties of filaments and filament bundles, to set parameters for simplified but far more tractable models of the macroscopic behaviors of full actin networks.

In this work, our objective was to design a coarse-grained Monte Carlo model of the actin filament network in a cell undergoing uniaxial cyclic stretch. We demonstrate a gradual alignment of the actin filaments that reflects the observed physiological and *in vivo* response of both endothelial cells and fibroblasts under cyclic stretch. We corroborate our model with experimental data showing gradual alignment of fibroblasts perpendicular to cyclic stretch over a period of 24 hours. Previous work on cyclic stretch simulations on actin networks have focused on areas such as continuum mechanics models [51, 53, 54] or cytoskeletal dynamics [55]. While there has been work on discrete models involving force-generating actin-myosin networks [56, 57] and passive actin networks under static stretch [58], to our knowledge this is the first discrete filament model that accurately captures the observed passive response of actin filament alignment under cyclic stretch. While we believe that incorporating active elements such as myosin as well as different cross-linking proteins will be a great next step, in this chapter, we have focused on developing a new model and showing its responses compared to defined experimental results.

2.3 Simulation methods

2.3.1 Cytoskeletal model generation

A stochastic model was developed to examine the distribution of forces and the reorganization of actin filament structures in response to cyclic stretching. The general overview of the model is outlined in pseudocode format in **Code 2-1** and the main code for execution of cell stretch (for dual-mode stimulation, which will be covered in **Chapter 4**) is shown in **Chapter 7.1 Dual-mode cell stretch execution.**

1. generate network
2. for every stretch cycle
   A. while network not fully stretched
      i. Stretch network by 1%
      ii. Relax network
   B. break filaments
   C. generate new filaments

Code 2-1: Pseudocode for "cellstretch" model undergoing single mode stretching

We used a two-dimensional circular solution space of prescribed radius. This radius was chosen to be 100 arbitrary units, representing an adhered and spread cell whose bulk lies in an approximately circular region of diameter 30 µm, such as a fibroblast. So as not to restrict the angular orientation of the filaments, an off-lattice model was chosen. The space is considered fixed to an underlying substrate by perimeter nodes at prescribed locations on the circumference of the circle (**Figure 2-1a**).

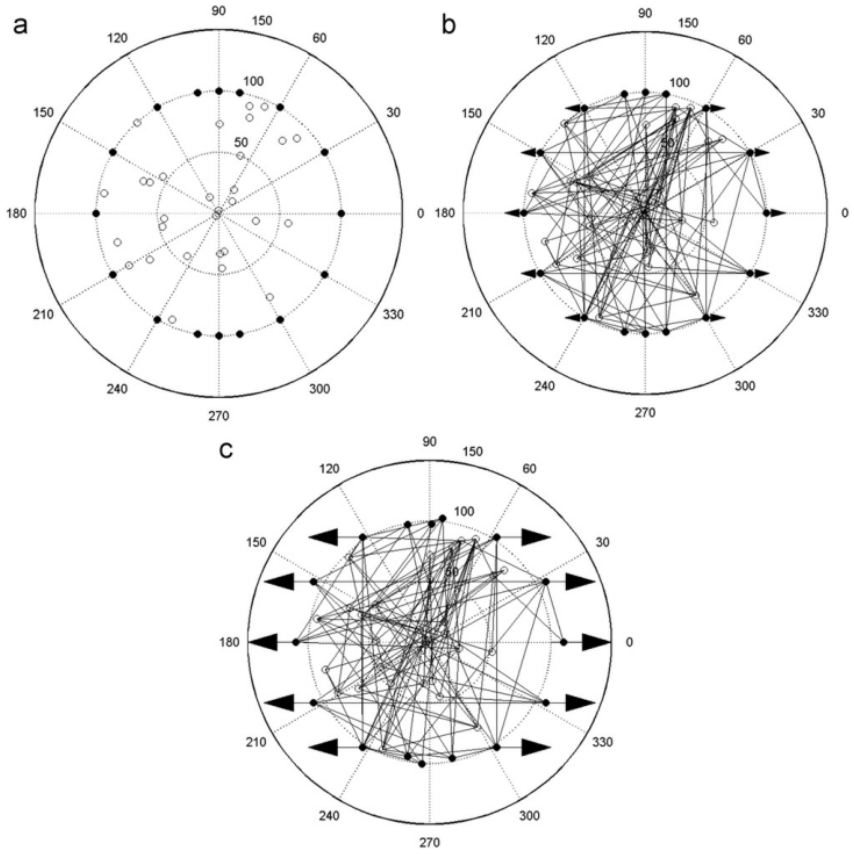

Figure 2-1: Our initial computational model for representing a simplified actin filament network of an approximately circular cell under mechanical stimulation. (a) The node distribution of the network of 100 arbitrary unit radiuses with filaments removed. 16 nodes are assigned to specific locations on the perimeter (filled circles) and can act as fixed connections (mimicking focal adhesions). 30 interior nodes (open circles) are placed randomly and function as links between filaments (mimicking linking proteins such as filamin). **(b)** 138 filament network with both nodes and filaments represented. Linear fibers are formed by randomly selecting two nodes for each fiber; the nodes locate the ends of a fiber and define its length and orientation. Arrows denote which perimeter nodes will be stretched and the direction of stretch. **(c)** Configuration after stretching the arrowed perimeter nodes by 10% of their X-axis position in the direction of the arrows and after node network equilibrium has been achieved. The model was considered in equilibrium when the summation of the absolute magnitude of all the nodal forces was less than a prescribed tolerance.

Within its interior, additional nodes are randomly placed that are not fixed to the substrate and can move when a net imbalanced force is applied to them. The nodes on the perimeter act as anchoring proteins, which are representative of focal adhesions, and the interior nodes model cross-linking proteins between filaments, such as filamin; multiple filaments per node are possible. A prescribed quantity of filaments is created by randomly assigning two nodes

per filament, which locates the filament ends and establishes its length and orientation within the space (**Figure 2-1b**). These filaments are assumed to represent either cross-linked single actin filaments or bundled filaments found in stress fibers. The filaments are considered linear members able to support both tensile and compressive loads. This assumption is reasonable if the applied stretch is at short time intervals, or the stress is weak, or for short filaments in the range of 0.1-1 μm long, which account for 80-90% of filaments found *in vivo* [59, 60].

2.3.2 Single-mode stretching and relaxation

The filaments and nodes are initially assembled in an unstressed state. All perimeter nodes except for those between 80-100° and 260-280° are then stretched horizontally on both sides (i.e., uniaxially) by an amount proportional to their initial X-axis positions so that those on the X-axis experience full stretching. The excluded nodes are near the vertical positions and are not considered fixed; this approach is used to simulate uniaxial stretching (**Figure 2-1c, see Movie M1**). The substrate is assumed to be sufficiently wide to exclude edge effects. A key assumption of the model is that mechanical stress on actin filaments is primarily responsible for the network's response and all other influences, including the properties of the binding proteins, are accounted for in the probabilities assigned for filament fracture.

The displacement of the nodes on the perimeter may cause some filaments to elongate and some to shorten (**Figure 2-2**). The resulting mechanical strain in a filament is defined as the ratio of the change in length to the original length **(**see **7.2 Strain summation** and **7.3 Angle calculation** for code). Using the assumption that filaments behave as Hooke's Law springs, strain is directly proportional to stress by the elastic modulus, which for actin filaments is approximately 2 GPa [61, 62]. It has been shown that individual actin filaments in living cells have a linear stress/strain relationship up to at least 12% strain [63] and that at frequencies <100

Hz, overall cytoskeletal elasticity is relatively independent of frequency [64]. The strain in our model is then directly proportional to the applied force and the forces exerted by the filaments on their connected nodes are equal and opposite; multiple filament connections per node are possible. A force balance—which translates to a strain balance—was applied to all internal nodes and the perimeter nodes at 80-100° and 260-280° (i.e. all nodes except for the fixed perimeter nodes).

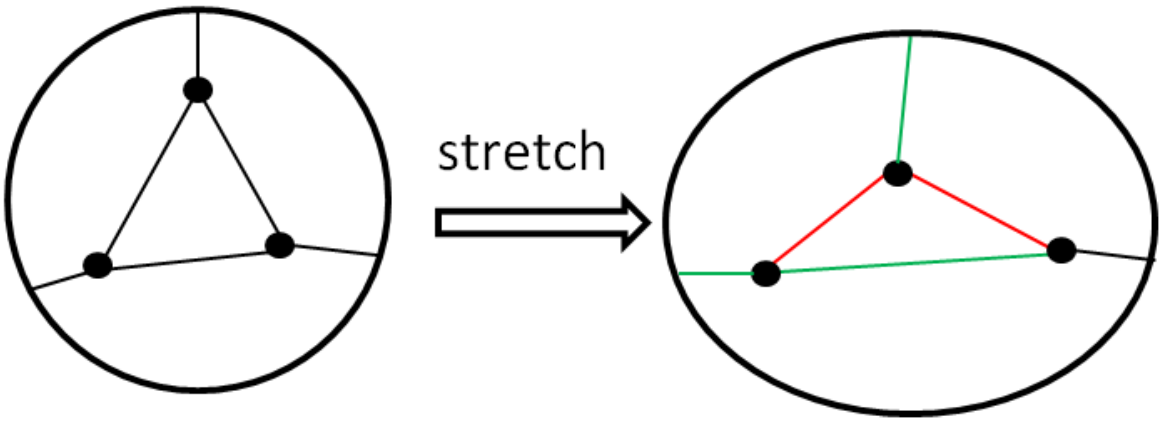

Figure 2-2: Simple schematic of stretching and resulting strains in free nodes. Cytoskeletal model has 6 filaments, 3 internal nodes, and 3 peripheral nodes. Green denotes extended filaments (positive strain). Red denotes compressed filaments (negative strain).

Based on the resultant forces, the position of the nodes were adjusted by an amount proportional to and in the direction of the resultant force. A Gauss-Seidel relaxation iteration was applied to adjust the node positions until all the nodal forces were balanced, minimizing the nodal stress in the network (see **7.1 Dual-mode cell stretch execution** for code). However, repositioning of the nodes can either increase or decrease stresses in the connected filaments. We consider the system to be at equilibrium when the sum of the absolute magnitudes of all the nodal forces is less than a prescribed tolerance (0.1 Pa in our model). We imposed a 10% total displacement by displacing perimeter nodes in 1% increments and relaxing forces in the system after each 1% adjustment until a total specified displacement of 10% was reached. Note that at

equilibrium, individual filaments may contain large positive (tensile) or negative (compressive) stress values but the net balance of these stresses on each node must be small.

2.3.3 Breaking and generating new filaments

Once the total prescribed displacement was reached and the model was in equilibrium (**Figure 2-1c**), the final strains in the individual filaments were checked to determine which would break. This was accomplished by first normalizing the strains using the largest strain value. The probability for any individual filament to break was then defined to be the absolute value of the normalized strain. Random numbers were generated between 0 and 1 to determine which filaments were removed, with a new filaments generated in the relaxed state between a random pair of nodes to replace each removed filament. This process of stretching, energy minimizing, and breaking and replacing filaments was considered a complete cycle. A new cycle was initiated by elastically returning the nodes back to their original positions while maintaining the filament connections. The network is now considered to be in an unscretched state. The network was again stretched and the cycle repeated. This continued for a prescribed number of cycles while the distribution of filaments, their orientations, and their stresses were determined. See **Movie M2** for a simulated actin filament network undergoing 25 cycles of horizontal uniaxial 10% stretching with filament breakage and replacement.

To calculate the variability in our model, we calculated the standard error of the mean of our measurements of filament angle and stress. The means are taken at each cycle over n=10 uniquely generated filament networks. These variabilities are shown in the relevant figures as error bars representing 95% confidence intervals. One assumption that makes this approach more computationally tractable is that the peripheral nodes acting as focal adhesions do not move

freely. While it has been shown that focal adhesions can move in response to tension [65], in the scope of this work we have not incorporated this yet.

2.4 Experimental methods

2.4.1 Mechanical Stimulation System

A device was fabricated to impose cyclic uniaxial tension on living cells [66]. A stretch frequency of 1 Hz was chosen since a normal adult resting heart rate is 60-100 beats per minute and experiments show that maximal alignment does not occur at less than 1 Hz [51]. The substrate used in our cell-substrate interactions was a ½ cm thick polydimethylsiloxane (PDMS) membrane. PDMS is created using a prescribed base-to-curing agent ratio, which was 10:1 for this study, resulting in an Elastic Modulus of 1882 kPa. We used the PDMS membrane to generate forces on adhered cells by clamping and stretching it in an air pressurization system. For the cyclic stretching, the cyclic pressure supply to the PDMS membrane was created through a bypass mechanism. This mechanism was constructed by modifying the feedback pressure control system of a microfluidic interface approach [67]. This control device enabled cyclic regulation of pressurized air onto the bottom surface of the membrane, which deformed the cells attached to the upper surface of the membrane. Nearly complete uniaxial (ratio of 20:1 of stretch in desired *vs.* normal direction) stretching was imposed on PDMS membranes through elliptically constraining the periphery of the membrane, and the cells that were attached to the membrane, were stretched simultaneously. Cyclic uniaxial strain at 20% was applied by adjusting the pressure to 10 psi using a frequency of 1 Hz for 3, 6, and 12 hour time periods.

2.4.2 Cell Culture

NIH 3T3 fibroblasts were washed once with phosphate-buffered saline (PBS), and then exposed to 0.05% trypsin-ethylenediamine-tetraacetate (Trypsin-EDTA) for 5 minutes. Following dissociation, the cells were counted and seeded, at a concentration of 1000 cells/cm^2, on PDMS substrates that were pre-coated with fibronectin (10 μg in 1 mL PBS; BD Biosciences, San Jose, CA, USA; No.: 39410). Cell cultures were maintained at 37ºC under 5% carbon dioxide in Dulbecco's modified Eagle's medium supplemented with 10% calf serum, glutamine, 0.3 mg/mL, streptomycin, 100 μg/mL, penicillin, 100 U/mL, and 20 mM N-2-hydroxyethylpiperazine-N'-2-ethanesulfonic acid at pH of 7.4. Cells were incubated for a minimum of 6 hours to allow for attachment and spreading; the media was replenished 24 hours before testing. A thermostatically regulated heat source maintained a temperature of 37ºC during the experiments.

2.4.3 Optical Microscopy

Following the application of mechanical stimulation, pressure was removed and the cells were immediately fixed for imaging with an optical microscope. Filamentous actin (F-actin) was visualized to investigate the effects of mechanical stimulation on actin filaments. F-actin were visualized by fixing the cells with 4% paraformaldahyde and then permeablizing them with 0.2% Triton-X 100, followed by staining with 6 μM Alexa Flour® 488 phalloidin (Molecular Probes, Carlsbad, CA, USA; No.: A12379). The cells were then mounted with fluoromount-G, sealed under a coverslip and examined using an inverted optical microscope (Zeiss Axiovert 200; Zander IVF, Vero Beach, FL, USA) with a 63X high numerical aperture oil immersion objective. A fluorescein isothiocyanate (FITC; correspondingly pseudo-colored green) filter set allowed us to visualize these filaments.

2.4.4 Analysis of Actin Filament Orientation

Following mechanical stimulation, the cells were stained for F-actin and fluorescent images were imported into ImageJ software (download from the National Institutes of Health; http://rsb.info.nih.gov/ij/download.html), which were used for analysis of actin filament orientation. Microfilament orientation was examined by fitting an ellipse to the cellular outline based upon an initial tracing of the cell periphery. A major and minor x' and y' axes was then defined on this ellipse. Because cellular orientation is a predictor of actin filament orientation [68, 69], we then quantified actin filament orientation by comparing the ellipse major axis orientation to the direction of uniaxial stretch. Only cells whose actin filaments exhibited a single orientation were used for analysis.

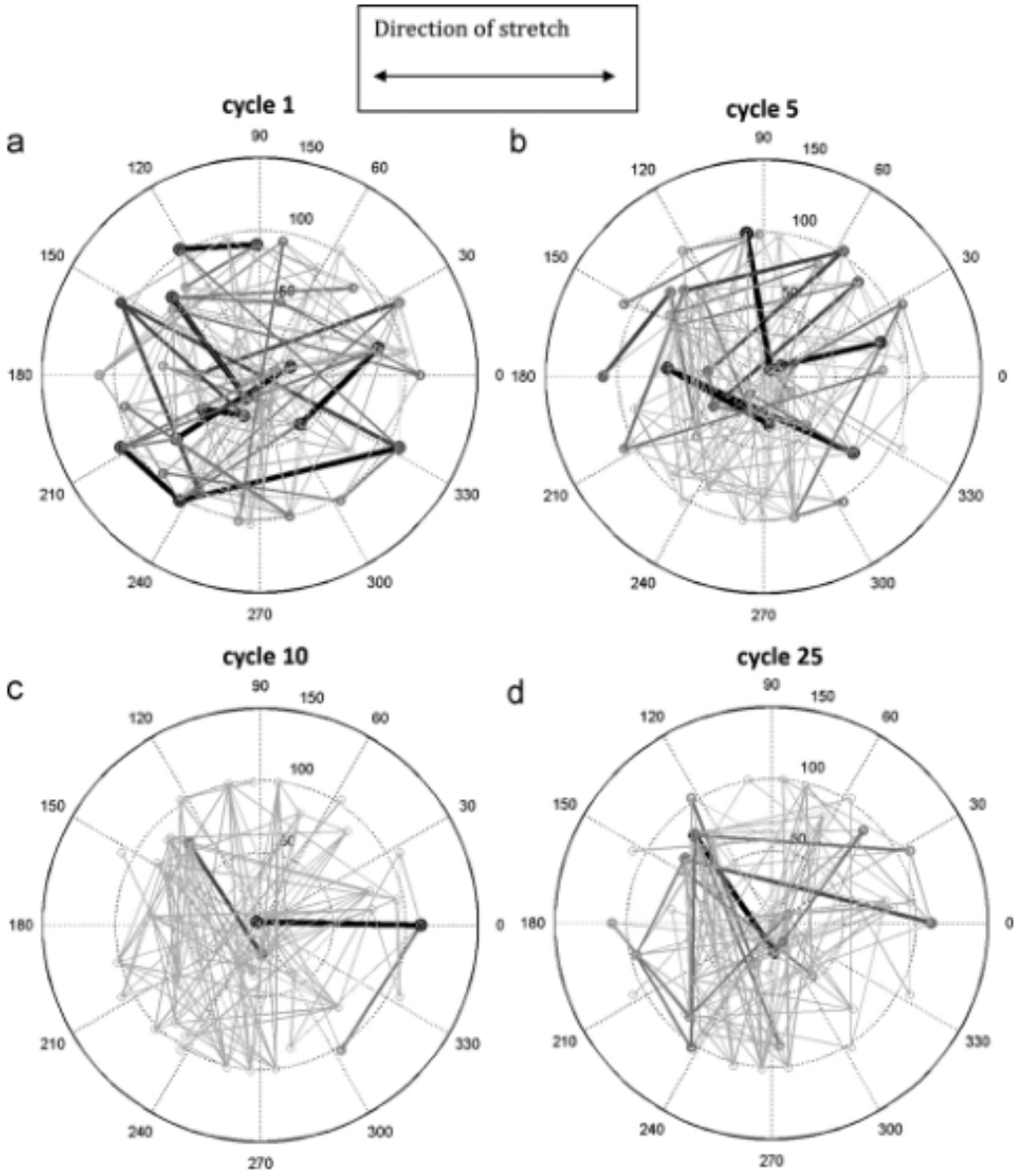

Figure 2-3: A filament network of 138 filaments, 16 prescribed perimeter nodes, and 30 randomly placed internal nodes under 10% uniaxial horizontal stretch after (a) 1, (b) 5, (c) 10, and (d) 25 iterative cycles. Stretch was imposed in 1% increments on all peripheral nodes from -60° to 60° and 120° to 240°followed by Gauss-Seidel relaxation to achieve network nodal force equilibrium. The depicted thickness/darkness of the filaments correspond to their relative stresses with the thickest/darkest being >75% of the maximum stress of the network and the thinnest/lightest being <25%. The length scale in this model is 100 arbitrary units, representing a cell whose bulk lies in an approximately circular region of diameter 30 μm, such as a fibroblast.

We studied the response of the actin filament model network by examining the network over time as mechanical stimulation was imposed on the system. **Figure 2-3** shows initial, intermediate, and final configurations of an actin filament network subjected to cyclic stretching corresponding to 1, 5, 10, and 25 cycles of stretching. There are 16 nodes on the perimeter of a circle of radius 100 units and 30 interior nodes with 138 filaments. In dividing non-muscle vertebrate cells, the number of actin filaments has been estimated to be in the tens of thousands [70-72] but due to the computational challenges with these number of filaments, we are assuming a model with fewer filaments. Nodes located on the perimeter from 80° to 100° and 260° to 280° are not stretched. Nodes from -60° to 60° and 120° to 240° are stretched 10% for 25 cycles. After each cycle, the normalized filament stress determines the probability for breaking. "Breaking" is a term used to encompass all of the different mechanisms by which a filament might cease linking two nodes, whether this is through depolymerization, disassembly, or physical breaking [73-77]. These are replaced by filaments that are randomly assigned new locations such that the total number of filaments is conserved.

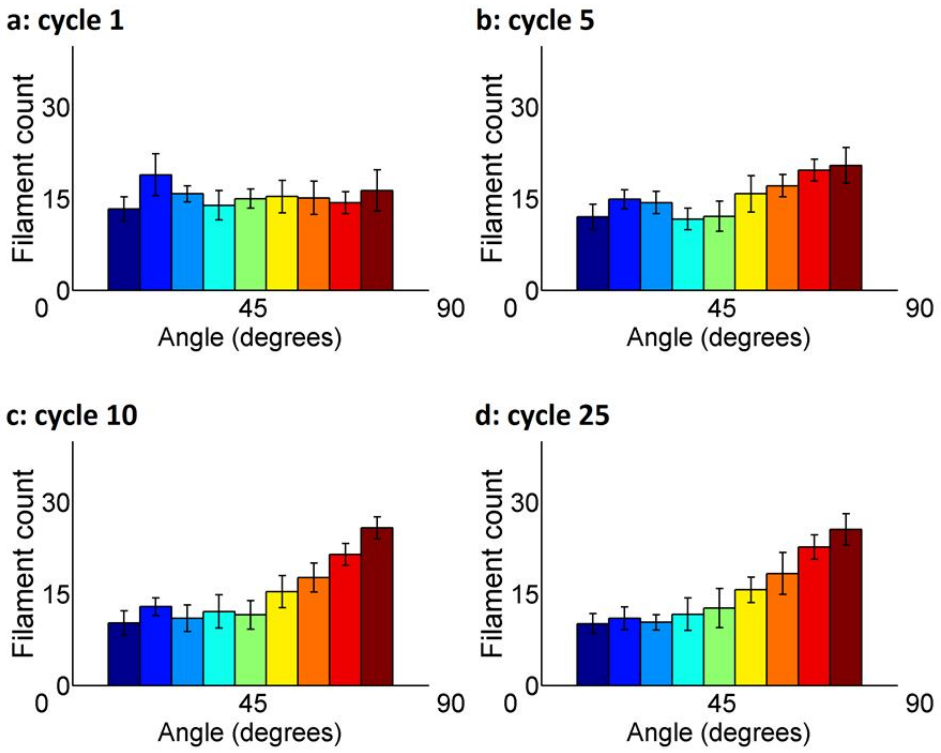

Figure 2-4: Histograms of angular orientation of filaments in nodal equilibrium after (a) 1, (b) 5, (c) 10, and (d) 25 iterative cycles of 10% uniaxial horizontal stretch. Averaged over ten uniquely generated filament networks, each of which consisted of 138 filaments distributed among 16 prescribed perimeter nodes and 30 randomly placed interior nodes. Each filament connects two nodes. Error bars denote 95% confidence interval.

In order to quantify filament orientation, we create histograms of all filament angles in the network, averaged over 10 uniquely generated networks (**Figure 2-4**; see **Appendix Figure 6-1** for full progression over 25 cycles**)**. A clear affinity for 90° vertical alignment appears as cycle number increases. This shift though can be detected in as few as 5 cycles. The error bars reveal that there is a small amount of variation in the distribution of the filament alignment, which is not unexpected in a stochastic model. Note that all filament angles have been transposed to the first quadrant of the Cartersian coordinate system to create these histograms so that we are able to similarly portray filaments from 90° to 360°.

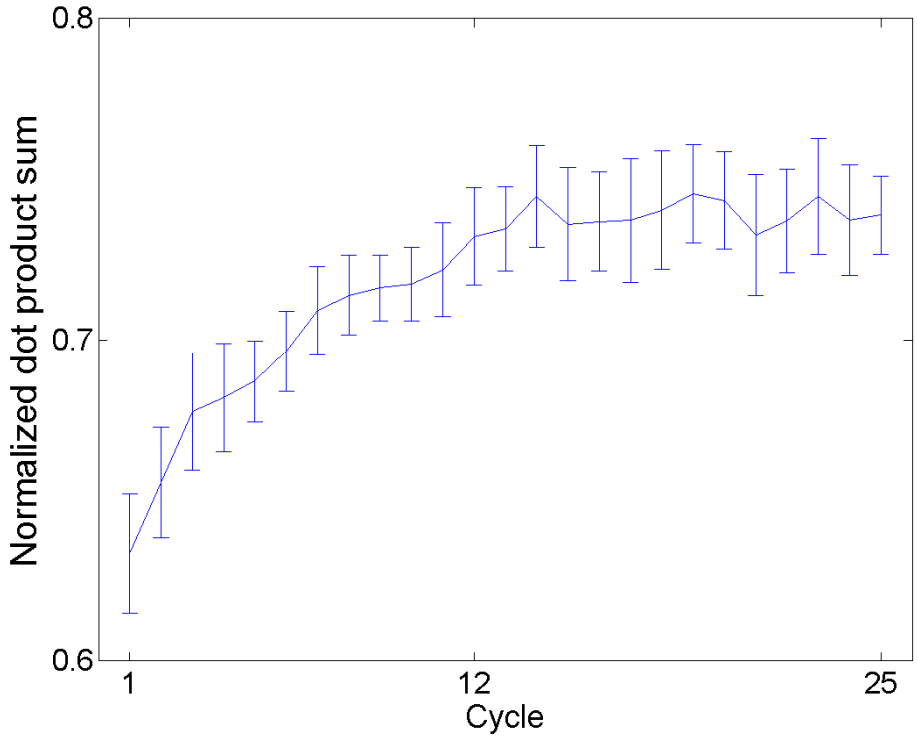

Figure 2-5: Normalized dot product between filament angles and the filament network mean angle at nodal equilibrium over cycles 1-25. For each cycle, filament lengths were all assumed to equal 1 and the average dot product between each filament angle and the mean filament network angle were averaged over 10 uniquely generated networks. All filament lengths were normalized to 1 to maintain equal representation among all filaments. If all of the 138 filaments aligned exactly with the filament network mean angle, the normalized dot product sum would be 1.0 for that cycle. Error bars denote 95% confidence interval.

To quantify filament angle alignment over all cycles, we normalized all filament lengths to 1 and determined the dot products between each filament angle and the mean filament angle of the network. We calculated this normalized dot product for each cycle from 1 through 25 and averaged the results over ten uniquely generated 138-filament networks (**Figure 2-5**). The normalized dot product increases immediately in the early cycles until a steady state is reached at approximately 14 cycles. The decision to normalize all filament lengths to 1 was made to allow equal representation among all filaments. If all of the 138 filaments aligned exactly with the filament network mean angle, the normalized dot product sum would be 1.0 for that cycle.

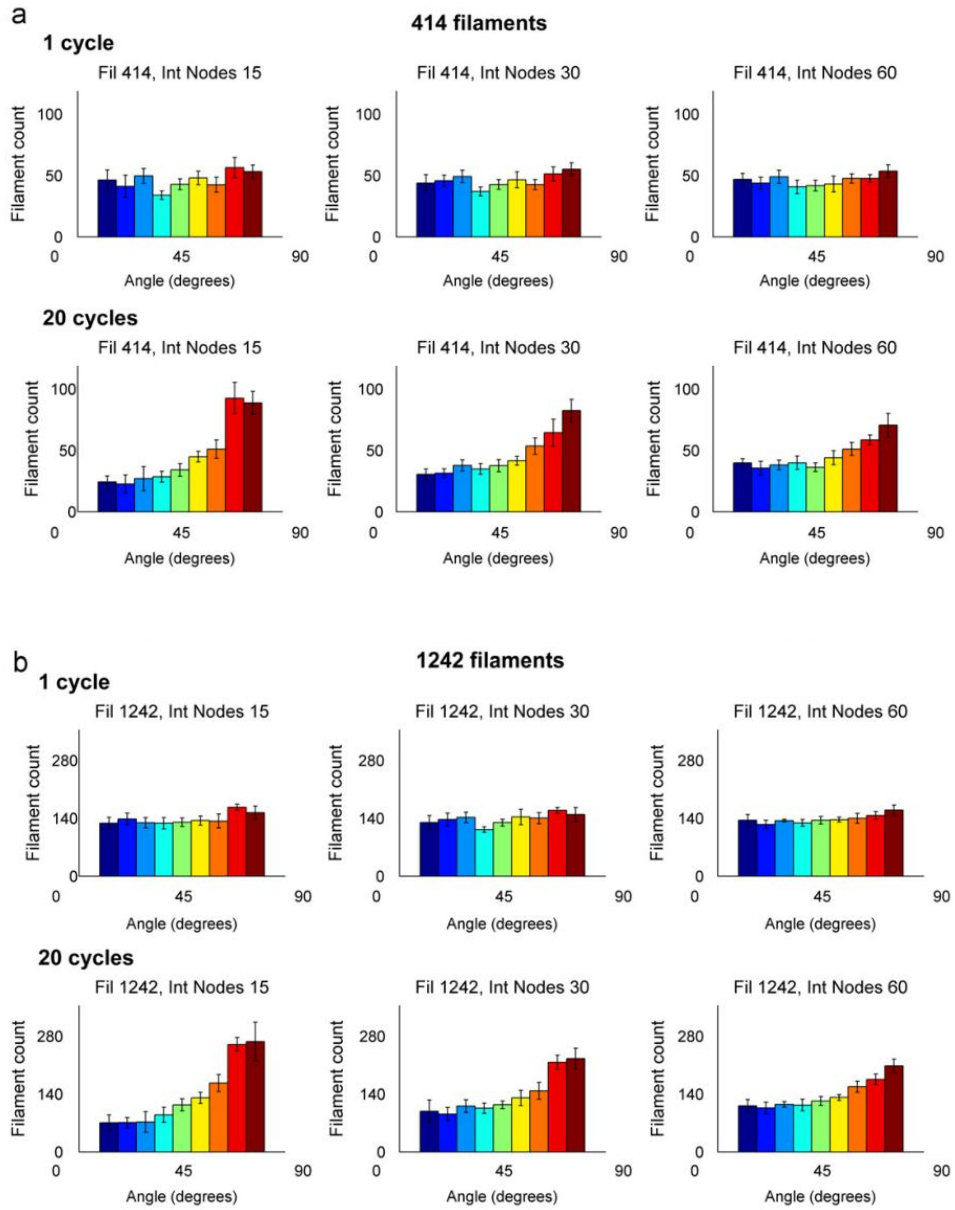

Figure 2-6: Histograms of angular orientation of filaments in nodal equilibrium after 1 cycle and 20 cycles for networks with (A) 414 and (B) 1242 filaments, which are 3 fold and 9 fold multiples of the previous filament number, 138. The number of internal nodes was varied as well from 15, 30, to 60 while peripheral nodes were held constant at 16. The results were averaged over eight uniquely generated filament networks. Error bars denote 95% confidence interval.

To determine the changes to our model under variation of important parameters, including filament number and internal node number, we increased the number of filaments to 414 and 1242 while varying the number of internal nodes between 15, 30, and 60. We tracked

filament angle orientation and present the results at cycle 1 and 20 (**Figure 2-6**). While there is no obvious alteration in filament orientation when increasing filament number, there is a slight shift towards vertical alignment when the number of internal nodes is decreased. We observed that with decreased number of internal nodes, more breakages occur while holding the filament number steady (data not shown). It is possible that fewer degrees of freedom to alleviate stress are causing higher filament strains when node number decreases, which subsequently leads to faster convergence to the perpendicularly aligned state.

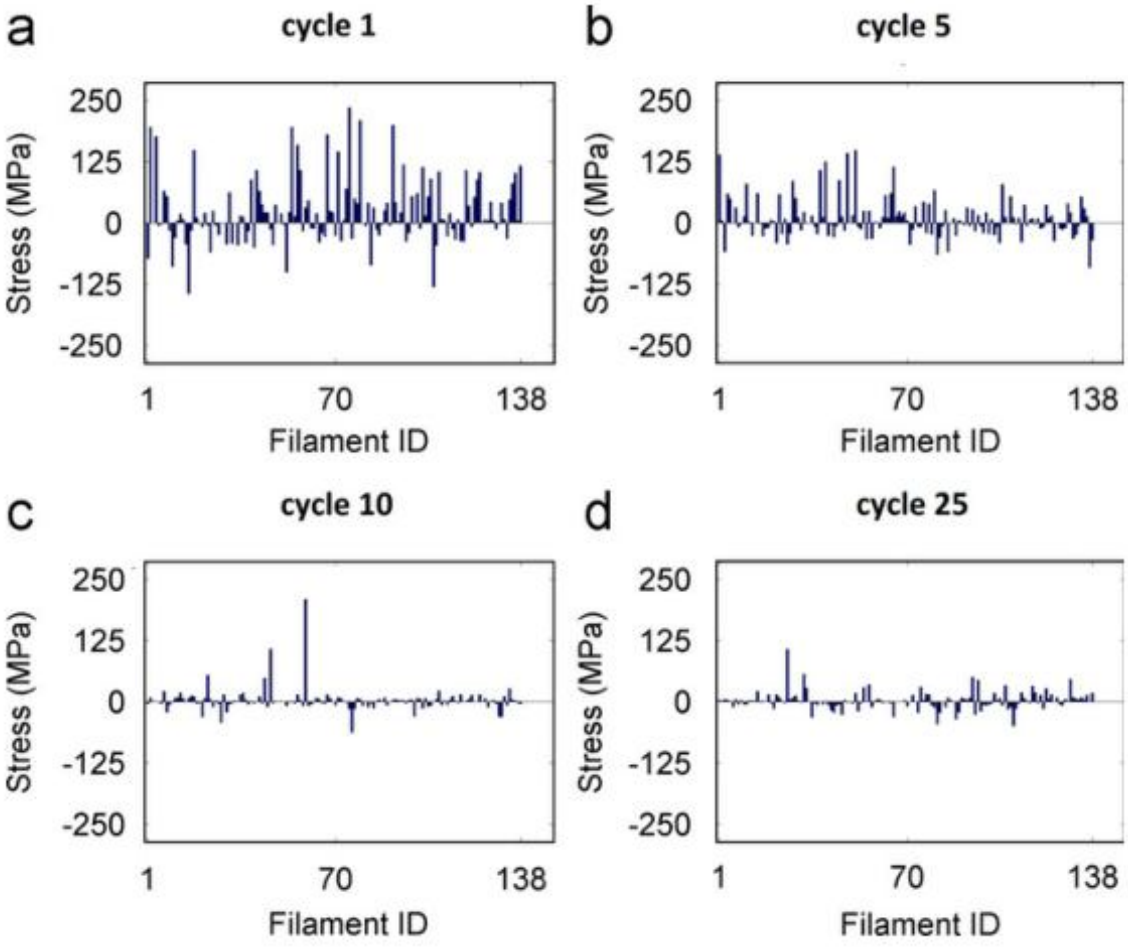

Figure 2-7 : Individual filament stress values in nodal equilibrium after a network was stretched uniaxially by 10% for (a) 1, (b) 5, (c) 10, and (d) 25 cycles. Positive stress (i.e., tension) denotes an increase in the length of the filament relative to the length before the stretching cycle and negative stress (i.e., compression) denotes a decrease in length. At the end of each cycle, filament breakage probability was defined to be the absolute value of the strain normalized to the largest strain value. Network parameters were 138 filaments, 16 perimeter nodes, and 30 internal nodes.

The filament stresses for each of the 138 filaments in the network for 1, 5, 10, and 25 cycles of stretching are analyzed (**Figure 2-7**). Positive stress (i.e., tension) denotes an increase in the length of the filament relative to the start of the stretch cycle and negative stress (i.e., compression) denotes a decrease in length. As the cycle number increases in **Figure 2-7**, a clear

trend towards decreasing stress is observed. At cycle 1, the range of filament stresses is [-100,200] MPa. By cycle 8, this has been reduced to [-100,100] MPa. At cycle 16, there are some spikes of higher stresses but by cycle 24, the filament stress range returns to [-100,100] MPa. These results are non-obvious as the model implies that stresses in not only tension but also compression are reducing in this uniaxial stretch based approach.

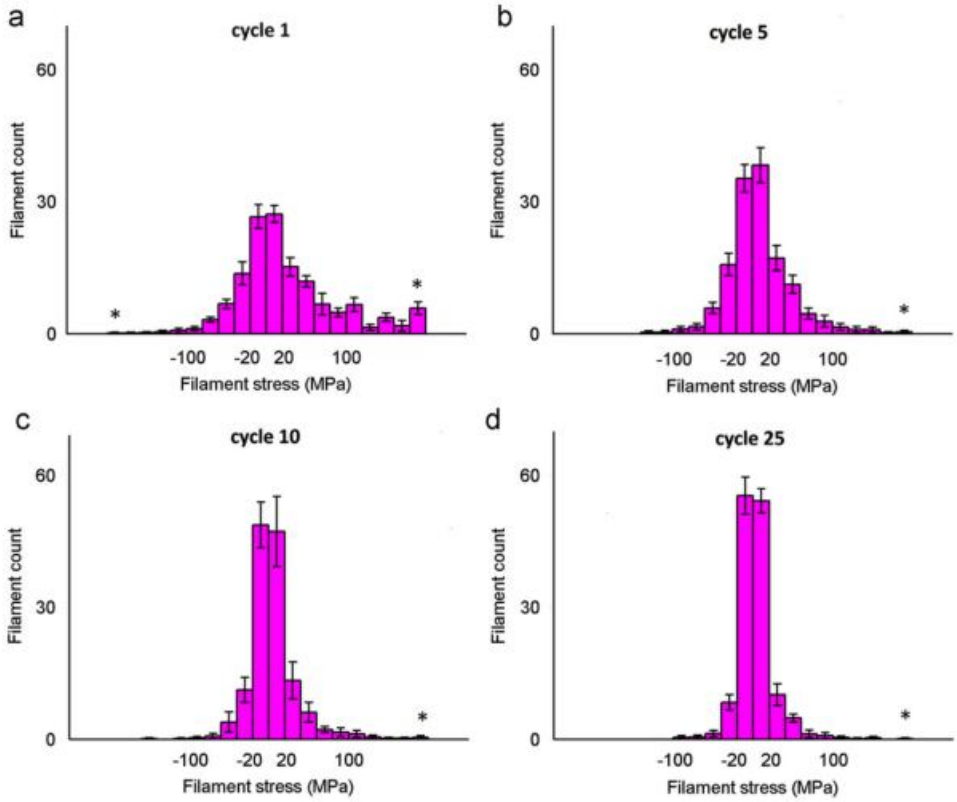

Figure 2-8 : Histogram of filament stresses in nodal equilibrium after (a) 1, (b) 5, (c) 10, (d) 25 iterative cycles of 10% uniaxial stretch averaged over 10 uniquely generated filament networks of 138 filaments, 16 perimeter nodes, and 30 internal nodes. The starred (*) leftmost and rightmost bins contain filaments with stresses less or greater than -180 and 180 MPa, respectively. Positive stress (i.e., tension) denotes an increase in the length of the filament relative to that before each stretching cycle and negative stress (i.e., compression) denotes a decrease in length. Note the large rightmost bin in (a) represents a large number of high-stress filaments initially present in the network, which decreases with additional cycles (b-d). Error bars denote 95% confidence interval.

Figure 2-8 quantifies the filament stress through histograms comparing tensile (positive) and compressive (negative) stresses for 1, 5, 10, and 25 cycles of stretching. Each bin covers a range of 10 MPa. The left-most and right-most starred (*) bins contain filaments with stresses less than and greater than -190 and 190 MPa, respectively, as these contained much smaller numbers of filaments. Initially the filament stresses are relatively widely distributed but as the number of cycles increases, a shift to a much higher number of filaments in the bins of lower tension and compression occurs. This result is consistent with the results presented in **Figure 2-6**. The peak in the right-most bin for the 1st cycle in **Figure 2-8a** is the result of a large number of high-stress filaments initially in the network, which decreases with greater number of cycles (**Figure 2-8b-d**).

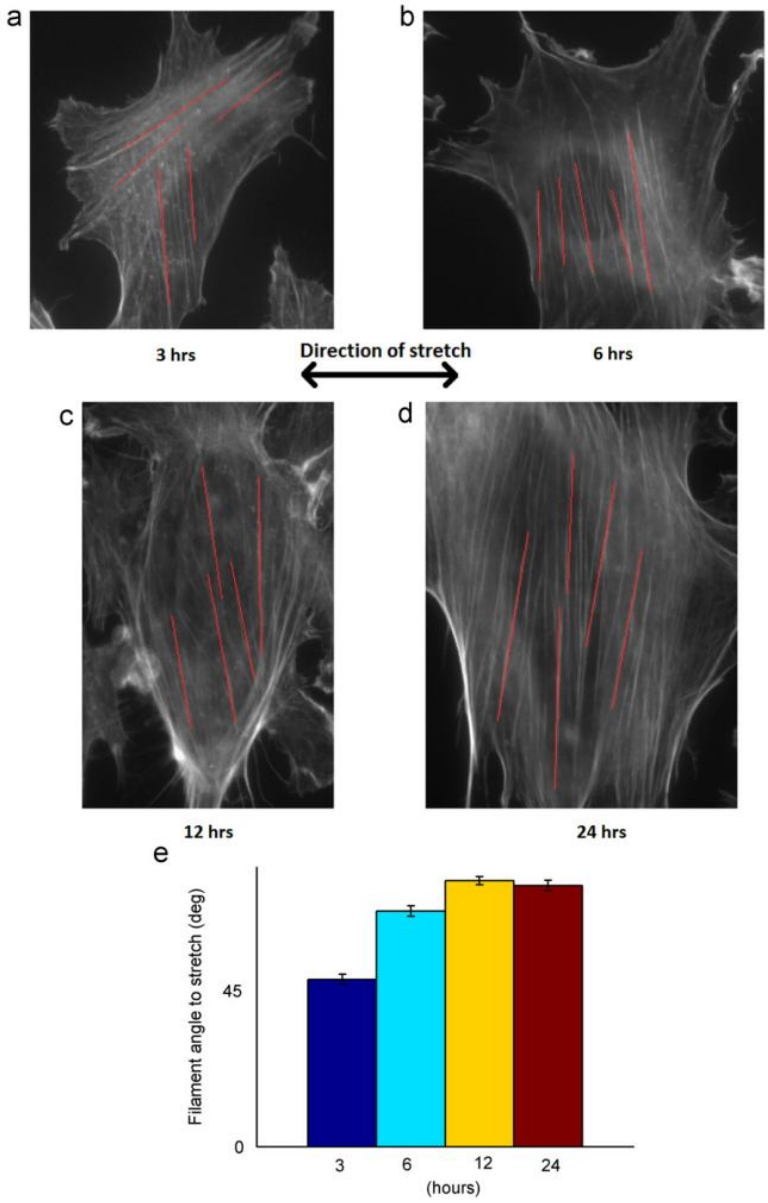

Figure 2-9: Images of NIH 3T3 fibroblasts exposed to 1 Hz vertical cyclic stretch uniaxial stretching after (a) 3, (b) 6, (c) 12, (d) 24 hours. Red lines indicate representative actin filaments measured for angle relative to stretch direction. (e) Average filament angle relative to stretch direction at all time points. 5 filament angles were measured per clearly visible non-dividing cell. For the 3, 6, 12, and 24 hour time points, we measured filaments in 47, 31, 22, and 10 cells, respectively. The cells were cultured on an elastomeric substrate, stretched, fixed with paraformaldahyde, and then stained with 6 µM Alexa Flour® 488 phalloidin stain for F-actin. These images were captured on an inverted Zeiss Axiovert optical microscope with a 63X high numerical aperture oil immersion objective. A fluorescein isothiocyanate (FITC) filter set allowed us to visualize the actin filaments. Error bars denote 95% confidence interval.

The orientation of cytoskeletal actin in NIH 3T3 fibroblasts exposed to 1 Hz cyclic uniaxial stretch after 3, 6, 12, and 24 hours was observed (**Figure 2-9a-d**). The cells were strained using the elastomeric membrane, fixed with paraformaldahyde, and then labeled using 6 μM Alexa Flour® 488 phalloidin stain for F-actin (green pseudo-colored). The filament outlines were enhanced in software using the convolution feature in ImageJ. For each time point, the angles of ten representative filaments relative to that of the cyclic stretch were measured and their average computed (**Figure 2-9e**). At 3 hours, we see that prominent actin filaments are arranged both parallel to and perpendicular to the axis of stretch. Over time, with an increasing number of stretch cycles, steadily increasing F-actin alignment in the direction normal to stretch is observed. To further support our observations, we measured the orientation of whole cells at the same time points as whole cell orientation generally follows intracellular cytoskeletal alignment (see **Figure 2-9**). This alignment is quantified showing a strong pattern moving toward vertical alignment (**Figure 2-10**). These experimental results reflect the modeling results in **Figure 2-4** and **Figure 2-5**.

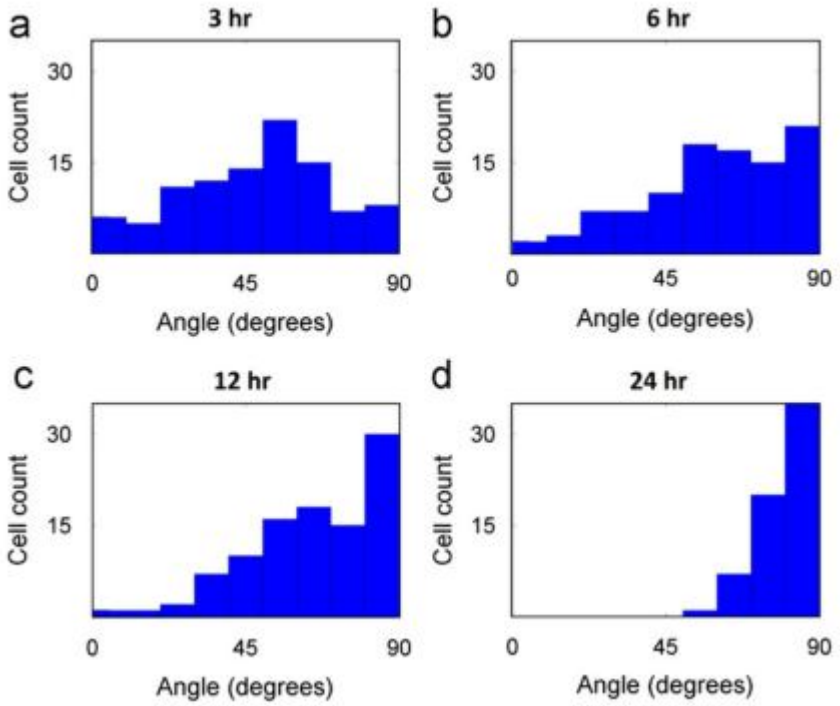

Figure 2-10: Whole cell angular orientation histogram of NIH 3T3 fibroblasts after (a) 3, (b) 6, (c) 12, and (d) 24 hours of uniaxial horizontal cyclic stretch. Following mechanical stimulation, the cells were stained for F-actin and fluorescent images were imported into ImageJ software for analysis of actin filament orientation. Orientation was examined by fitting an ellipse to the cellular outline based upon an initial tracing of the cell periphery. A major and minor x' and y' axes was then defined on this ellipse. Actin filament orientation was then quantified by comparing the ellipse major axis orientation to the direction of uniaxial stretch. Only cells whose actin filaments exhibited a single orientation were used for analysis. 100 cells were sampled. At time 0, the cell orientation was the most uniformly distributed.

2.6 Discussion

2.6.1 Filament alignment patterns

Through our computational simulations, we have shown that a minimal model of coupling of mechanics to a stress based approach results in a realignment of filament networks under cyclic stretching. Initially the filaments in the model are randomly oriented (**Figure 2-4a**) but begin to exhibit a distinct alignment in the vertical direction as they experience additional cycles of stretching (**Figure 2-4b-d). Figure 2-5** clearly shows a trend towards filament co-alignment with further cycles. Taken together, **Figure 2-4** and **Figure 2-5** show that under cyclic stretch, our model demonstrates not only gradual vertical alignment but also increased similarities in the distribution of filament angles. As shown in Figures **Figure 2-9** and **Figure 2-10**, a comparable alignment in response to cyclic stress occurs in cultured cells. Initially, the cells show little alignment, but by 12 hours under uniaxial cyclic stimulation, the cytoskeletal actin and whole cell alignment of NIH 3T3 cells acquire a defined alignment in the vertical direction. This alignment begins to appear as early as 6 hours. Our model predicts this alignment by 25 cycles, which would correspond to approximately half a minute assuming a typical heart rate of 60 cycles per minute. We believe this discrepancy results from the fact that the probabilistic method of our network realignment algorithm forces at least one filament to break and reform on each iteration of energy relaxation, while the true system might pass through many cycles of stretching between filament breakages. In this regard, then, each cycle in our method can be considered to represent a sequence of potentially many cycles without any filament breakage culminating in a cycle in which some rearrangement occurs. This decision to effectively simulate only “eventful” rounds of cycling is needed because the computational cost of each individual cycle would make it prohibitive to directly simulate the tens of thousands of

cycles needed to explicitly simulate every cycle of the true multi-hour time course of realignment. While the selective sampling procedure we use prevents us from attaching an explicit time scale to our simulations, we plan in future work to extend it using standard stochastic simulation methods to allow more realistic sampling of times between eventful cycles [51, 78, 79].

2.6.2 Filament stress patterns and imposed strain

Along with the alignment perpendicular to the direction of cyclic stretch, the stress within the individual filaments was observed to decrease with increasing number of cycles. The alignment can be attributed in part to the model being stretched in the horizontal direction and the highest strains therefore occurring in the horizontally positioned filaments. This result suggests that certain cells may be altering their morphology in order to minimize the energy of external mechanical stress. These findings are supported by continuum models of cytoskeletal alignment under cyclic stretching [51, 80]. There were several further interesting and non-obvious findings. For the nodes from 80-100° and 260-280°, which were not fixed to the underlying substrate, the vertical filaments attached to these nodes could be expected to experience higher compressive strains similar to that experienced in a uniaxial stretch of a solid body obeying Poisson's ratio, described as a simple elongation model [11]. This, though, did not seem to be the case here. The stress plots suggest that both tensile (positive) and compressive (negative) stress levels proceeded toward a low baseline with more cycles of stretching (**Figure 2-7**). **Figure 2-8** quantifies this trend and, when taken with the alignment of the filaments, indicates that the filaments may have reorganized to minimize stress. However, if the filaments in compression were assigned a higher probability of breaking, as has been suggested in prior experimental work [81] , the final results may have been more biased towards an oblique

alignment of the filaments. In addition, if all the perimeter nodes were fixed in a different initial configuration, the filament response may have differed. Furthermore, the results may be dependent on the total magnitude of stretching applied as experiments have shown that cell reorientation is primarily dependent on stretch magnitude as opposed to rate [11]. A strain of 10% was used based on previous cellular and physiological experiments and conditions. For example, under normotensive conditions, stretch has been reported to be 9-12% in the aorta and 6-10% in the pulmonary arteries in humans [82-84]. In addition, arterial motion is predominantly in the circumferential direction with little longitudinal movement [85], which suggests that a uniaxial circumferential stretch model may accurately simulate physiological arterial stretch. Previous studies have demonstrated that the variation of cytoskeletal elasticity with respect to frequency lies in two domains: at high frequencies >100 Hz the elasticity is dependent on frequency with a universal exponent of 3/4 in a regime akin to semiflexible polymers whereas at lower frequencies the elasticity is relatively independent of frequency consistent with a soft-glass regime [64, 86]. While our model is independent of frequency and these cytoskeletal elasticities relate to the whole cell rather than individual filaments, in the future, the alignment and stress patterns could be compared to empirical results after parameterizing the elastic modulus of our filaments for frequencies between 60-100Hz and beyond 100 Hz.

2.6.3 Filament breakage and reassembly

In our model, we normalize probabilities of filament breakage to the highest individual stress value of the given filament network. Our goal is to have a single measure that attempts to account of the variety of different filament responses that might occur at high stresses, including physical breaking and depolymerization. However, it has been shown *in vitro* that actin

breakage might be more accurately modeled as occurring reliably at a threshold strain [75] rather than probabilistically over a range of strains. This observation may hold *in vivo* as well. Our data shows the average filament stress dropped from 71 MPa at cycle 1 to 8 MPa by cycle 8. The averaged stayed at approximately 8 MPa by cycle 16 before dropping to 3 MPa by cycle 24. These data suggest that even though our model uses a relative probability for filament breakage, the model still is relatively effective at simulating pseudo-thresholds in these cycle ranges.

In addition, although the total filament length remains relatively constant, new filaments are assumed to form instantaneously and independently of current fiber orientation or shape in our model. In reality, new filament formation may be more gradual and dependent on multiple factors including current cell orientation. It has been reported that endothelial elongation can drive filament orientation [87]. Conversely, stress fiber orientation has been suggested to drive endothelial cell elongation [88]. An interesting result during reassembly that we observed in our simulations was when nodes moved outside the boundaries of the cell during the force equilibrium phases (see **Movie M2**). Our model was not formulated to constrain this from occurring and interestingly, this might have implications for cell motility as motility is directly related to polymerization of the actin cytoskeleton [73]. As our model is based on passive force balance, one factor that we have not modeled is the generation of active force by myosin motors. While it is known that myosin II is involved in unbundling individual actin filaments and their depolymerization, the functions of various myosins and actin turnover separate from actin-based motility is not well understood [89]. Thus, we maintain a minimalistic model without multiple layers of complexity. Additionally, while it is known that various focal adhesion and actin cross-linking proteins such as α-actinin and zyxin have different mechanical properties related to

adhesion, motility and orientation [90], in this current work, we are not modeling these specific differences in this minimalistic model.

2.7 Conclusion

We have developed a simulation model of the gel-like lattice-crosslinked actin networks typically seen in the mechanically and biochemically-active cell cortex to investigate the morphological response of actin filaments under single-mode mechanical stimulation in the form of stretching. We present this minimalistic model to isolate observed behavior and test the sufficiency of a defined set of components critical to understanding complex biological systems, as modeling billions of molecules in single cells completely in terms of spatial and temporal organization will be far beyond computational resources for the foreseeable future. These minimal or coarse-grained models are in principal suited to understanding how mechanical stimulation influences actin cytoskeleton structure and dynamics. With this model, we are able test the hypothesis that a first-principles mechanical model of filament assembly in a confined space may be capable of yielding the remodeling behavior observed both experimentally and *in vivo* for cytoskeletal actin networks subjected to mechanical stimulation. We have found that the filaments in our model align preferentially in the vertical direction when experiencing cyclic horizontal stretching, which were similar to our experimental cyclic cell stretching responses.

We also observed that the stress in the individual filaments decreased with the increasing numbers of stretch cycles, indicating that the aggregate behavior of this network can decrease the local stress in the individual filaments. While this is a simplified model of cell structure, it is intended to approach a minimal model to allow exploration of fundamental questions about the mechanisms underlying cytoskeleton rearrangement in response to mechanical stimulus that do

not lend themselves to direct experimental investigation. It therefore contains only those mechanisms we propose to be necessary to the observed phenomena, in order to test whether those mechanisms specifically are sufficient to give the observed behaviors. The fact that the network moves toward a minimal energy state with increasing numbers of cycles suggests that the driving factor for actin cytoskeletal morphological response to cyclic stretching is to minimize the stress of the network. This theory is supported by others working with continuum models of cyclic stretching of actin networks [51, 80].

Future directions of this work include correlating our simulation and experimental data to find an accurate physiological threshold stress, integrating multiple modes of mechanical stimulation, and linking these network responses to biochemical alterations. We believe this computational model in combination with experimental results will provide insight into a wide range of areas at the intersection of mechanics and biochemistry, including mechanobiology, material science, and polymer physics.

2.8 Expansions to model

In this section, we discuss a new cytoskeletal actin network model that we adapted from our model discussed previously in the chapter. We call this model the "intersection model" based upon the method for the generation of interior nodes. The intersection model is designed for mechanotransductive analysis and contains independent modular functions for network generation, stretching, relaxing, and filament breakage. This model is also highly parameterizable with provisions for altering the number of elements (interior nodes, perimeter nodes, filaments), the geometry of the elements (random, deterministic +/- noise), the type of

stretching (apical, peripheral), the type of breakage (count-based, conservation of mass), as well as many other refining parameters.

Similarly to our original published model, when cyclically stretched, our intersection model demonstrates a perpendicular alignment of the filaments to the direction of stretch. We also observe decreasing filament stresses over increasing cycles of stretch.

2.8.1 Rationale

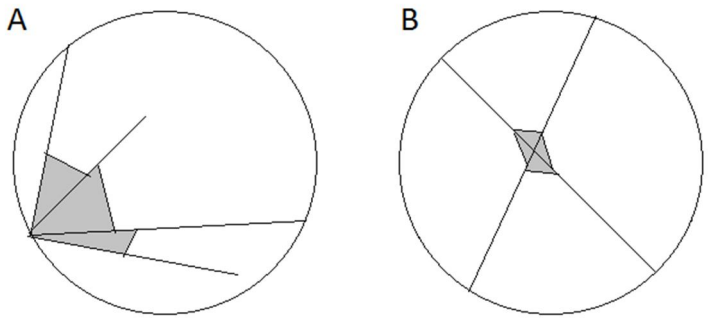

Figure 2-11: Schematic of how interior angles (grey) are determined for A) focal adhesion complexes and B) actin crosslinking complexes

Due to existing literature [36, 37, 91] describing exposure of cryptic binding sites involved at either focal adhesion complexes (peripheral nodes) or crosslinking proteins (internal nodes), we extended our model to analyze the internal angles between filaments and binding proteins. The location of these internal angles is schematically depicted for both focal adhesion complexes and actin crosslinking complexes in **Figure 2-11**. We will delve into the mechanotransductive aspects of our model further in 0.

Additionally, we sought to improve the modularity and number of alterable parameters in our initial coarse-grained Monte Carlo model of the actin filament network in a cell undergoing uniaxial cyclic stretch. The overall nature of the intersection model is to simulate a quasi-

realistic cytoskeletal model under mechanical stimulation in a similar manner as our original model as outlined in **Code 2-1**. We test and validate our intersection model by performing similar analyses such as filament angle and stress analysis as per our published work [52].

We believe our "intersection model" (based upon the creation of internal nodes) is a more physically realistic model for an energy minimization model as it prevents certain internal nodes from being heavily loaded on one side with connections, which is energetically unfavorable for force balancing. Additionally, this new type of network is also more suggestive of the mesh-like actin gel-like networks seen in regions of the cytoskeleton such as the cell cortex (**Figure 2-12** and **Figure 2-13**), which is a rich area for signaling, as opposed to the thick bundled stress fibers that are more easily observed in microscopy. Additionally, this model is primed for further analysis at binding angles at the crosslinking complexes since the majority of the nodes are formed by an intersection of two filaments to create four potential binding sites for signaling molecules.

2.8.2 Methods

We modified our initial cellular network model to be more biologically realistic in capturing actual cytoskeletal morphology and repolymerization behavior. Our goal was to develop a new stochastic platform that could be used to both examine the distribution of forces and the reorganization of actin filament structures in response to mechanical stimulation as well as recapitulate crosslinker-driven mechanotransductive responses seen in experimental systems [37]; we will describe the mechanotransductive response in 0.

Aesthetically, we aim for our model to represent a top-down apical view of an epithelial cell, such as endothelial cells lining the vasculature. In an epithelial cell, focal adhesion

complexes located at the basal surface of the cell fix the cell to the substrate underneath via transmembrane integrin proteins. In the interior of the cell, various actin binding proteins such as alpha-actinin and filamin act as crosslinkers for actin filaments. One important region of the cell is the cortex, which lies just underneath the plasma membrane. The cortex is composed of actin filaments crosslinked in a loose, meshed gel-like arrangement [92] and is responsible for mechanical support and movement, as well as being highly rich in protein signaling [93]. Visualizations in literature of the cortical actin cytoskeleton show a well-connected mesh network of actin filaments providing structural support to the cell, as well as signaling capabilities, as seen in red in **Figure 2-12** [94] and green in **Figure 2-13** [95].

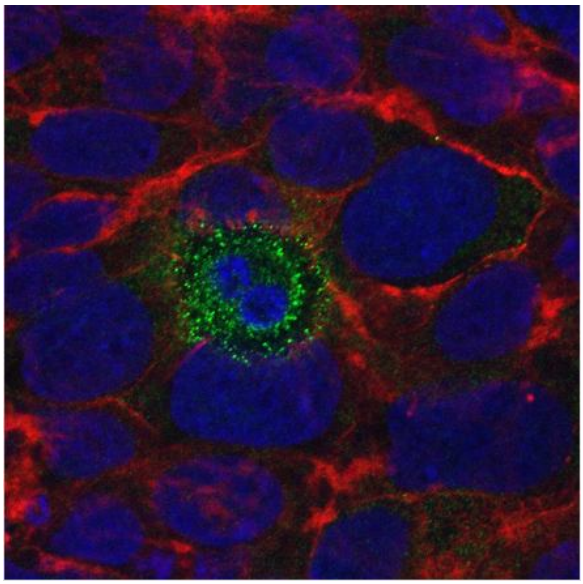

Figure 2-12: Apoptotic cells produce and transmit the bioactive lipid sphingosine-1-phosphate (S1P) during extrusion. In this confocal Z-series, an antagonist to the S1P receptor, S1P2, was used to block signaling. High levels of S1P accumulate in the dying, unextruded cells but not in surrounding cells. The nucleus is in blue**,** the actin-myosin ring at the basolateral surface is in red and S1P receptor is in green [94]. This image is licensed under a Creative Commons Attribution, Non-Commercial Share Alike License.

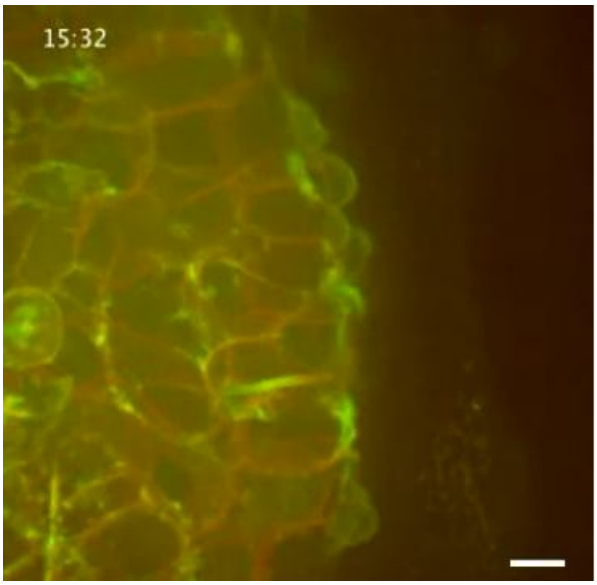

Figure 2-13: Bleb formation is enhanced in myo1b morphant prechordal plate progenitors. Animal view of the leading edge of the prechordal plate of an embryo injected with myo1b-MO. Plasma membrane (GPI-RFP) is red; actin cortex (Lifeact-GFP) is green. Scale bar = 10 μm. This frame is from 15:32 of Video S9 from [95]. This video is licensed under the Creative Commons Attribution 2.5 Generic license.

The cortical actin cytoskeleton is also visualized exquisitely in the 2nd place entry for the 2013 "Art of Science" Biophysical Society image contest[2] where a mouse embryonic fibroblast was fixed with methanol and stained with phalloidin to highlight actin filaments. The mesh like nature of the cortical cytoskeleton is visualized close up in the atomic force microscopy (AFM) figures of the cortical mesh from bovine endothelial cells by Pesen et al. [92].

Here, we seek to recreate the basic mechanical components of the cell in a coarse-grained two dimensional manner where the components of the cells are compressed from 3D into 2D

[2] http://biophysics.org/AwardsOpportunities/SocietyContests/ArtofScienceImageContest/2013ImageContest/tabid/4483/Default.aspx

space with a focus on the cell cortex. We conceptualize our model as a contained circular solution space with both external connections to the surrounding environment as well as internal intracellular connections. As before, we use a two-dimensional circular solution space of prescribed radius of 100 arbitrary units representing an adhered and spread cell whose bulk lies in an approximately circular region of diameter 30 μm, such as a fibroblast. So as not to restrict the angular orientation of the filaments, an off-lattice model was chosen. The cellular solution space is considered fixed to an underlying substrate by perimeter nodes representing focal adhesions at prescribed locations along the circumference.

In order to more closely model the meshed network configuration of the cell cortex, we alter the generation of the actin filament network in our model. Instead of specifying peripheral nodes and randomly generating internal nodes followed by interconnecting filaments as described previously in our original model **(2.3.1 Cytoskeletal model generation**), our new model generates peripheral nodes along the periphery first, then links peripheral nodes together to create initial connections. Subsequently, we generate internal nodes at intersections of these filaments to create multiple smaller filaments from one filament, thus generating a well-connected "intersection" meshed network when compared to our previous model **(Figure 2-14**). This novel network generation methodology allows us to more closely simulate the signaling-rich areas of the actin cortical cytoskeleton as opposed to the previous method that was more akin to simulating stress fibers enhanced by cell-substrate adhesions.

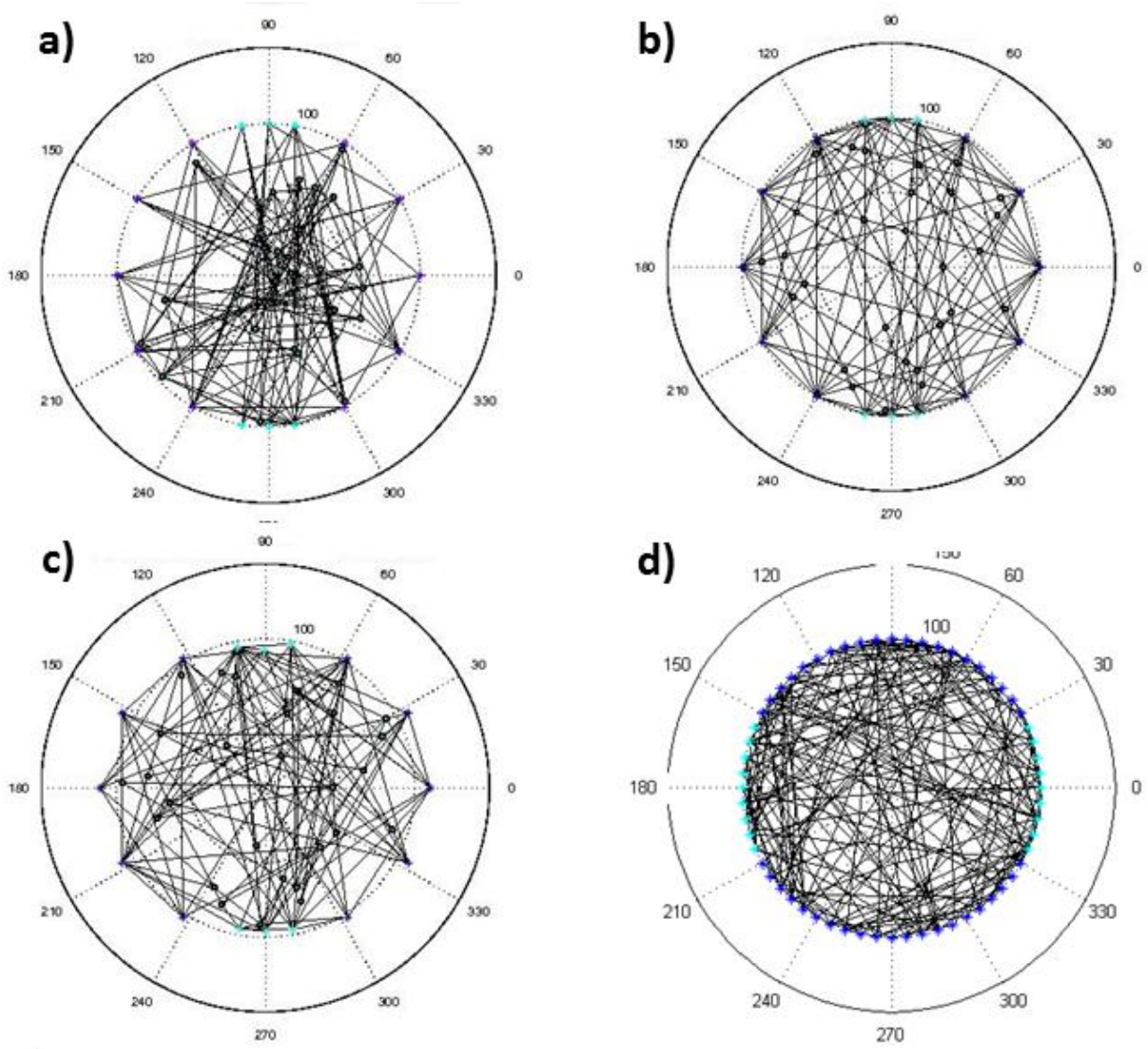

Figure 2-14: Comparison of original published and expanded "intersection" methods for cytoskeletal network model generation. **(a)** Original published model under 0% stretch with 30 internal nodes, 16 peripheral nodes, and 138 filaments. **(b)** Intersection model under 0% stretch with 30 internal nodes, 16 peripheral nodes, and 138 filaments. **(c)** Intersection model under 10% uniaxial horizontal stretch with 30 internal nodes, 16 peripheral nodes, and 138 filaments. **(d)** Intersection model under 0% stretch with 421 internal nodes, 60 peripheral nodes, and 960 filaments. These more dense parameters in **(d)** were used in the mechanotransduction simulations in 0.

For use concurrently with the intersection model, a new method for filament replacement at the end of each stretch cycle that more closely approximates conservation of mass of actin subunits was developed. Instead of simply replacing broken filaments with *n* new filaments, we

instead track the cumulative length of the filaments and prevent generation of new filaments once cumulative length of the new filaments has exceeded this original limit (**Code 2-2**). While the previous method for filament generation would on average maintain conservation of mass over many runs, this new methodology guarantees conservation on every run.

1. Set "sum of net strains" to max
2. While "sum of net strains" > threshold
   A. Find strains of all filaments connected to free nodes
   B. Adjust position of free nodes in direction of net strain from connected filaments
   C. Store "sum of net strains" for all free nodes
   D. Break if number of iterations > limit

Code 2-2: Pseudocode for a relaxation of the model network using a variant of Gauss-Seidel relaxation

This process of stretching, energy minimizing, and breaking and replacing filaments was considered a complete cycle (**Code 2-1**). A new cycle was initiated by returning the nodes back to their original positions with the filaments in an unscretched state. This continued for a prescribed number of cycles while the distribution of filaments, their orientations, and their stresses were determined. See **Movie M3** for an intersection network model undergoing 25 cycles of horizontal uniaxial 10% stretching with filament breakage and replacement.

To calculate the variability in our model, we calculated the standard error of the mean of our measurements of filament angle and stress. The means are taken at each cycle over n = 30 uniquely generated filament networks. The variability is shown in the relevant figures as error bars representing 95% confidence intervals.

2.8.3 Results

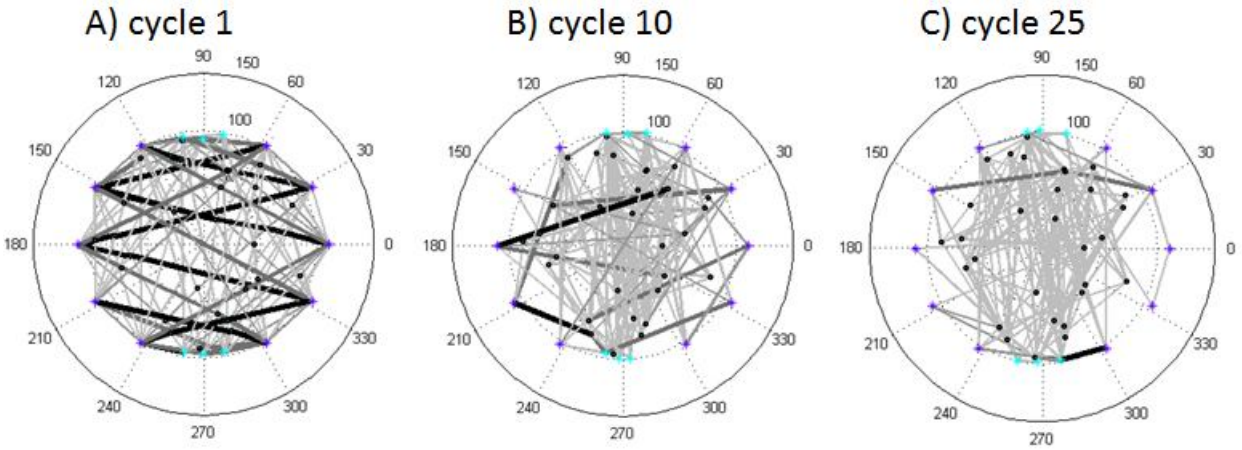

Figure 2-15: A filament network generated using the intersection method containing 138 filaments, 16 prescribed perimeter nodes, and 30 randomly placed internal nodes under 10% uniaxial horizontal stretch after (a) 1, (b) 10, and (c) 25 iterative cycles. Stretch was imposed in 1% increments on all peripheral nodes from -60° to 60° and 120° to 240° followed by Gauss-Seidel variant relaxation to achieve network nodal strain equilibrium. The depicted thickness/darkness of the filaments correspond to their relative stresses with the thickest/darkest being >75% of the maximum stress of the network and the thinnest/lightest being <25%. The length scale in this model is 100 arbitrary units, representing a cell whose bulk lies in an approximately circular region of diameter 30 μm, such as a fibroblast.

We studied the response of the actin filament model network by examining the network over time as mechanical stimulation was imposed on the system. **Figure 2-15** shows initial, intermediate, and final configurations of an actin filament network subjected to cyclic stretching corresponding to 1, 10 and 25 cycles of stretching.

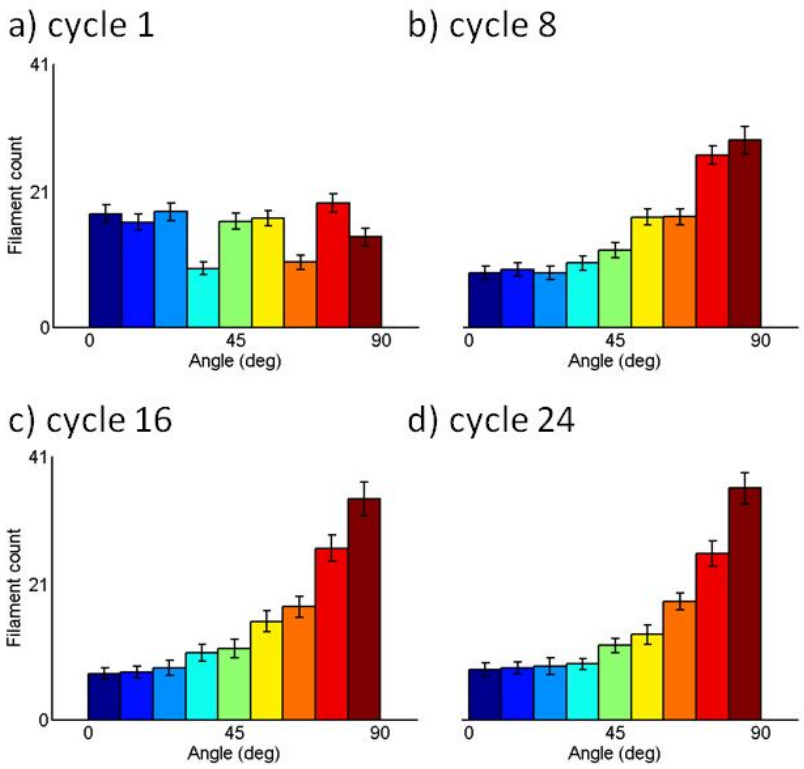

Figure 2-16 Histograms of equilibrium angular orientation of filaments in our intersection model after (a) 1, (b) 5, (c) 10, and (d) 25 cycles of 10% uniaxial horizontal stretch. Averaged over 30 uniquely generated filament networks, each of which consisted of 138 filaments distributed among 16 prescribed perimeter nodes and 30 randomly placed interior nodes. Each filament connects two nodes. Error bars denote 95% confidence interval.

In order to quantify filament orientation, we create histograms of all filament angles in the network, averaged over 30 uniquely generated networks. Compared to our previous model given the same number of nodes and filaments, the intersection model gives a much more pronounced perpendicular alignment to the direction of force stimulation as we increase the number of uniaxial stretch cycles (**Figure 2-4** versus **Figure 2-16**). We also analyze the stress states of the filaments to determine whether the same putative mechanism of energy minimization is driving the filament alignment. We see that energy is minimized to a steady state earlier in the number of stretch cycles than the original model with the same parameters, both in terms of individual filament stresses (**Figure 2-7** versus **Figure 2-17**) and overall

distribution of stresses (**Figure 2-8** versus **Figure 2-18**). Thus, given these results presented, we are confident our intersection model can be used for further investigations wherever our original published model is appropriate.

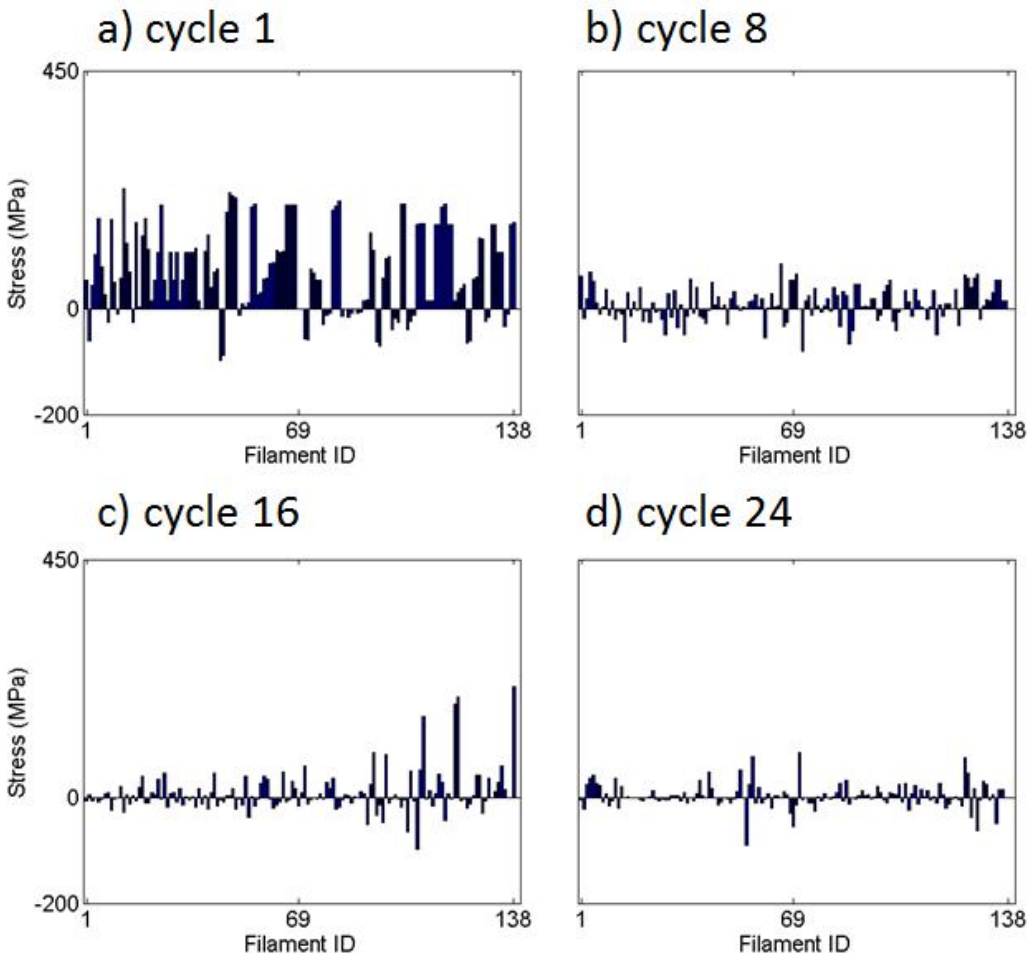

Figure 2-17 : Intersection model's individual filament stress values in nodal equilibrium after a network was stretched uniaxially by 10% for (a) 1, (b) 8, C) 16 and (c) 24 cycles. Positive stress (i.e., tension) denotes an increase in the length of the filament relative to the length before the stretching cycle and negative stress (i.e., compression) denotes a decrease in length. At the end of each cycle, filament breakage probability was defined to be the absolute value of the strain normalized to the largest strain value. Network parameters were 138 filaments, 16 perimeter nodes, and 30 internal nodes

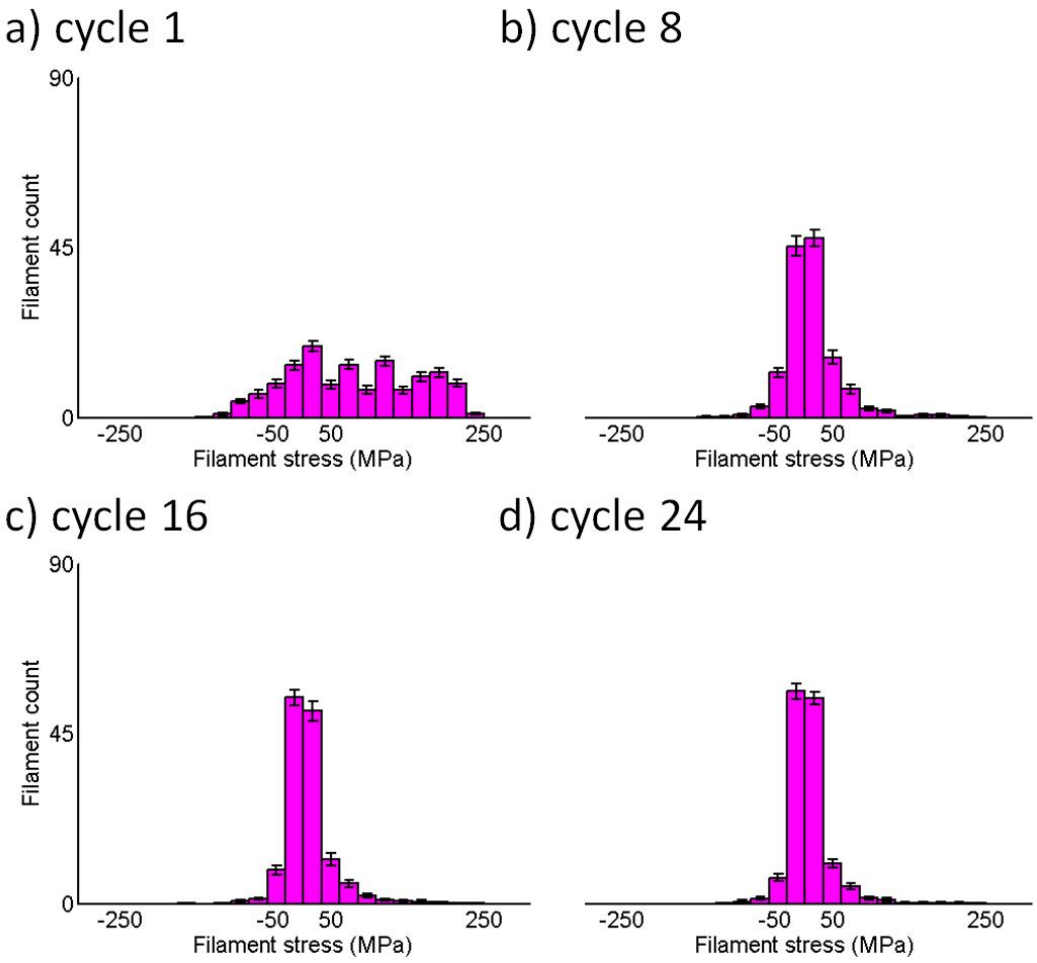

Figure 2-18 Histogram of filament stresses in nodal equilibrium after (a) 1, (b) 6, (c) 12, (d) 24 iterative cycles of 10% uniaxial stretch. Positive stress (i.e., tension) denotes an increase in the length of the filament relative to that before each stretching cycle and negative stress (i.e., compression) denotes a decrease in length. Error bars denote 95% confidence interval. Results averaged over 30 uniquely generated filament networks of 138 filaments, 16 perimeter nodes, and 30 internal nodes.

Chapter 3 : Interfacing cytoskeletal morphology under stretching with mechanotransduction[3]

3.1 Abstract

Mechanotransduction is a critical mechanism for linking cellular to tissue-level function, yet how cells sense and respond to external mechanical signals is still highly debated. While biochemical signaling and cell mechanics are well studied, there is a poor understanding of direct molecular links between physical forces and biological activity. Mechanotransduction can be divided into three stages: mechanotransmission (the rapid transmission of forces across mechanotransductive elements), mechanosensing (force-induced alterations of protein conformation and subsequent function), and mechanoresponse (cellular signaling output of the force-sensitive networks). One emerging viewpoint is that the same structural cellular components are involved in all three stages, yet there has been no proposed model or mechanism that unifies these functions. Here, we seek to bridge the gap between emerging molecular models of mechanotransductive proteins and a systems-level understanding of mechanotransduction through a multi-scale coarse-grained model of discrete networked actin filaments and associated binding proteins that captures the three stages of mechanotransduction in a single approach. First, we incorporate mechanotransmission through simulating stretch across a discrete network of actin filaments and binding proteins. These forces cause conformation changes at the crosslinking molecular complexes and we assess three potential geometric mechanosensing mechanisms for activation. Lastly, we simulate the release of signaling factors from mechanosensitive crosslinking proteins using time-dependent mechanoresponse model. We use experimental results of the mechanically-governed release of

[3] Adapted from manuscript in preparation. John Kang, Kathleen M. Puskar, Philip R. LeDuc, Russell S. Schwartz. *Exploring Structural Influences on Cell Mechanotransduction through Multiscale Modeling.*

Rho GTPase FilGAP in an *ex vivo* actin-filamin A network to benchmark our approach. Our results suggest that the mechanosensing for filamin-FilGAP interaction follows an angle bandpass mechanism where FilGAP is more favorably released from flexible binding junctions when binding angles fall outside of a specific range. Additionally, our results imply that a more random actin network environment such as that found inside a cell is more beneficial for regulating mechanotransduction through the robustness of the response. Our results have implications in a range of fields including mechanotransduction, robust system behavior, and protein-protein interactions.

3.2 Introduction

Mechanotransduction is a rapidly expanding area of study with important medical applications ranging from wound healing to anti-cancer therapeutics [2, 3, 96]. Recent developments in the field include modulating extracellular matrix forces to control everything from stem cell fate [25, 97, 98] to cancer metastasis [99] to neovascularization [100]. While the macroscale understanding of the extracellular effects of mechanical stimulus on cell physiology continues to grow, much remains unknown about cellular mechanotransduction response. We know that mechanical forces are transduced from outside the cell via transmembrane integrins to the cytoskeleton via focal adhesion complexes [35, 101]. Actin cytoskeleton dynamics are in turn heavily regulated by the signaling pathway of the Rho family of GTPases, particularly RhoA (Rho) and Rac1 (Rac), which themselves are both influenced by and influencers of mechanical forces [102]. A possible key mechanistic step was recently demonstrated by Ehrlicher et al. [37], who found that stretching a reconstituted filamin A-crosslinked actin filament network could influence release rate of fluorescently-labeled FilGAP, an inhibitor of Rac that binds to filamin A [103]. This observation provides a potential direct molecular link

from mechanical stimulation of the cytoskeleton back to regulation of cytoskeletal assembly by Rho/Rac.

At the cellular level, mechanotransduction involves a highly integrated set of mechanistic interactions including mechanotransmission, mechanosensing, and mechanoresponse [34]. These interactions can be related to cryptic binding sites within cells [104], rupture forces between actin filaments and filamin A crosslinkers [105], the mechanical instability of different filamin A domains under the same loading rate [106], the stretching of talin rods to expose cryptic sites for vinculin binding [36], and catch bonds [34, 107, 108]. One recent area of study that is linking forces to biochemistry involves filamin. Filamin is a natural homodimer and studies have shown that the carboxy-terminal rod 2 domain responsible for dimerization has a compacted structure [109] yet can undergo conformational changes at 10pN or less [106] whereas filamin as a whole unfolds at much higher forces [105], strongly implicating rod 2 as having mechanosensitive function. What makes the rod 2 domain especially intriguing is both its promiscuity—binding over 90 partners including key mechanotransductive proteins such as FilGAP [103, 110], Rho [111], Rac [111], Cdc42 [111], ROCK [112], ICAM-1 [113], and integrin [114, 115]—while also directly bordering the self-association homodimerization hinge domain which flexes during mechanical stimulation of crosslinked actin network. The exact atomic structure for the FLNa rod 2-FilGAP interaction is unknown [109] and high resolution structures of full-length filamin characterizing relevant binding angles are lacking due its large, flexible nature and complex scaffolding [116, 117].

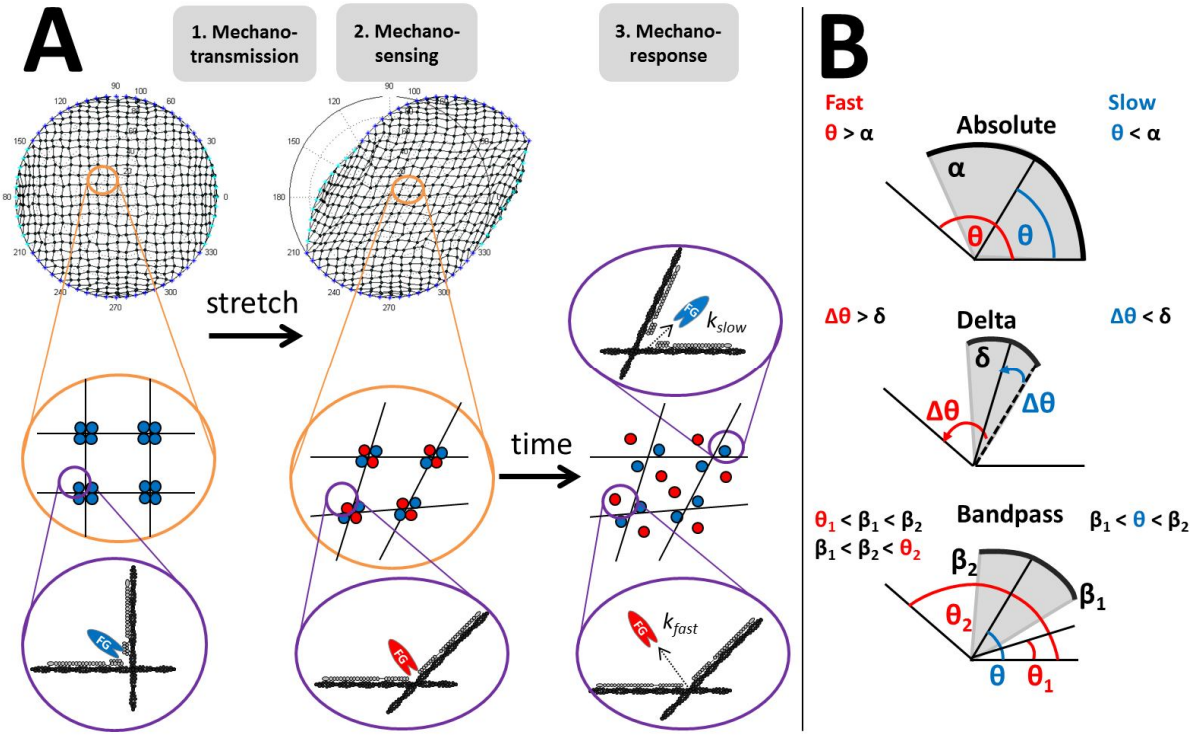

Figure 3-1: Structurally governed multiscale cellular mechanotransduction of force transmission, sensing and response. **(A)** Schematic of the integration of the three phases of mechanotransduction: mechanotransmission, mechanosensing, and mechanoresponse. **(A, Top)** We generate a connected network of square-grid actin filaments crosslinked by hinged filamin A (FLNa) homodimers at filament intersections. This network is initially stretched by holding a subset of the peripheral nodes stationary and displacing a subset of internal nodes while balancing forces on the internal nodes (mechanotransmission). The transmission of force across the network changes the intersection angles between filaments at crosslinks, altering FLNa conformations and affecting binding site affinities (mechanosensing). (**Orange insets**) Here, as an example, we represent an absolute threshold of 90° at the intersection to examine whether a filamin-bound signaling molecule is released at slow rate k_{slow} (**blue dots**) or fast rate k_{fast} (**red dots**). In this example using an absolute angle threshold of 90°, when the specific crosslinking angle is below or above 90°, the bound signaling molecule is marked to be released at rate k_{slow} or k_{fast}, respectively. (**Purple insets**) Lastly, we simulate the time-dependent release of the signaling factors such as FilGAP at each crosslink depending on whether it is categorized as k_{slow} or k_{fast} release (mechanoresponse). Actin filaments in dark grey, FLNa in light grey. **(B)** Representation of the three different threshold models (absolute, delta and bandpass) to examine whether a signaling molecule is being released at a slow rate k_{slow} or fast rate k_{fast}. These thresholds represent simplified models of protein deformation whereby if an angle has not passed a threshold, the filamin A crosslink is considered to be in a conformational state of slowly releasing FilGAP at a rate k_{slow}. Once an internal angle has passed a threshold, the crosslink is considered to be in a conformational state of quickly releasing FilGAP at a rate k_{fast}. For absolute thresholding, fast release is activated if the angle exceeds a defined maximum value α. For delta thresholding, fast release is activated if the angle changes relative to its starting value by at least some threshold parameter value δ. For bandpass thresholding, fast release activates if the angle falls outside a specific range [β1, β2].

Here, we focus on the ability to examine filamin mechanotransductive response by building a multiscale structural model to examine integrated mechanotransmission (the rapid transmission of forces across structural elements), mechanosensing (force-induced protein conformation and function changes), and mechanoresponse (signaling through the force-sensitive biochemical networks) [34] **(Figure 3-1A)**. First, we incorporate mechanotransmission through simulating stretch across a discrete network of actin filaments and associated binding proteins. These forces cause conformation changes at the crosslinking complexes and we hypothesize three geometric mechanosensing mechanisms for protein activation **(Figure 3-2)**. Lastly, we simulate the release of signaling factors from mechanosensitive crosslinkers using time-dependent mechanoresponse mixture model that we parameterize with experimental data [37]. To our knowledge, a unified model which incorporates all three aspects of mechanotransduction has not been developed before.

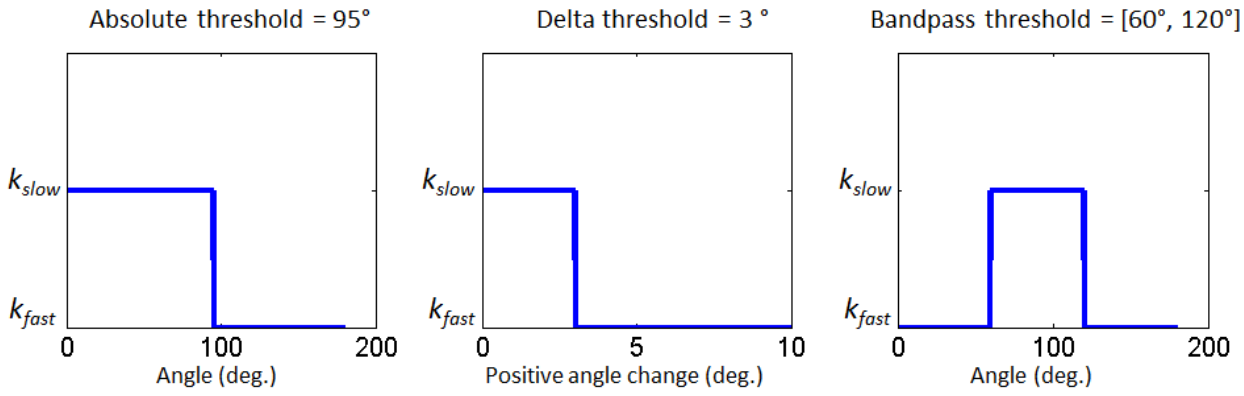

Figure 3-2: Examples of threshold vs. angle response graphs for three thresholding models (absolute, delta, and bandpass) for determining rate of release of a molecule at a crosslinking angle. (Left) absolute angle thresholding with threshold of 95 degrees, **(Middle)** delta angle thresholding with threshold of 3 degrees, **(Right)** bandpass angle thresholding with threshold band of [60, 120] degrees. For further details of the thresholding models, see **Figure 3-1B.**

3.3 Methods and Results

Our model consists of force-driven architectural model of discrete actin filaments (mechanotransmission) coupled to a geometry-dependent activation model for cytoskeletal-associated signaling molecules (mechanosensing), which ultimately will alter downstream signaling (mechanoresponse). We specifically favor a simple, minimal model that abstracts away most cytoskeletal binding proteins and other elements of cellular architecture in order to test whether the specific components modeled alone are sufficient to account for observed responses. This modular model allows us to explore a range of possible mechanisms and parameters for linking changes in actin network structure to molecular release, specifically in the critical area of mechanosensing. We benchmark this model using data from published literature describing analogous experimental work using the molecule FilGAP [37] and use the results to test three possible coupling mechanisms by the degree to which they can be reconciled with the experimental data. The resulting fits allow us to identify a specific mechanosensing model of bandpass angle thresholding (**Figure 3-1B, Figure 3-2)** that best explains the FilGAP data, suggesting a detailed quantitative mechanism by which the release mechanism suggested by Ehrlicher et al. [37] can give rise to systems-level mechanotransductive behavior and providing a basis for quantitative modeling of mechanotransduction in conjunction with biochemical networks.

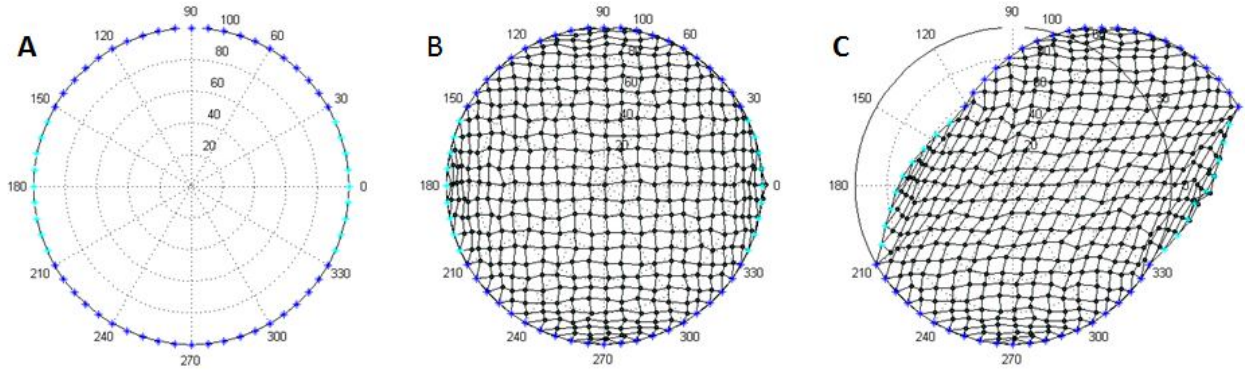

Figure 3-3: Square-grid actin network generation and stretching. (A) Fixed perimeter nodes (blue) and mobile perimeter nodes (cyan) are generated along the periphery. **(B)** Opposing perimeter nodes are connected to form filaments and the intersecting crosslinks are represented as black dots with 3% noise. Each intersection represents a molecular complex containing four potential binding sites at four angles. **(C)** The apical fixed perimeter nodes have been displaced by 28% to the right (defined as the ratio of the rightward displacement over the height of the cell) causing strains on the mobile nodes (cyan and black). The stretched network reaches equilibrium after the mobile nodes iteratively relax their strains such that the sum of the strains on each node is minimized.

We first represent an actin network as a discrete set of filaments in a two-dimensional circular solution space of prescribed radius. This network is considered fixed to an underlying substrate at pre-determined perimeter nodes, representative of focal adhesions fixing a cell on a substrate **(Figure 3-3A)**. Filaments representing actin filaments are formed by crosslinking opposite focal adhesions on the periphery; these crosslinks can either be determinate in a square-grid network (**Figure 3-3B**) or random (**Figure 3-9A**). Filaments are formed by crosslinking opposite focal adhesions on the periphery. Intersections formed by crosslinked filaments form nodes which represent molecular complexes of associated molecules (e.g., filamin A and FilGAP) with actin filaments at each of the four angles created by those intersecting filaments. This work builds on prior mechanical models of actin networks developed by our group and discussed in Chapter 2 [118] **(Figure 2-1)**. The actin network simulation parameters used are

421 internal nodes, 60 peripheral nodes, and 960 filaments based on optimization of response; altering these parameters did not qualitatively affect our results.

We first implement a square geometric network to model the *in vitro* system used in previous experimental studies and then extend to a more realistic randomly-connected network intended to better model a typical actin cytoskeleton *in vivo*. For either variant, we can create a well-connected network of nodes and filaments that models the loose gel-like actin filament-filamin crosslinked networks found in specific areas of the cell, such as the cortex [116]. Mechanical stretching is simulated by displacing the perimeter nodes, which due to their filament connections, creates imbalanced forces on free nodes that are iteratively relaxed until force equilibrium is achieved (**Figure 3-3C**) [118]. The internal nodes act as force-movable hinges formed by intersecting filaments. These hinges at internal nodes model locations of the actin binding protein filamin A, which is known to form relatively orthogonal angles in both truncated constructs [119] and natively while crosslinking actin filaments [109, 117].

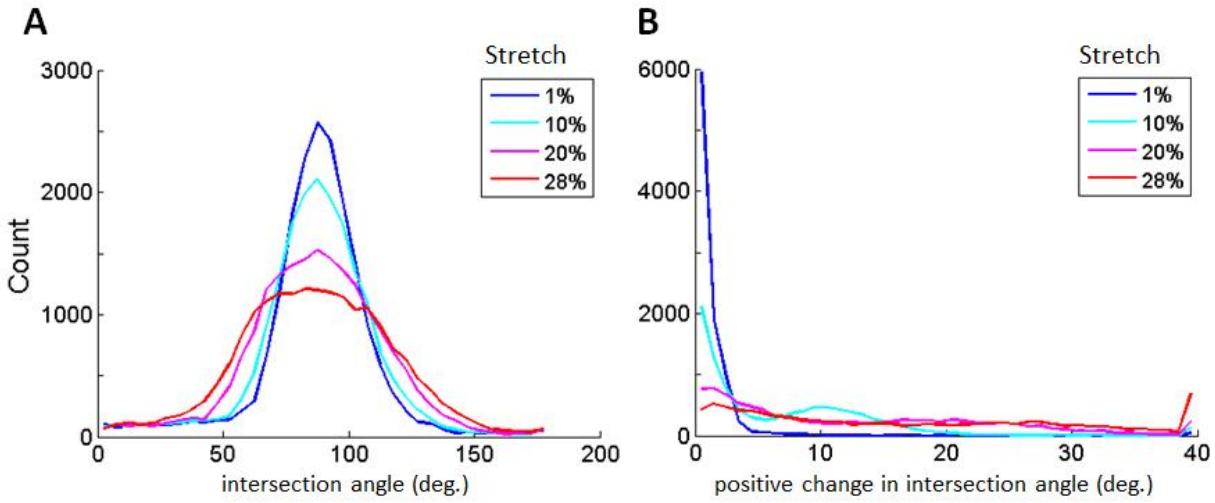

Figure 3-4: Distribution of (A) intersection crosslinking angles and (B) positive increases in intersection angles (i.e., delta angles) in a square-grid actin network model. Results averaged over 10 runs. Model parameters are 421 internal nodes, 60 peripheral nodes, and 960 filaments (see **Figure 3-5**).

We first examined the direct effects of applied stretch on the distribution of intersection angles in the simulated actin networks. As stretch is applied, the intersecting angle distribution transitions from a more peaked to a flatter distribution while remaining centered at 90° (**Figure 3-4A)**. The difference in the stretched angle relative to the non-stretched angle ("delta angle") observed a shift in distribution under the same stretch amount (**Figure 3-4B)**. At 1% stretch, the delta angles are small with almost no angle changes greater than 5 degrees, but at higher levels of stretch, the observed delta angle distribution is almost uniform. These histograms reflect similar results to simulations performed by Ehrlicher et al. to model their experimental system even though their simulations had different overall morphologies and boundary conditions [37].

3.3.2 Mechanosensing: linking network architectural changes to filamin deformation

Our model implements mechanosensing by linking structural changes in the actin network to biochemistry through molecular deformation of actin bound molecules that then release complementary molecules. A system that has been implicated in this approach is the FilGAP release from the actin crosslinking protein filamin A [37].

We assume each internal node intersection holds a maximum of four FilGAP molecules—one at each angle—and that the rate of release of FilGAP is a function of the angular deformation of the binding site (**Figure 3-1A**). Based on the intersection angles in the network, we assign either a slow or fast rate of release of the embedded molecule from the binding site. To connect force-induced cell architecture changes with protein conformation changes, we postulate three geometric mechanosensing mechanisms at individual molecular complex crosslinks based on known geometric molecular concepts [37, 120]: absolute angle thresholds, delta angle thresholds, and bandpass angle thresholds **(Figure 3-1B**, **Figure 3-2)**. These

thresholds represent simplified models of protein deformation whereby if an angle has not passed a threshold, the filamin A crosslink is considered to be in a conformational state of slowly releasing FilGAP at a rate k_{slow}. Once an internal angle has passed a threshold, the crosslink is considered to be in a conformational state of quickly releasing FilGAP at a rate k_{fast}. We initialize the model by assuming FilGAP is present at each binding site below threshold. For an absolute threshold of α, an angle θ is considered to be below or above threshold when $\theta < \alpha$ or $\theta > \alpha$, respectively. For a delta threshold of δ, a positive change in angle $\Delta\theta$ is considered to be below or above threshold when $\Delta\theta < \delta$ or $\Delta\theta > \delta$, respectively. For a bandpass threshold of $[\beta_1, \beta_2]$, an angle θ is considered to be below threshold when $\beta_1 < \theta < \beta_2$ and above threshold when $\theta < \beta_1$ or $\theta > \beta_2$. Once an angle is above threshold, we assume that it is constitutively activated to release at rate k_{fast}. Using these thresholding models, we can identify and simulate subsets of fast-releasing and slow-releasing binding sites over time as mechanical stimulus is applied to the network.

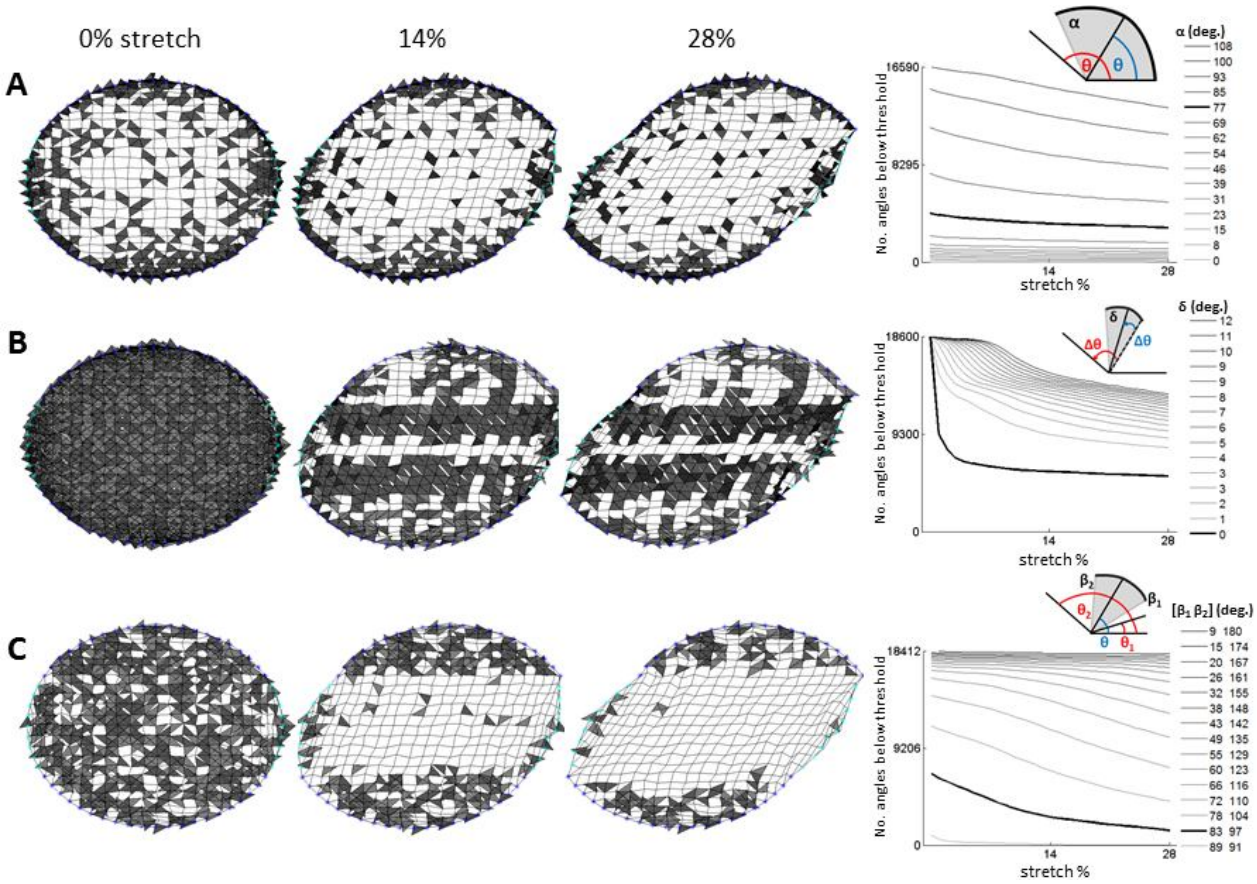

Figure 3-5: The interior angles at the intersections that exceed fast-release thresholds vary with the type and degree of angle thresholding. We examine three different mechanosensing models (A: absolute, B: delta, C: bandpass) that are based on FLNa homodimer angle conformation. As the network undergoes 0-28% stretch, shaded regions represent angles below threshold (i.e., to be released at slow rate) with darker regions denoting smaller angles. Clear regions represent angles above threshold (i.e., to be released at fast rate). We show representative square-grid actin filament networks from 0-28% stretch under (A) a 77° absolute threshold; (B) a 0° delta angle threshold (i.e., any angle increase passes the threshold); and (C) a 90±7°range bandpass angle threshold. These specific threshold values are illustrated as they were optimized to experimental FilGAP release data (**Figure 3-7** and **Figure 3-8**). The rightmost graphs are corresponding numbers of angles under threshold at increasing amounts of stretch for a range of threshold values (averaged over 10 runs). The bolded line represents the best-fit threshold between the simulated cell stretch and experimental data. The actin network simulation parameters used are 421 internal nodes, 60 peripheral nodes, and 960 filaments based on optimization of response.

We next examined how changes in network morphology under stretch would manifest in distributions of binding sites above or below the fast-release threshold for absolute, delta, and bandpass thresholding. **Figure 3-5** demonstrates the results of absolute (**Figure 3-5A**), delta

(**Figure 3-5B**), and bandpass (**Figure 3-5C**) angle thresholding models being applied to a square-grid actin network under 0-28% stretch in 1% steps (see **Appendix Figure 6-2, Figure 6-3,** and **Figure 6-4** for animation frames). These threshold models allow visualization and calculation of specifically which angles are considered to be below threshold (i.e., to be released at rate k_{slow}) versus which angles are considered to be above threshold (i.e., to be released at rate k_{fast}). For the whole cell views of the actin network model, the shaded angles indicate that the internal angle is below threshold, with lighter shades denoting larger angles. If an angle is not shaded, it denotes that the internal angle is above threshold. The numbers of angles below the fast release threshold (i.e., angles being released at rate k_{slow}) at different threshold values are plotted in the right panel for their respective threshold models.

Our model provides for a sensitive mechanical system by which a cell could finely modulate biochemical signals in response to the same or varying mechanical inputs. Small changes in stretching force can yield a variety of angle distributions that provides the information necessary for our model to modulate its response, allowing for fine control of individual mechanical switches (**Figure 3-4**). Furthermore, as **Figure 3-5** reveals, small changes in model parameters can substantially shift the ratio of fast to slow release molecules at the magnitude of stretch, providing a mechanism by which a cell can in principle support multiple mechanically-sensitive switches with distinct response patterns.

3.3.3 Mechanoresponse: linking filamin deformation model to molecular release

We next apply our mechanosensing filamin deformation model to a mechanoresponse model. Each variant of the filamin deformation angle model (i.e., absolute, delta, or bandpass threshold) has a set of parameters that first is trained and validated on experimental data. The experimental data consists of fluorescence decay measurements showing fluorescent readouts of the concentrations of FilGAP as functions of time at stretch values of 0% and 28% [37]. To couple our models of angle deformation with biochemical signaling, we developed and integrated a time-dependent release mixture model of two exponential decays **(Eqn. 1).** For a given actin network under a stretch, the two decays represent the network's time-dependent release of molecules such as FilGAP at both angles favorable for slow release (angles below threshold) and angles favorable for fast release (angles above threshold). The overall signal N is defined as the number of signaling molecules remaining in a specific network configuration. N is modeled as a sum of these two decays:

$$N = A\exp(-t/k_{slow}) + B\exp(-t/k_{fast}) + C \quad (1)$$

The first exponential term describes slow decay: A represents the number of angles below threshold and k_{slow} describes the rate of slow release. The second exponential describes fast decay: B describes the number of angles above threshold and k_{fast} describes the rate of fast release. C is the noise, including background fluorescence. A and B are dependent on the number of angles below and above the fast release threshold, respectively, and are determined by simulation of stretch on the actin network model.

Curve fitting to experimental data was performed using Levenberg-Marquardt nonlinear regression to determine k_{slow} = 4.0669s, k_{fast} = 0.1876s, and C = 0.0006 (**Table 1**). Our chosen

mixture model improved fitting over existing models in literature without introducing model complexity (i.e., the number of fitted parameters) [37]. By assuming a common set of parameters (k_{slow}, k_{fast} and C) is intrinsic for both unstretched and stretched networks, we can simulate overall network time-dependent rate of release of a molecule such a FilGAP by deriving A and B from stretch simulations of the overall morphology of the network. This approach allows us to expand the model to novel configurations such as using a randomized filament network while maintaining the same baseline parameters for k_{slow}, k_{fast}, and C to better understand how the mechanosensing thresholding approaches alter mechanotransduction response under different network geometries.

Table 1: Fitting parameters to three alternative models tested and our chosen model ("Mix model, dual fit"). Curve fitting was performed to determine the rate constants k_{slow}, k_{fast}, and C for slow release rate, fast release rate, and background noise, respectively. Here, we compare the parameters determined using alternative models to our final choice of a dual fit mixture model, which uses one set of parameters to fit both unstretched and stretched data. To also compare our parameters with published results, we corrected for diffusion by subtracting 0.5e^(-t/0.15s) from the normalized raw data per Ehrlicher et al. to generate diffusion-removed normalized data [37]. Curve fitting was performed via the "nlinfit" MATLAB function using Levenberg-Marquardt nonlinear least squares algorithm for non-linear regression. "Ehrlicher et al., *Nature* 2011" uses the single exponential fit that was performed in the eponymous paper (4 parameters fit for 4 degrees of freedom, d.f.) [37]. "Mix model fixed k" uses a two-exponential model where we assume the constants used by Ehrlicher et al. describe the characteristic release rates for FilGAP (2 d.f.). "Mix model free k" uses a two-exponential fit where all the parameters are freely floating such that a different set of parameters could be fit for unstretched vs. stretched data (6 d.f.). "Mix model dual fit" was the model used in our analysis and also uses a two-exponential fit where the parameters must be constant between both unstretched and stretched data (3 d.f.).

Model	Objective function	d.f.	Raw: 0% stretch	Raw: 28% stretch	Corrected: 0% stretch	Corrected: 28% stretch
Ehrlicher et al. *Nature* 2011	$exp_0(t) = A_0 e^{-\frac{t}{k_{slow}}} + C_0$ $exp_{28}(t) = A_{28} e^{-t/k_{fast}} + C_{28}$	4	k_{slow} = 2.301 C_0 = 0.023	k_{fast} = 0.252 C_{28} = 0.012	k_{slow} = 3.643 C_0 = 0.015	k_{fast} = 0.567 C_{28} = 0.020
Mix model fixed k	$exp_0(t) = Ae^{-t/3.6} + Be^{-t/0.6} + C_0$ $exp_{28}(t) = Ae^{-t/3.6} + Be^{-t/0.6} + C_{28}$	2	C_0 = 0.014	C_{28} = 0.007	C_0 = 0.018	C_{28} = 0.003
Mix model free k	$exp_0(t) = Ae^{-t/k_{slow,0}} + Be^{-t/k_{fast,0}} + C_0$ $exp_{28}(t) = Ae^{-t/k_{slow,28}} + Be^{-t/k_{fast,28}} + C_{28}$	6	$k_{slow,0}$ = 3.520 $k_{fast,0}$ = 0.185 C_0 = -0.002	$k_{slow,28}$ = 3.630 $k_{fast,28}$ = 0.144 C_{28} = 0.007	$k_{slow,0}$ = 4.451 $k_{fast,0}$ = 1.103 C_0 = 0.002	$k_{slow,28}$ = 4.327 $k_{fast,28}$ = 0.278 C_{28} = -0.008
Mix model dual fit	$\left(exp_0(t) - A_0 e^{-\frac{t}{k_{slow}}} - B_0 e^{-\frac{t}{k_{fast}}} - C\right)^2 + \left(exp_{28}(t) - A_{28} e^{-\frac{t}{k_{slow}}} - B_{28} e^{-\frac{t}{k_{fast}}} - C\right)^2 = 0$	3	**Simultaneous fit with 0% and 28% stretched data:** k_{slow} = 4.067, k_{fast} = 0.188 C = 6.120e-04		**Simultaneous fit with corrected 0% and 28% stretched data:** k_{slow} = 3.980, k_{fast} =0.291 C = -5.441e-004	

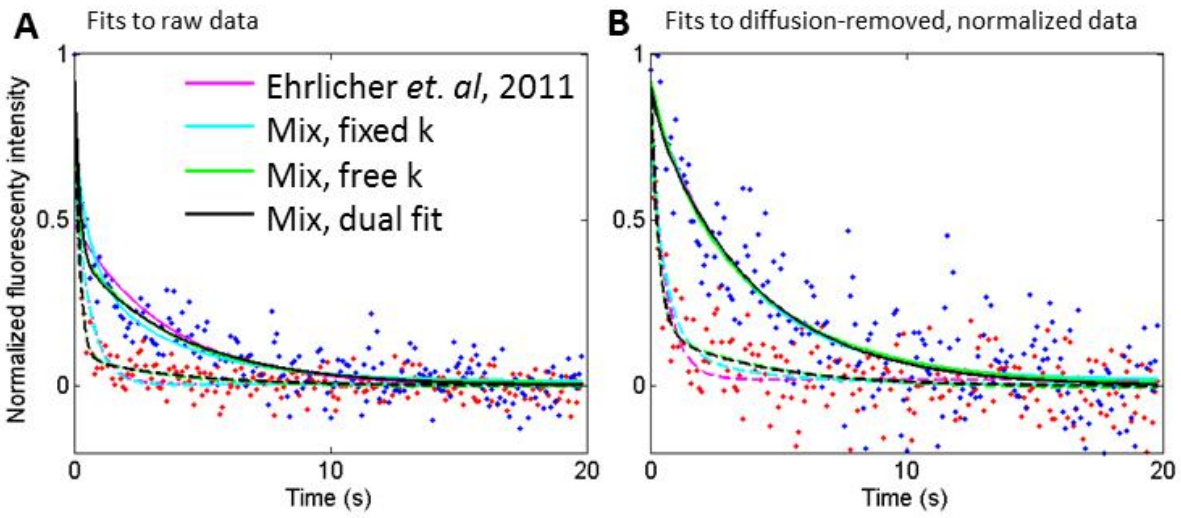

C **Raw data**

0% stretch	RMSE	r^2
Ehrlicher	0.0725	0.73
Fixed K	0.0636	0.793
Free K	0.06	0.815
Dual Fit	0.0602	0.815

28% stretch	RMSE	r^2
Ehrlicher	0.0517	0.717
Fixed K	0.0517	0.717
Free K	0.0385	0.843
Dual Fit	0.0387	0.843

D **Diffusion-removed, normalized data**

0% stretch	RMSE	r^2
Ehrlicher	0.124	0.74
Fixed K	0.124	0.74
Free K	0.124	0.742
Dual Fit	0.124	0.74

28% stretch	RMSE	r^2
Ehrlicher	0.0891	0.563
Fixed K	0.0869	0.585
Free K	0.0836	0.616
Dual Fit	0.0837	0.615

Figure 3-6: Fits of three alternative models and our chosen model ("Mixture model, dual fit"). Plots demonstrating model fits to **(A)** raw and **(B)** diffusion-removed data. Unstretched data in blue, stretched data in red. Solid lines denote fits to unstretched data, dashed lines to stretched data. See **Table 1** for the fitted parameters for each model. Tables demonstrating root mean squared error (RMSE) and squared correlation coefficients (r2) for the models' best fits to **(C)** raw data and **(D)** diffusion-removed data.

We first benchmarked our integrated model to experimental FLNa-FilGAP release data for unstretched and stretched networks to identify the release model best able to fit the experimental data [37] (**Figure 3-7**).

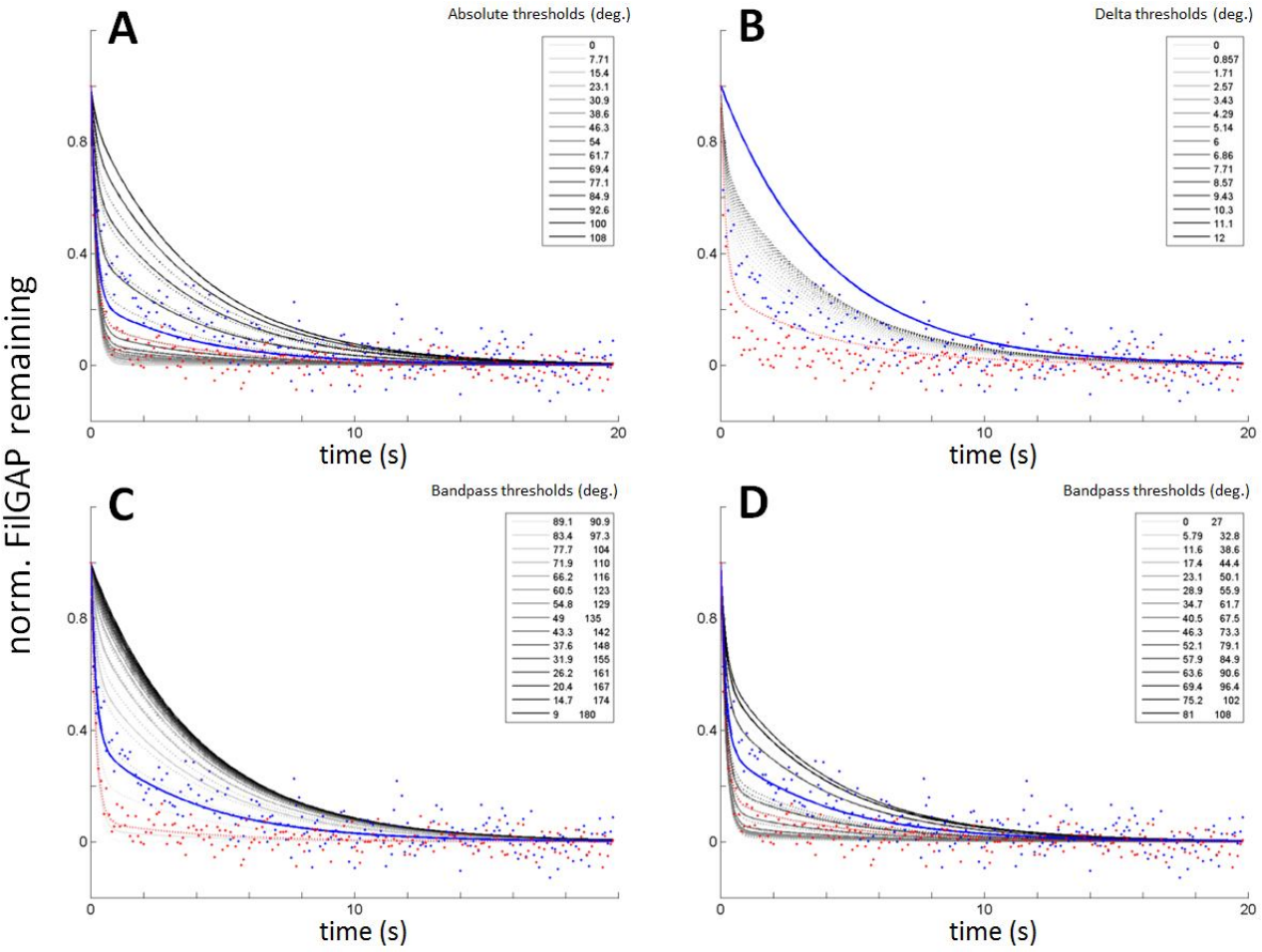

Figure 3-7: Finding the optimal thresholds for the three thresholding mechanosensing models. We search a range of 15 threshold values for each model. Experimental data show as red (28% stretched network) and blue (unstretched network). Best fit lines are colored in red (for stretched) and blue (for unstretched). **(A)** Absolute angle thresholds from 0° to 108°in 7.7° steps. Best fit at 77.1° with RMSE = 0.122. **(B)** Delta angle thresholds from 0° to 12°in 1° steps. Best fit at 0° with RMSE = 0.258. **(C)** Bandpass angle thresholds with constant 90° center widened from [89.1°, 90.9°] to [9°, 180°] bands in 5.7° steps. Best fit at [83.4°, 97.3°] with RMSE = 0.100. (D) Bandpass angle thresholds with constant width 27° width shifted from [0°, 27°] to [81°, 108°] by 5.8° steps. Best fit at [57.9°, 84.9°] with RMSE=0.107.

When examining the three mechanosensing thresholding models, the best model overall was the bandpass model with a least root mean square error (RMSE) of 0.100 and a 90±7 degree band, which is reasonably close to the natural orthogonal angle of filamin A-crosslinked actin filaments [110] **(Figure 3-8C)**. The best absolute threshold model had an RMSE of 0.123 and a

cutoff of 77 degrees (**Figure 3-8A)**. The best delta threshold model had an RMSE of 0.262 and a cutoff of 0 degrees **(Figure 3-8B)**.

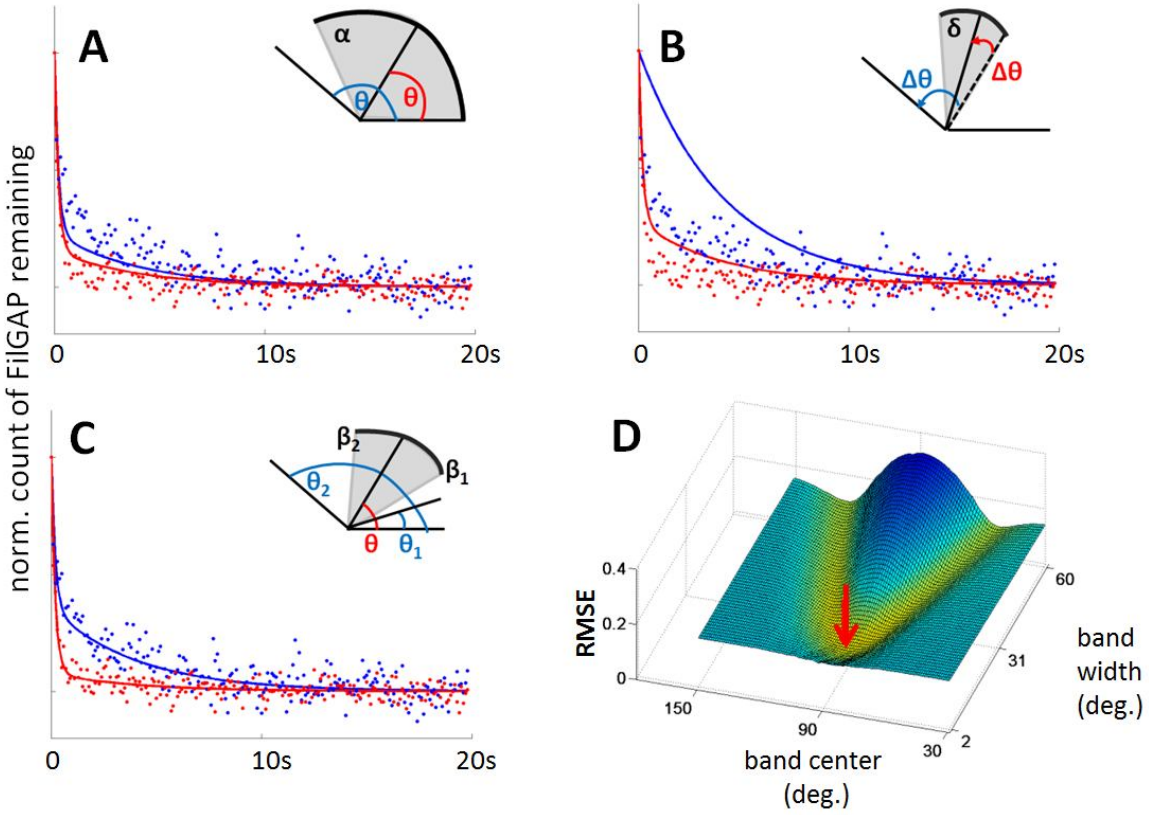

Figure 3-8: Examining three threshold models for a square-grid network corresponding to experimental results. We model the initial stages of mechanoresponse by simulating time-dependent release of FLNa-bound FilGAP signaling factor in a square-grid actin network for **(A)** absolute, **(B)** delta, **(C)** bandpass thresholds. We show here the best fits from a threshold parameter searches (**Figure 3-7**). We also plot fluorescent intensity data of tagged FilGAP release from unstretched and stretched in vitro actin networks in blue and red, respectively [37]. For each thresholding method, we plot the best fits found via our mixture model for unstretched and stretched simulated actin networks in blue and red, respectively. **(A)** For absolute thresholding, we tested a range of thresholds from 0-108° and the 77° threshold fit best with a 0-10s RMSE of 0.145 and an overall 0-20s RMSE of 0.123. **(B)** For delta thresholding, the 0° threshold (i.e., any increase in angle) fit best with a 0-10s RMSE of 0.356 and an overall 0-20s RMSE of 0.262. **(C)** For bandpass threshold, the 90±7° threshold fit best with a 0-10s RMSE of 0.103 and an overall 0-20s RMSE of 0.100. **(D)** To further study the bandpass threshold approach, which exhibits dual parameter sensitivity, we examined simultaneous variation of width and center. We perform a parameter sweep by varying the center of the band (30 to 150° in 1° steps) and the width of the band (from 2 to 60° with 1° steps) and compare the results to raw data to find that the optimum point for the bandpass threshold with two degrees of freedom is 92±8° with RMSE 0.099 (arrow). The cell network parameters for all simulations were 421 internal nodes, 60 peripheral nodes, and 960 filaments. Data presented was averaged over 10 runs.

By allowing two degrees of freedom to control both the width and the center of the bandpass threshold, we determine further that a band of 92±8 degree allows a marginally better fit with RMSE 0.099 compared to 0.100 for the single parameter bandpass fit **(Figure 3-8D)**. The minimal improvement gained from optimizing over two parameters suggests that our single degree of freedom bandpass model can accurately model the experimental behavior. Furthermore, based on the valley of low RMSE values observed as we perform the two dimensional parameter sweep of band width and center, we see that different centers can be compensated for by altering widths and vice versa (**Figure 3-8D)**. This suggests that cells may be able to fine-tune molecular release for different molecules in order to control release rates.

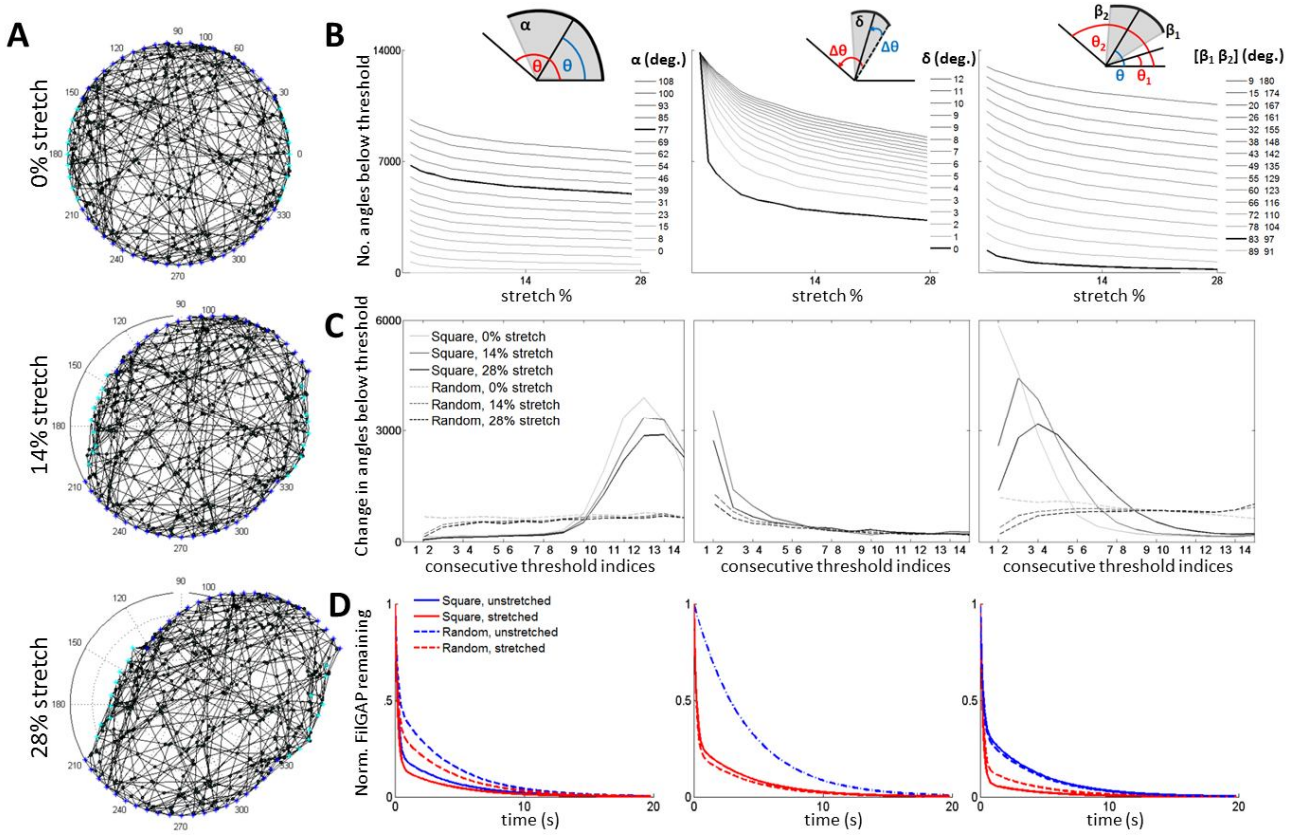

Figure 3-9: Randomized non-square grid actin networks enable more linear mechanosensitive response than do square-grid networks. While maintaining the same parameters used in square-networks, we generated randomized configurations of actin networks that are intended to be more representative of *in vivo* networks. Results were averaged over 7 runs. **(A**) Actin filament network with randomly-generated filament orientations, crosslinks, and internal nodes under 0%, 14% and 28% stretch. **(B)** For absolute (left), delta (middle) and bandpass (right) thresholding models, we track the number of angles below threshold as stretch increases for a range of threshold values. The bolded lines represents the best fit threshold values found previously using square networks (77° for absolute, 0° for delta, and 90±7° for bandpass). **(C)** For absolute (left), delta (middle) and bandpass (right), we compare the marginal increase in number of angles below threshold for square (**Figure 3-5**) vs. random networks (**Figure 3-9**) as we increment consecutive thresholds. As we compare the number of angles below threshold at successive threshold values, the randomly generated networks present more uniform changes in the number of angles below threshold at all stages of stretch when compared to the square networks. **(D)** Mixture model predictions for FilGAP release for square vs. random networks using the best fit threshold values.

A key question for modeling is whether the square network used in data-fitting (in order to approximate the *ex vivo* actin network system of Ehrlicher et al.), would yield similar behavior

to a random network model expected to better represent a cellular actin network. To explore this question, we examined model outputs for a network model with randomized connections **(Figure 3-9A)** using the same methodology as before while keeping the square-grid optimal parameters, which we assume describe characteristic geometry-independent FLNa-FilGAP behavior (**Figure 3-9B, C**; see **Appendix Figure 6-5, Figure 6-6, Figure 6-7** for animation frames).

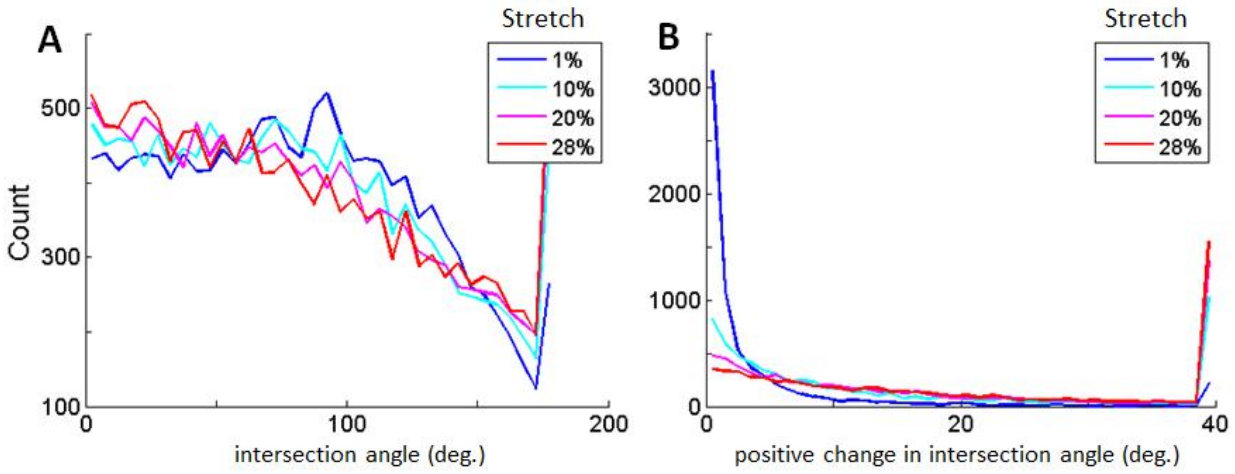

Figure 3-10: Distribution of (A) intersection crosslinking angles and (B) positive increases in intersection angles (i.e., delta angles) in a random non-square-grid actin network model. Results averaged over 7 runs. Model parameters are 421 internal nodes, 60 peripheral nodes, and 960 filaments (**Figure 3-9**).

We first find that the extension to random networks leads to a flatter distribution of angles due to more inherent noise in the system **(Figure 3-10)**. However, the distributions of angles that have not passed threshold in random networks are more uniformly spaced compared to those of a square network (**Figure 3-9B** vs. **Figure 3-5 plots)**. The number of angles below threshold in a random network varies nearly linearly with the threshold, whereas in a square network this increase is much more dependent on the specific threshold values, with negligible

change at smaller threshold values but noticeable increases at higher values (**Figure 3-9C)**. This pattern of random networks giving more predictable changes to the distribution of angles below thresholds than square networks is also reflected in bandpass thresholding and, to a lesser extent, delta thresholding **(Figure 3-9C)**.

These results suggest that more regular *in vitro* models, while qualitatively capturing the behavior of a more random system expected *in vivo,* would in fact likely substantially understate the sensitivity and responsiveness of the more random true system. More biologically-realistic random networks may allow the cell to more finely tune control of molecular release since small variation in threshold can lead to a predictable change in the distribution of angles passing mechanosensitive thresholds. Together with the leeway in the center and band width of the bandpass thresholds (**Figure 3-9D)**, these results suggest that the cell has considerable architectural parameters it can vary to output a specific signaling response.

3.4 Discussion and Conclusion

While we chose our parameters carefully in this study to emulate FilGAP response, this is just one potential use of our model. Given filamin's three isoforms (FLNa, FLNb, FLNc) and over 90 binding partners [109]—of which many, such as Rho, Rac, Cdc42, ROCK, ICAM-1, and integrin, bind within or in close proximity to the rod 2 hinge region—we can predict a similar model to be applicable to many other mechanotransductive signaling pathways. One potential problem this model may help solve is how the cell is able to localize the many mediators necessary in complicated motility signaling; having different crosslinker angular conformational thresholds for different players would give the cell another control system to direct morphology changes. Furthermore, this model could also be expanded to incorporate not just slip-bond-like

release of molecules due to conformation changes, but also the observed catch-bond-like behavior seen between integrin and filamin [37, 120].

In conclusion, we have generated a structurally-based mechanotransduction model incorporating mechanotransmission, mechanosensing, and mechanoresponse that can be parameterized using experimental data. We model mechanotransmission using a coarse-grained discrete element model of the cytoskeleton that uses force balancing to simulate stretch on the cytoskeleton. Architectural changes to the cytoskeleton results in deformations at crosslinking proteins and we determined that an angle bandpass model of mechanosensing most closely fits experimental data. By selecting crosslinkers as either fast or slow releasing bound signaling molecules, we can model the final time-dependent mechanoresponse output of the cellular system as a mixture of these two components. When we randomized the model architecture, we observed the putative mechanosensing mechanism was robust over a wide parameter range, suggesting that small alterations in mechanosensitive proteins can allow the cell to predictably fine-tune its signaling response. We believe our model provides a platform for generating and testing further hypotheses in mechanotransduction.

Chapter 4 : Generating a modular platform for single- and dual-mode stretching and shearing

4.1 Introduction

Fluid shear stress—physiologically, the movement of fluids over the surface of epithelial cells— is an indispensable mechanical stimulation necessary for proper function in not only endothelial cells [121, 122], but also other epithelial cells found in the lung [56] and bladder [123]. At vascular branches where blood flow transitions from laminar to turbulent flow, proatherosclerotic genes are upregulated that promote the development of atherosclerosis in the vessels [124]. Under healthy laminar flow, it is observed that endothelial cells and fibroblasts align parallel to cyclic fluid shear stresses in *in vitro* studies [27, 28, 41]. Previous models to understand shearing have focused on continuum models using differential equations of fluid dynamics [68], or modeling the red blood cell [125] or flow itself [126]. To our knowledge, there exists no published method for shearing of a discrete filament model in order to capture alignment characteristics. As there was also no discrete filament model of the cytoskeleton capable of capturing cyclic stretch characteristics until our published model discussed in Chapter 2 [52], our combined dual-mode cyclic shear and stretch model is also a novel finding.

In this chapter, we introduce cyclic (*i.e.*, pulsatile) shearing to our actin network model of cyclic stretching to generate a dual-mode stimulation model capable of experiencing cyclic stretch and/or shear. First, we characterize single-mode cyclic shearing and compare this type of mechanical stimulation to single-mode cyclic stretching. Next, we will analyze dual-mode stimulation of stretching and shearing simultaneously. We investigate parameters such as the number of internal nodes sheared and how we manage relaxation cycles in the context of dual-mode stimulation. Where relevant, we compare our results between our published model and our

revised “intersection” model. After simulations are performed, we will assay the orientation of filaments as well as their stresses with respect to cycles of stretch and/or shear. Tracking filament stresses would inform us whether compressive or tensile forces are predominant and help us address the question of whether the network is responding to the mechanical stimulation through minimizing network stress. This would be a logical explanation for why biological elements, which are known to be extremely adaptive, would alter their position and orientation.

Our final step will be coupling the shear and the stretch models into a common framework, which will represent cyclic shear on a subset of internal nodes and cyclic stretching displacement of the peripheral focal adhesions. This coupled framework will help explore the coupled effects of forces at varying magnitudes and directions. Existing literature describing *in vitro* experiments have suggested that the effects of stretch and shear may be linear under certain conditions. A previous study by the Yin group showed that the orientation-inducing effects of the two forces could sum linearly if they were both in phase and equipotent, resulting in a cooperative alignment [27]. This study represents occurrences under normal physiological function and does not capture pathologic conditions well. Our approach is well suited for examining such pathological conditions where the shear and stretch may not be equipotent or in phase.

4.2 Single-Mode Shearing

4.2.1 Rationale

Our first objective in this chapter is to characterize single-mode cyclic shearing and compare it to single-mode cyclic stretching in order to ensure that we can simulate each type of force independently of the other. To achieve this objective, we first aim to adapt our cytoskeletal network to support shear stress in an orthogonal direction of force stimulation compared to our previous single-mode stretching model (**Figure 4-1**).

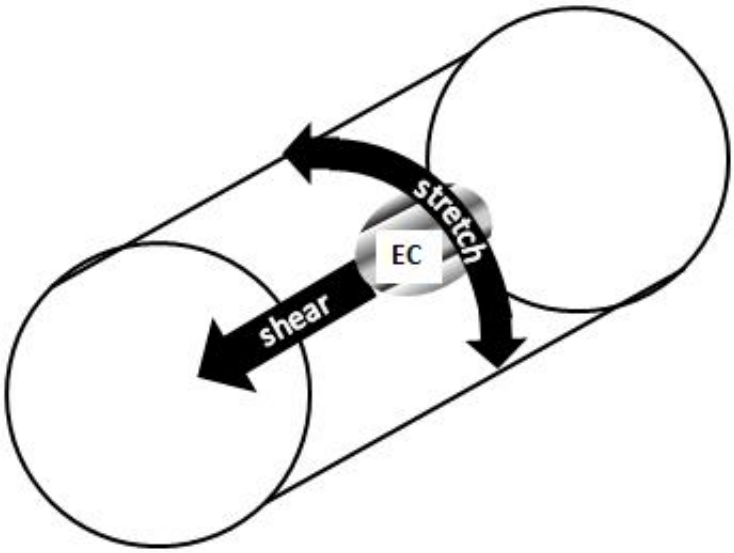

Figure 4-1: Schematic of orthogonal orientation between shear and stretch stresses on a typical epithelial cell sitting on the inside surface of a lumen such as a blood vessel

Secondly, we will run multiple simulations of single-mode cyclic shearing and run the same type of analyses comparing filament alignment and stresses in order to compare these results with single-mode cyclic stretching.

4.2.2 Methods

We first create a single-mode stimulation model for cyclic shear flow in a similar manner to our methodology for our single-mode cyclic stretch model described in Chapter 2 and

published work [52]. We propose a two-dimensional circular space to simulate a whole cell. The cell will be fixed to an underlying substrate at prescribed perimeter nodes and a number of unstressed filaments will be randomly created to connect nodes. Shear force will be emulated by applying an external uniaxial force to a random subset of the moveable interior nodes, representing simulated apical flow across a cell from a two-dimensional viewpoint (**Figure 4-2**).

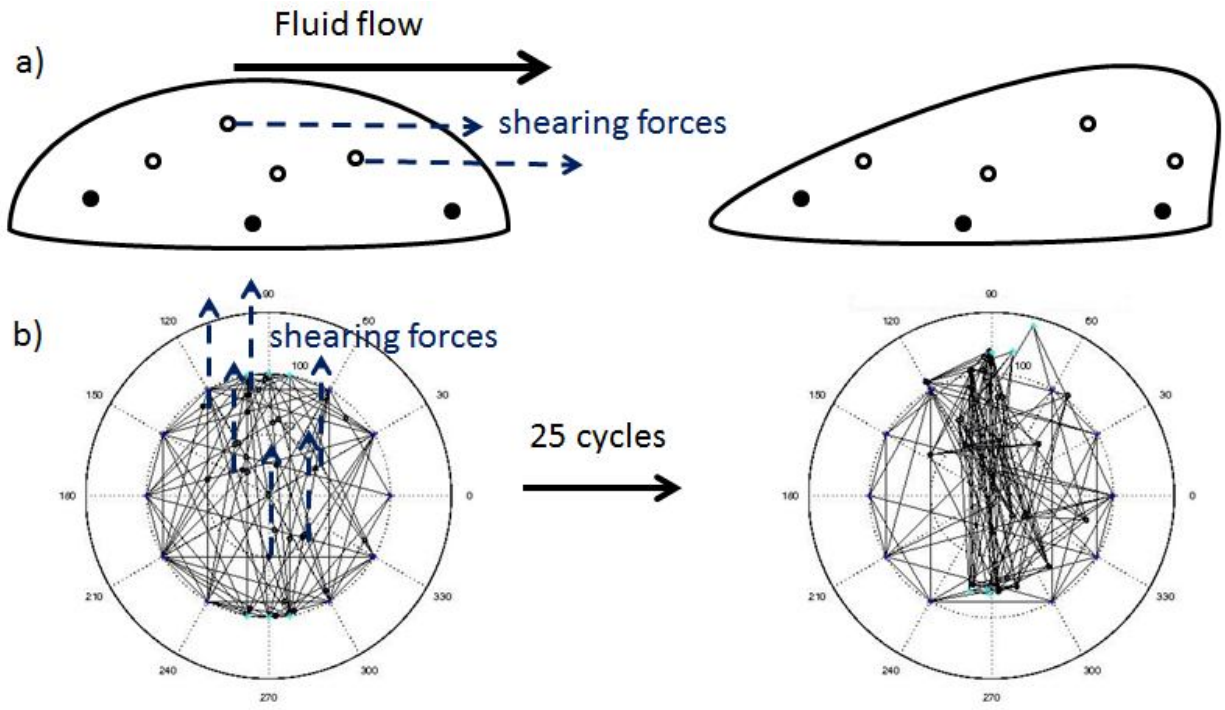

Figure 4-2 : Shearing single-mode stimulation in (a) schematic form and (b) on our actin network model. (**a)** Side view schematic of epithelial cell under shearing forces. Filled nodes are internal nodes that are fixed to the substrate. Clear nodes are internal nodes that are sheared by simulated displacement. (**b)** Top down 2D view of actin network model under shearing forces in the vertical direction. 50% of the internal nodes are displaced upwards to mimic epithelial cells under shearing forces as displayed schematically in **(a)**. Model parameters are 30 internal nodes (15 sheared), 16 peripheral nodes, and 138 filaments.

After the application of each incremental shear stress, we use a variant of Gauss-Seidel relaxation to iteratively adjust interior node positions not under the influence of shearing itself to find the state of minimum stress. This force application-relaxation methodology is similar to that used in our single-mode stretching model described in Chapter 2 (**Code 2-1**). Once the

network is in a minimum stress state, we apply our "normalized to maximum strain" filament breakage model and reform filaments using our conservation-of-mass model. We repeat this shear-relax-breakage-reformation process over 25 cycles (see **Movie M4** for an example of an intersection network model undergoing 25 cycles of 10% uniaxial shear).

4.2.3 Results

Here, we apply our cyclic shear stress method to our intersection network generation model described in Chapter 2 (**Figure 4-3**). As a point of reference, we also apply the same method to our original published model [52] and compare the filament alignment and stress results. Whereas both our original published model and our intersection model experience experimentally-observed perpendicular alignment of actin filaments to cyclic stretch (**Figure 2-4** and **Figure 2-16** , respectively), we see that in the case of experimentally-observed parallel alignment of actin filaments to cyclic shear, only our intersection model can recapitulate this behavior. This difference in our two models supports the hypothesis that the intersection model which more closely resembles the gel-like meshed networks seen in the cell cortex is a more realistic biophysical model for actin networks.

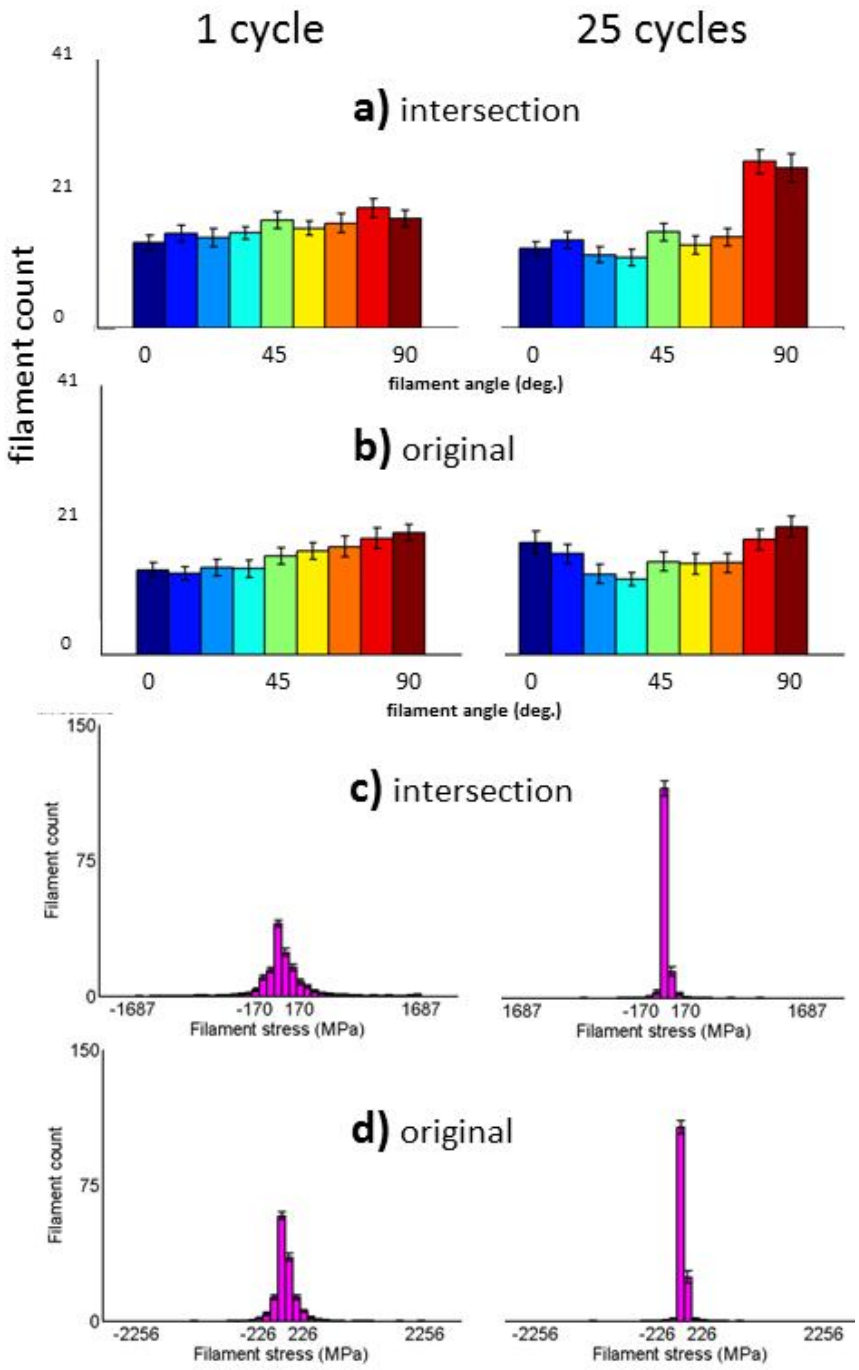

Figure 4-3: Comparing uniaxial single-mode cyclic shear stress in the vertical direction between our intersection model and original published model [52]. Filament alignment histograms for **(a)** intersection and **(b)** original models under 1 cycle (left) and 25 cycles (right) of 10% shear stress. Filament stress histograms for **(c)** intersection and **(d)** original models under 1 cycle (left) and 25 cycles (right) of 10% shear stress. Example networks of intersection and original models in insets of **(a)** and **(b)**, respectively. Model parameters are 30 internal nodes, 16 peripheral nodes, and 138 filaments. 50% of internal nodes were displaced vertically to simulate fluid shear stress. Elastic modulus of actin filaments was assumed to be 2 GPa. Results averaged over 30 runs. Error bars denote 95% confidence interval.

The interface surface area and downward pressure between fluid flow and the apical surface of the cell presents a potential critical area of control for the cell, as evidenced when hypertension is an underlying factor in various vascular diseases [127]. Here, we investigate this interaction by displacing more or less internal nodes in the direction of shear. We compare filament alignment results from 25% (**Figure 4-4a**), 50% (**Figure 4-4b**), and 75% (**Figure 4-4c**) of internal nodes uniaxially sheared vertically for 25 cycles. We see that there is a significant correlation in increased parallel alignment to cyclic shear as we transition from 25% to 75% of internal nodes being cyclically displaced. These results support the hypothesis that the magnitude of cyclic stresses is an important factor in determining alignment responses as previously suggested for stretch responses [11].

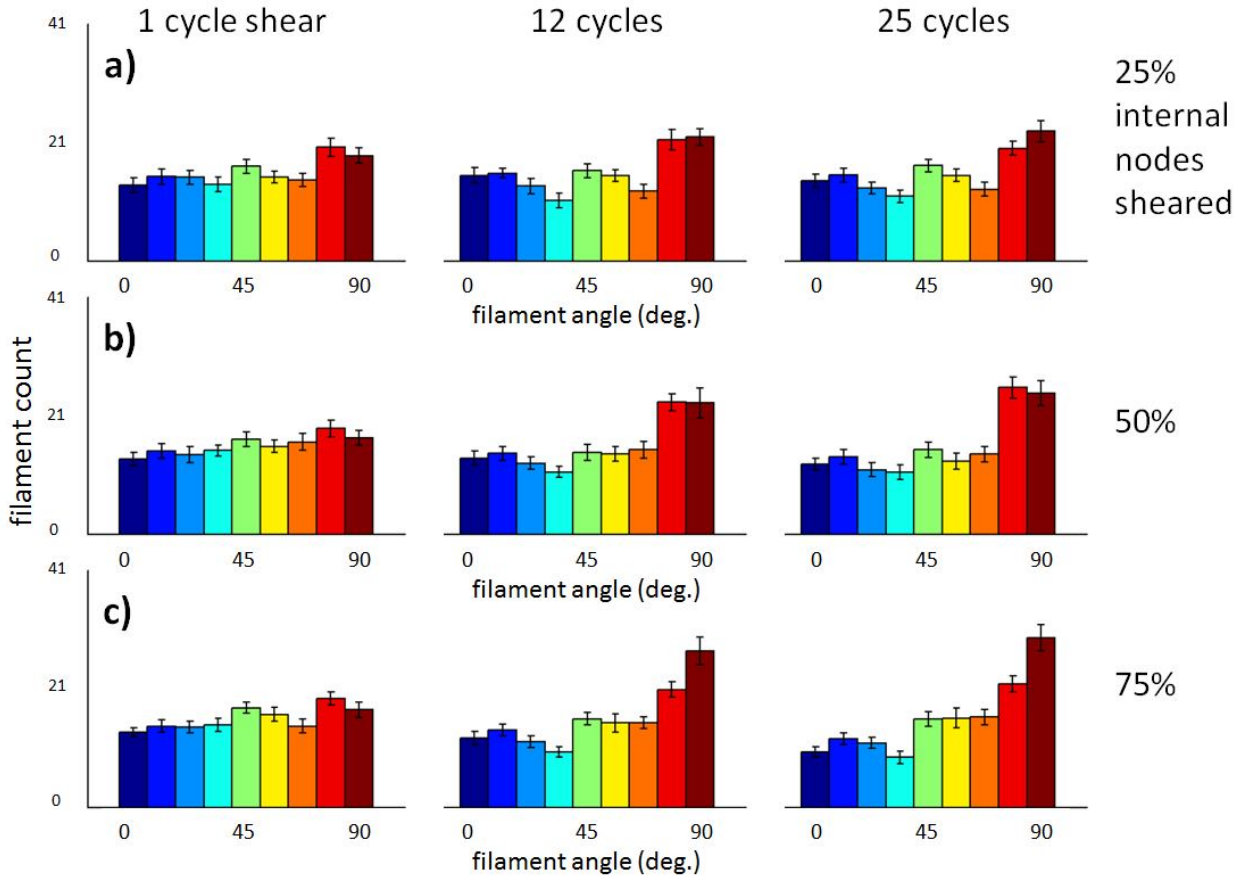

Figure 4-4: Filament alignment histograms when (a) 25%, (b) 50% and (c) 75% of internal nodes are uniaxially cyclically sheared in the vertical direction. Model parameters are 30 internal nodes, 16 peripheral nodes, and 138 filaments formed using the intersection method. Network was cyclically sheared by 10% for 25 cycles. Results averaged over 30 runs. Error bars denote 95% confidence interval.

Next we compare the stresses that the filaments experience over multiple shear cycles for 25%, 50%, and 75% of internal nodes uniaxially sheared vertically for 25 cycles (**Figure 4-5**). Here, we also see significant correlation between increased proportion of internal nodes being cyclically sheared from 25% to 75% and lower stressed filaments.

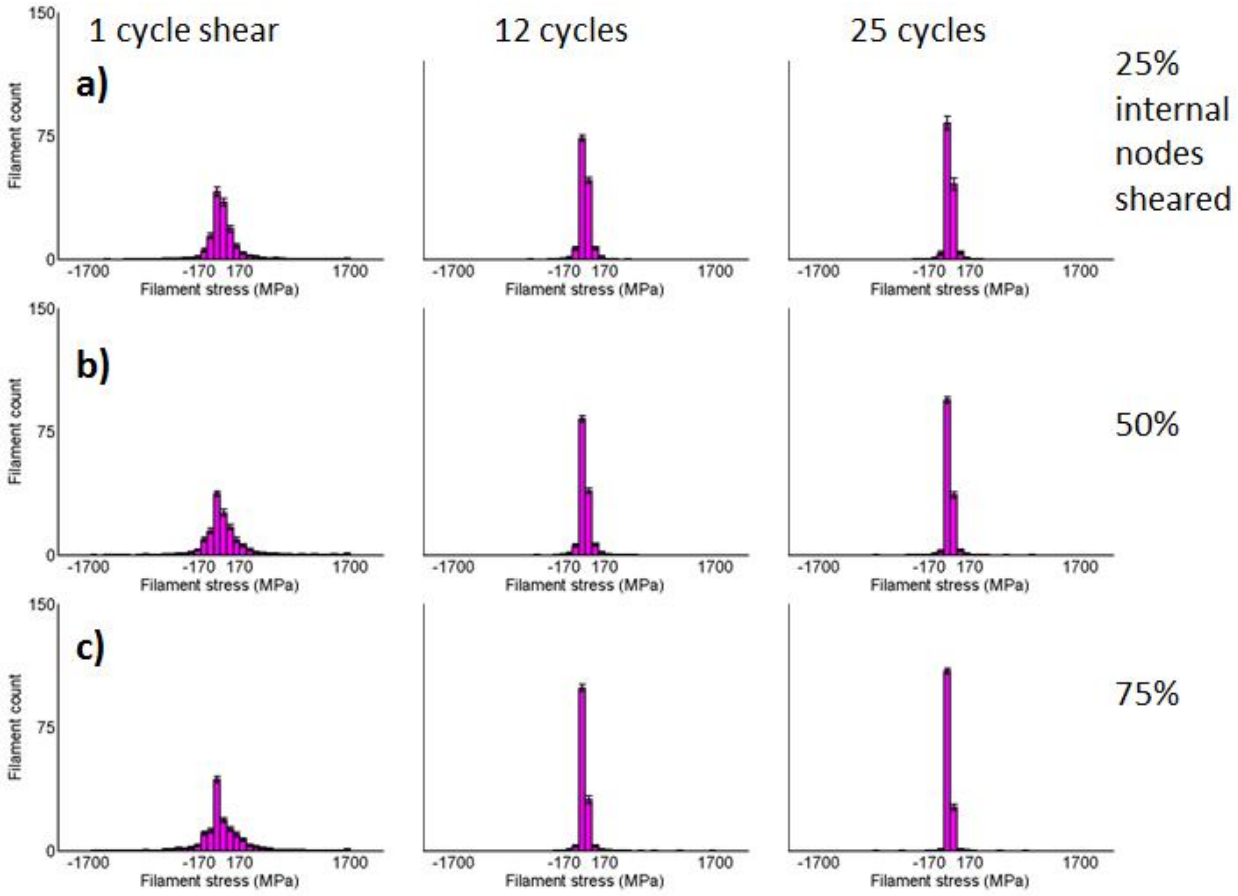

Figure 4-5: Filament stress histograms when (a) 25%, (b) 50% and (c) 75% of internal nodes are uniaxially cyclically sheared. Model parameters are 30 internal nodes, 16 peripheral nodes, and 138 filaments formed using the intersection method. Network was cyclically sheared by 10% for 25 cycles. Results averaged over 30 runs. We assume actin filaments have a 2 GPa elastic modulus. Error bars denote 95% confidence interval.

4.3 Dual-mode Stimulation: simultaneous stretching and shearing

4.3.1 Rationale

The two main forces acting on endothelial cells are cyclic stretch and shear [128]. These two forces are physiologically perpendicular to each other but typically cooperate to align endothelial cells and fibroblasts in the direction of blood flow [27, 41]. Cyclic shear and stretch forces are strongest in the arteries and arterioles [122], but these pulsatile forces have also been shown to alter angiogenesis-related capillary behavior. Examples include regulating cell orientation and stimulating mechanosensitive TRPV4 ion channels to activate integrin receptors and downstream cytoskeletal remodeling [129]. Cyclic strain has also been shown to mediate expression of various matrix metalloproteinases in capillary endothelia, which are critical for ECM dissolution in the inception of angiogenesis [81, 130]. Shear and stretch have also been shown to increase and direct angiogenesis [131, 132].

Although mechanotransductive signaling is intimately involved in angiogenesis, there is no one specific known mechanism that can explain the micrometer precision of vascular growth that results in controlled development of vascular patterns. It has been suggested, though, that the fractal-like patterns of angiogenesis cannot be explained by mitogen gradients alone and that local micromechanics plays a major role [133]. The importance of local micromechanics is also implied by the findings that frequency-dependent response [27, 134] occurs at frequencies too high for tissue factor gradients to change substantively; this suggests that force itself—inherently a non-specific factor—is a remodeling agent. More recently, this hypothesis has been supported by the reports of a new type of vascularization called “looping angiogenesis" whereby tension was sufficient to induce and direct vascularization [135]. We believe generating a dual stimulation model could help us further understand the local micromechanics that cells

experience and how they affect morphological behavior. Developing a mechanical stimulation model of cytoskeletal actin arrangement not only provides a platform to test theories but also can help us answer open questions about endothelial behavior, such as why high shear flow increases the mechanical stiffness of cells *in vitro* [136, 137].

Our guiding hypothesis is that mechanical stresses are primarily responsible for the microenvironment network's response and that the effects of these mechanical stresses can be adequately described by their influence on depolymerization of filaments in cytoskeletal networks. Our previous work described in this dissertation demonstrated that a coarse-grained model of cyclic stretch can qualitatively simulate both cyclic stretch and cyclic shear stress responses of actin networks in living cells. Here, we propose to combine these two effects and exert them on our network model simultaneously to determine their coupled response.

4.3.2 Methods

Here, we generate a stochastic dual-mode mechanical stimulation model that combines the single-mode stimulation described in **Chapter 2.3** and the single-mode shear stimulation in **Chapter 4.2** to examine the force distribution and reorganization of intracellular actin cytoskeleton in response to simultaneous pulsatile shear and tensile stresses. Please see the respective sections for more detailed methods. Briefly, these filament structures may represent either cross-linked single actin filaments found in the cell cortex or bundled filaments found in stress fibers. The specific hypothesis guiding this work is that mechanical stresses are primarily responsible for the network's response and all other influences are accounted for by their effects on the probability of filament depolymerization as a function of stress. We assume that one need not explicitly model altered expression of actin cofactors or their interaction with the

cytoskeleton to account for orientation of the cytoskeleton under external mechanical stimulation.

We first test two variants for the relaxation stage in our dual stimulation model to test well-behaved characteristics. We compare a single-relaxation stage method and a double-relaxation stage method (**Code 4-1**). Physiologically, stretching and shear would be more "in phase" (single-relaxation stage) but it is possible the model would not be well-behaved without an intermediate relaxation stage (double-relaxation stage).

1. generate network
2. for every cycle
   A. while network not fully stimulated
      i. Stretch network by 1%
      ii. Shear network by 1%
      iii. Relax network
   B. break filaments
   C. generate new filaments

1. generate network
2. for every cycle
   A. while network not fully stimulated
      i. Stretch network by 1%
      ii. Relax network
      iii. Shear network by 1%
      iv. Relax network
   B. break filaments
   C. generate new filaments

Code 4-1 : Comparing (left) single- and (right) double-relaxation stages for coupled cyclic stretch and shear stress simulation.

4.3.3 Results

When we compare single- and double-relaxation stage coupled cyclic stretching and shearing, we discovered that there was no discernible difference from the results **(Appendix Figure 6-8)**. As the single-relaxation stage model is simpler, we will present all results using that model. See **Movie S5** for an example of an actin network undergoing 25 cycles of dual-mode cyclic 10% stretch and cyclic 10% shear under single relaxation.

We examine mean and median filament angles for dual-mode simulations run at sixteen combinations of cyclic shear and stretch (**Figure 4-6**) ranging up to 30% cyclic shear and stretch.

When examining the effect of coupled stimulation on the actin network, we find that the two modes of force stimulation act in an unexpectedly negatively reinforcing but linear fashion. Since both modes of stimulation serve to align filaments in a 90 degree orientation independently to horizontal cyclic stretch and vertical cyclic shear in our model simulations, we expect that when dual stimulation is applied to our network model, we would see increased perpendicular alignment earlier in the stretch cycles. However, what we observed was that the best alignments were achieved with 0% shear and 30% stretching. When cyclic shear stress was added in, this served to actually decrease filament alignment in a monotonically descending fashion (**Figure 4-6**; **Appendix Figure 6-9**). This type of non-reinforcing behavior is reminiscent of regions of disturbed blood flow such as arterial bifurcations [3, 33] which are host to a number of pathologies such as atherosclerosis but as our model is not modeling non-laminar shear, this is a surprising result.

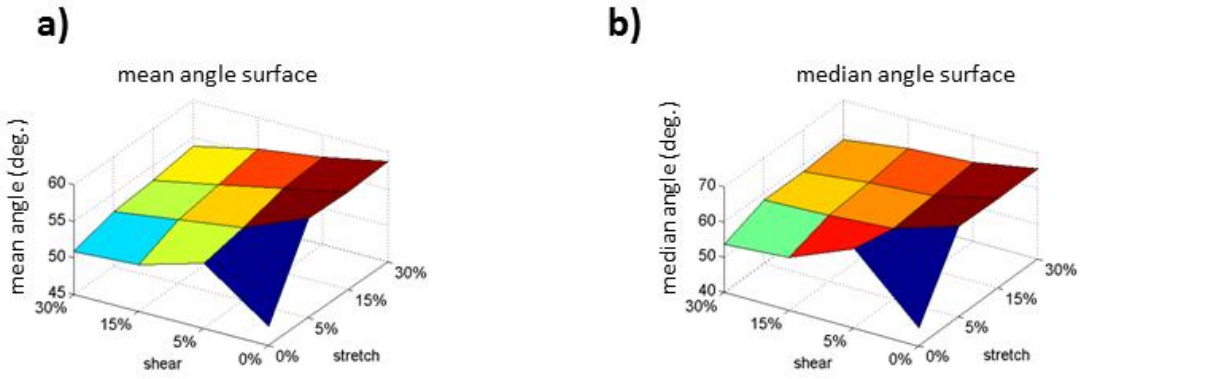

Shear % \ Stretch %	0	5	15	30
0	47.7	58.6	58.4	58.7
5	54.0	55.0	56.5	57.0
15	51.4	53.7	54.7	55.8
30	50.9	52.5	53.0	53.8

Shear % \ Stretch %	0	5	15	30
0	45.0	65.7	65.3	65.6
5	62.5	60.0	61.2	62.5
15	55.0	58.8	59.7	61.2
30	53.7	58.2	57.9	58.8

Figure 4-6: Mean and median filament angles for dual stimulation cyclic stretching and shearing at cycle 25. Surface mesh of mean (**a**) and median (**b**) filament angles at different magnitudes of cyclic stretch and shear (range from 0-30%) at cycle number 25. Below the mesh graphs is the raw data used to generate the surface plots.

One possible explanation for why we did not see cooperative behavior for cyclic stretching and shearing is that the magnitudes of stretch and shear we are examining here are too spread apart and we are overlooking local minima. The alignment increases as we increase from 0% to 5% shearing, but drops as we increase shearing magnitude further to 15% and 30%. Similarly, when we increase from 0% to 5% stretching, we see an increase in alignment but there is not much improvement when we transition from 5% to 15% or 30%. Thus, there could be local minima in the search space between 5-10% that may warrant further investigation. Another explanation for this phenomenon is that simultaneous shear and stretch is overloading the cell's ability to relax filament stresses to align its cytoskeleton [80].

For future directions, we propose a method whereby full stretch and relaxation cycles are performed consecutively for stretching and shearing (**Code 4-2**; compare with **Code 4-1**). This would allow the network to fully relax before undergoing an additional stress. Additionally, we would like to investigate the effects of non-reinforcing oblique directions for cyclic stretching and shearing to determine whether our model can capture directional effects observed *in vitro* [11, 27]. Non-reinforcing stresses may be able to capture more complex stresses seen at arterial bifurcations where pathologies often occur [3, 33].

1. generate network
2. for every cycle
   A. while network not fully stretched
      i. Stretch network by 1%
      ii. Relax network
   B. break filaments
   C. generate new filaments
   D. while network not fully sheared
      i. Stretch network by 1%
      ii. Relax network
   E. break filaments
   F. generate new filaments

Code 4-2 : New proposed dual stimulation algorithm for coupled cyclic stretching and shearing

Chapter 5 : Conclusion

In this dissertation, we discussed three main results. First, in Chapter 2, we introduce a coarse-grained model of the cytoskeleton capable of experiencing simulated uniaxial single-mode stretching. We analyze the response of the actin filament alignment and stress responses to suggest that minimizing stresses is a driving factor in filament alignment (**Figure 2-4** and **Figure 2-8**) which is also seen in certain cell types such as fibroblasts and endothelial cells *in vivo* [6, 10]. To our knowledge, this is the first discrete actin network model that can recapitulate the known phenomenon of actin filament alignment to cyclic stretch and we published our findings [52]. Since publication, our findings have been supported by the work of Stamenovic group that described a continuum model for cytoskeletal fluidization to reach a similar conclusion that actin filaments fluidize and reorient themselves perpendicular to the direction of cyclic stretch [80].

In 0, we apply our model to investigate key questions surrounding mechanotransduction, which is currently an area of intense research [3, 34] due to being largely undiscovered territory for medical applications in vascular diseases and cancer. The driving question we sought to answer is that given the cell has a common set of structural components, how can it use these same components to convert a pure mechanical signal such as stretching into a biochemical response at the cellular level? To explore this problem, we built a multiscale model of mechanotransduction summarized in **Figure 3-1** that encompasses the three recognized stages of mechanotransduction: mechanotransmission (the rapid transmission of forces across mechanotransductive elements), mechanosensing (force-induced alterations of protein conformation and subsequent function), and mechanoresponse (cellular signaling output of the force-sensitive networks). Our mechanotransmission model was built upon a modified model of our original paper [52] with modifications to the internal node generation and stretching

modality. For the key mechanosensing step, we postulated three geometric-based mechanisms by which a mechanosensitive actin crosslinker may undergo conformational changes to alter biochemical signal release. For the mechanoresponse stage, we generated a time-dependent mixture model of populations of actin crosslinkers above and below activation thresholds. We trained and validated our mixture models on published data by the Stossel group [37]. Our findings suggest that the filamin A-FilGAP mechanotransductive response may be utilizing an actin crosslinker bandpass angle at a coarse-grained level to determine whether the associated FilGAP signaling molecule is being released quickly or slowly (**Figure 3-8**). Additionally, the noisy, stochastic environment of the *in vivo* cell may actually be beneficial in terms of allowing finer linear control of signal release (**Figure 3-9**). We have finished writing up our results in a manuscript and will be submitting them shortly pending correspondence from a collaborator.

In Chapter 4, we tackle the question of whether our energy-minimization actin network model can also recapitulate observed cyclic fluid shear stresses in addition to cyclic stretch. For example, endothelial cells experience both cyclic shear flow stress from blood flow passing over them as well as cyclic hoop stress from vessel deformation. We first modified the model to simulate single-mode cyclic shear by itself and were able to capture observed parallel alignment of epithelial cells to shear flow (**Figure 4-3**, **Figure 4-4**). Next, we incorporated both cyclic stretch and cyclic shear to stimulate the actin network simultaneously. Our initial results suggest that the two modes of force stimulation do not act in a cooperative fashion and that cyclic shear may actually be counteracting the effects of cyclic stretch in a monotonically descending fashion (**Figure 4-6**). One possibility is that the network model is under too much stress from forces acting on it in orthogonal directions and is thus not able to relax correctly.

Future work would involve investigating this clashing phenomenon further through different avenues. First, tightening the threshold for force equilibrium and thus forcing the network to balance the nodal stresses further. Secondly, using a finer search space for stretch and shear magnitudes to look for local energy minima. Lastly, allowing the network to undergo full relaxation and filament breakage/reforming cycles after both stretching and shearing steps (**Code 4-2**). Additionally, our dual stimulation model can be used to investigate the oblique, directional effects of stretch and shear on cellular morphology.

In summary, in this dissertation we have confronted challenges in biology that are not straightforward to solve experimentally due to limitations in current laboratory technology. However, with the use of computer modeling and simulations, we can explore these specialized problems that would otherwise go unperturbed for the time being and generate *in silico* platforms upon which we can test novel hypotheses that can further be investigated *in vitro*.

Chapter 6 : Appendix

6.1 Complete history of angle alignment for actin filament network

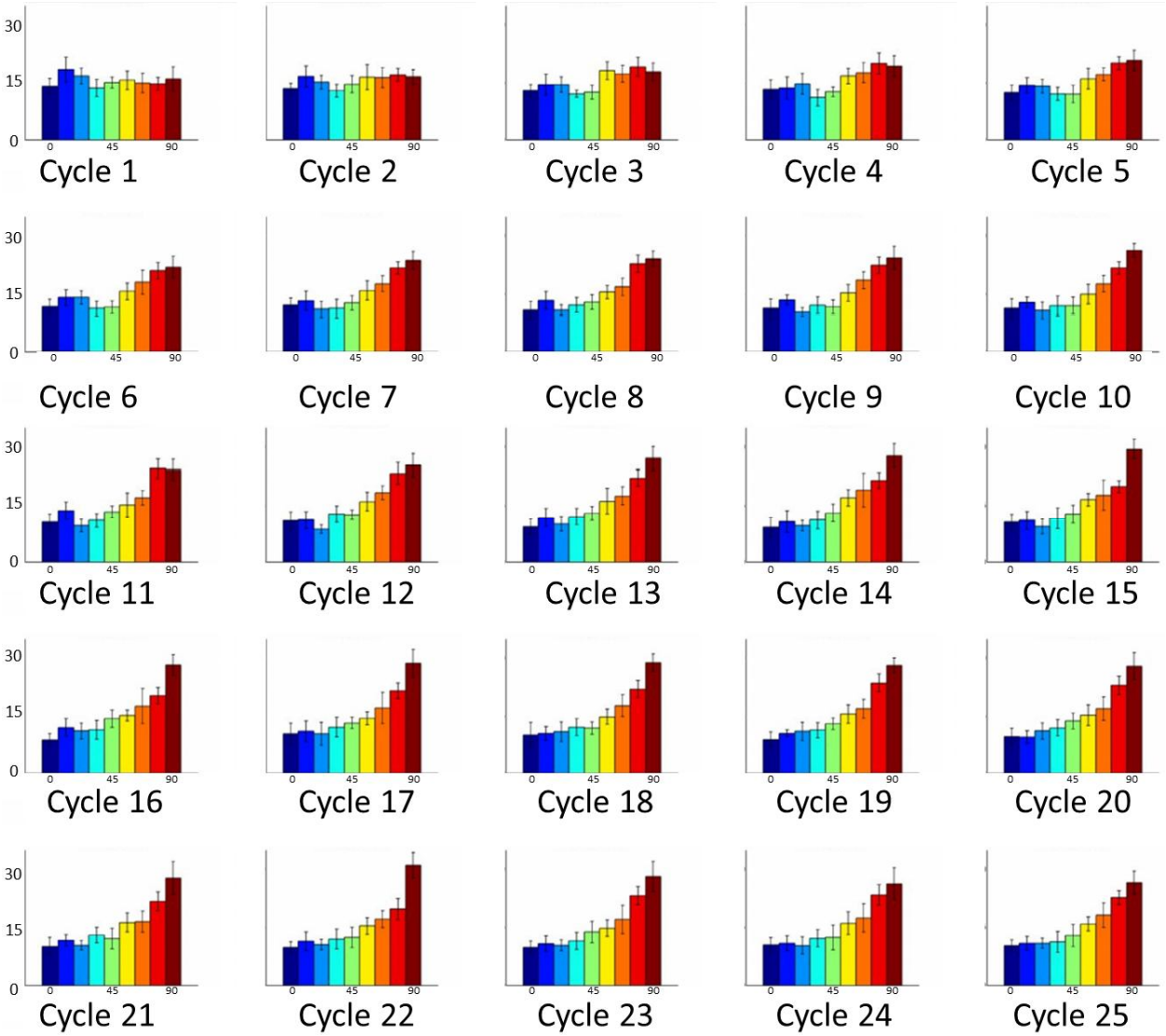

Figure 6-1: Histograms of angular orientation of filaments in nodal equilibrium after 1-25 iterative cycles of 10% uniaxial horizontal stretch. Averaged over ten uniquely generated filament networks, each of which consisted of 138 filaments distributed among 16 prescribed perimeter nodes and 30 randomly placed interior nodes. Each filament connects two nodes. Error bars denote 95% confidence interval.

6.2 Mechanotransduction: visualizing different network configurations and thresholding models

Supplemental Movie Frames (Figure 6-2 through Figure 6-7): For all movie frames, we show the networks under 0%, 14%, and 28% stretch. Shaded regions represent angles below threshold (i.e., to be released at slow rate) with darker regions denoting smaller angles. Clear regions represent angles above threshold (i.e., to be released at fast rate). Simulation parameters used were 421 internal nodes, 60 peripheral nodes, and 960 filaments.

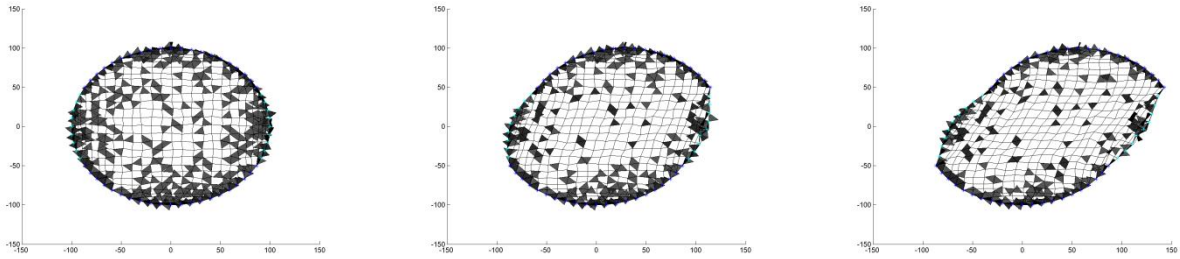

Figure 6-2 : Square grid network, absolute threshold of 77°

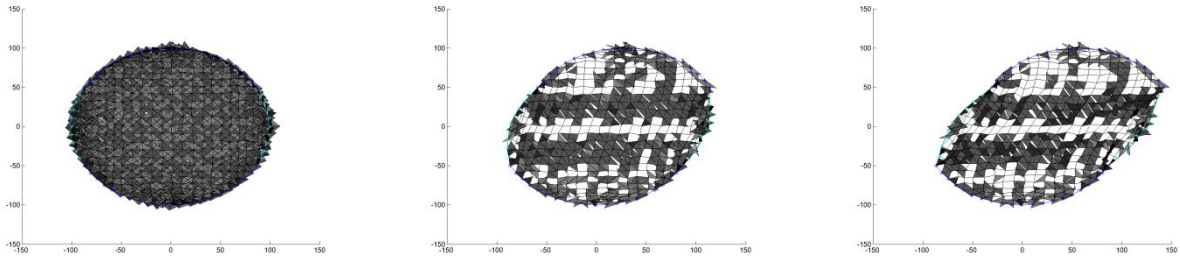

Figure 6-3 : Square grid network, delta threshold of 0°

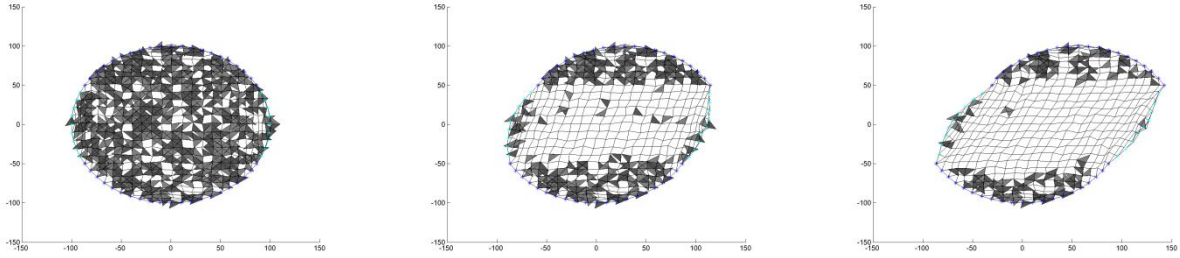

Figure 6-4 : Square grid network, bandpass threshold 90±7°

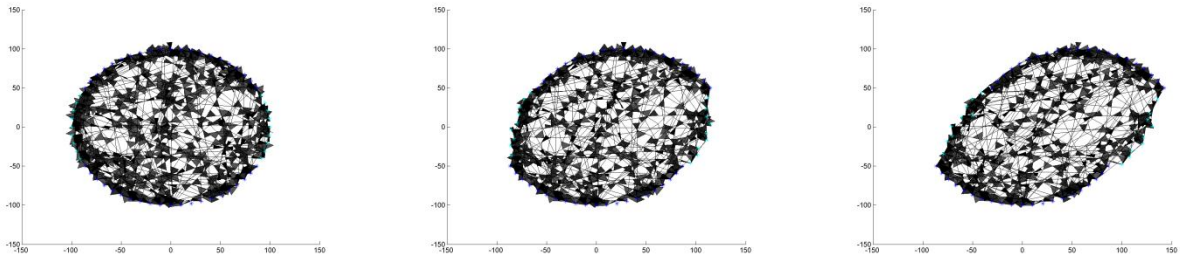

Figure 6-5 : Random non-square-grid network, absolute threshold of 77°

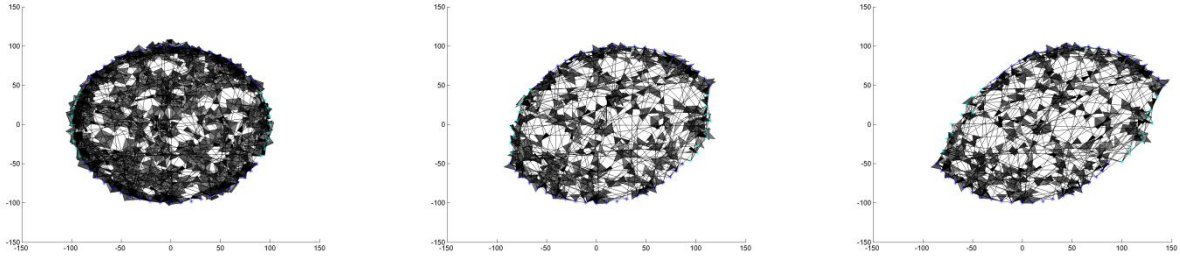

Figure 6-6 : Random non-square-grid network, delta threshold of 0°

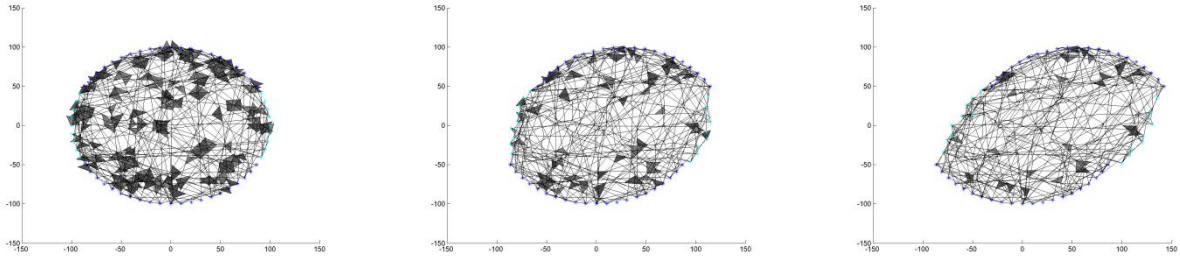

Figure 6-7 : Random non-square-grid network, bandpass threshold of 90±7°

6.3 Dual-mode stimulation: single-relaxation vs. double-relaxation stages

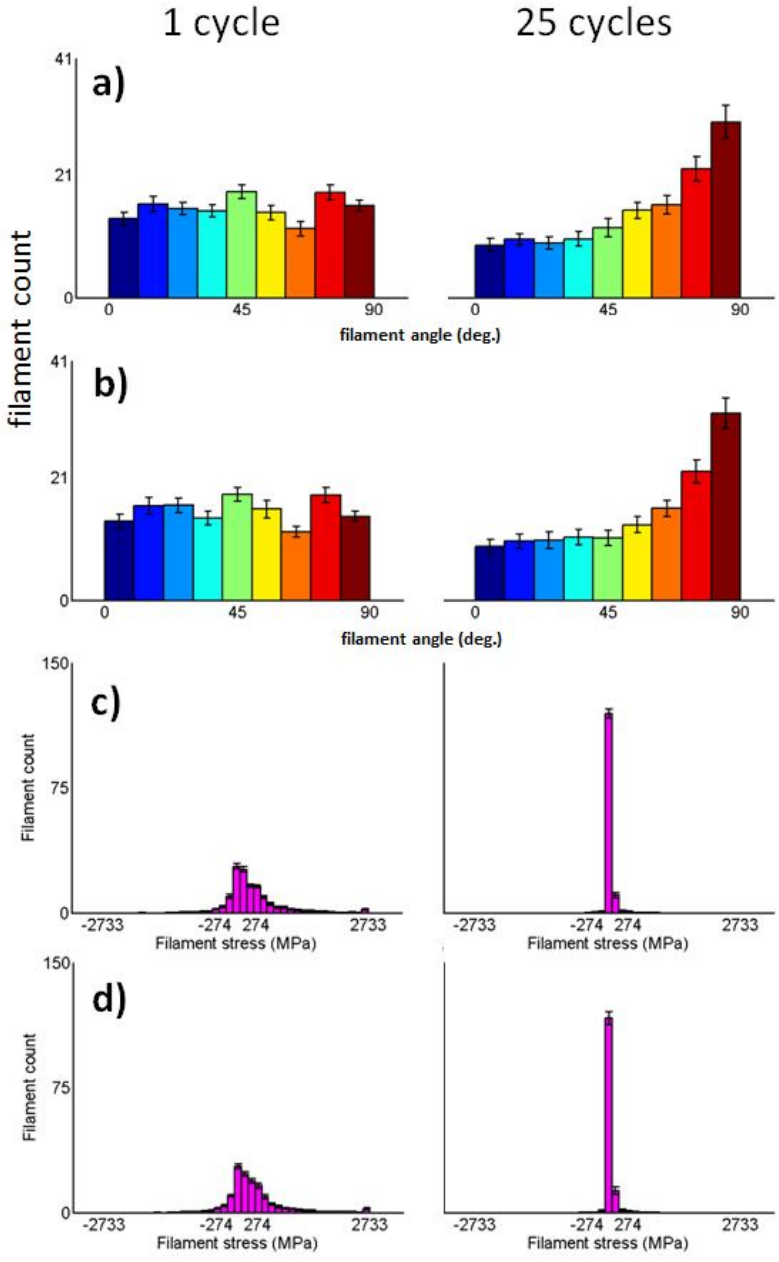

Figure 6-8: comparing single- and double-relaxation stages in coupled cyclic stretching and shearing. See **Code 4-1**. Filament alignment to horizontal axis cyclic stretching and vertical axis cyclic shearing at **(a)** 1 cycle and **(b)** 25 cycles. Filament stress histograms at **(c)** 1 cycle and **(d)** 25 cycles. Model parameters are 30 internal nodes (15 sheared), 16 peripheral nodes (10 stretched) and 138 filaments. Results averaged over 30 runs.

6.4 Dual-mode stimulation: mean and median filament angles

a)

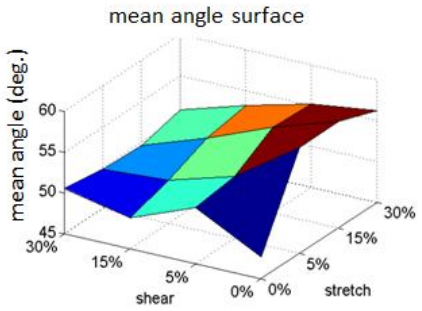

Shear % \ Stretch %	0	5	15	30
0	47.7	58.0	58.0	56.3
5	51.9	52.6	55.5	55.2
15	48.8	50.3	52.3	53.2
30	50.6	49.8	49.6	50.8

b)

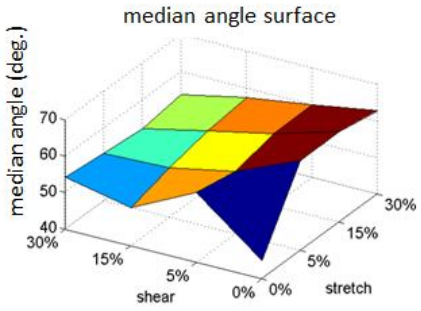

Shear % \ Stretch %	0	5	15	30
0	45.0	64.8	65.0	62.9
5	59.1	57.2	59.8	60.0
15	50.4	53.6	55.9	57.3
30	54.2	53.0	52.0	53.7

Figure 6-9: **mean and median filament angles for dual stimulation cyclic stretching and shearing at cycle 10.** Surface mesh of mean (a) and median (b) filament angles at different magnitudes of cyclic stretch and shear (range from 0-30%) at cycle number 10. Below the mesh graphs is the raw data used to generate the surface plots.

Chapter 7 : Code

7.1 Dual-mode cell stretch execution

```
function [lastCycle]=cellstretchDM_john_execute_relaxBreakX2(...
    SAVE_DIR,...
    whichRun,...
    numCycles,...
    datasetDescription,...
    doElasticNodes,...
    intNodePositioning,periNodePositioning,...
    vertOffset,...
    stretchMethod,stretchMag,...
    breakMethod,breakFactor,...
    doRotate,...
    cellRadius,...
    intNodeNoise,...
    elastMod,...
    nIntNodes,nPeriNodes,nFilaments,...
    shearMethod,shearVal,shearFactor,...
    delX,...
    relaxThresh,...
    iMax,...
    doSaveNetworkBeforeBreak,...
    figOptions)

%12/01/23: changed from tracking forces (which depends on elastMod) to
%tracking strains.  Subsequently changed relaxation threshold from a sum of
%squared forces to a sum of squared displacements [PENDING]

%12/01/17: changed the way ministretch is performed from 1:delX:stretchMag
%to delX:delX:stretchMag.  Track the amt of stretch (currStretch) rather
%than the number of ministretches (miniStretchCount)

% disp(['[Run ' int2str(whichRun) '] Begin run at ' GetCurrentTime() ]);
disp('***Start cellstretchDM_john_execute_relaxBreakX2***');
disp(['[R' int2str(whichRun) '] Folder name: ' SAVE_DIR]);
disp(['[R' int2str(whichRun) '] Dataset description: ' datasetDescription])
disp(['[R' int2str(whichRun) '] delX = ' num2str(delX) ', relaxThresh = ' num2str(relaxThresh)]);
rand('state',sum(100*clock));   %resets random generator to a different state each time

%% Setup initial network

%GENERATE INITIAL NETWORK
disp(['[R' int2str(whichRun) '] ' GetCurrentTime() ' generating dual-mode network...' ]);
[intPol_0, periPol_0, nIntMobile, nPeriMobile,
filNodeLUT]=GenerateNetworkDM(nIntNodes,nPeriNodes,intNodePositioning,periNodePositioning,vertOffset,stretchMethod,nFilaments,she
arMethod,shearFactor,cellRadius,intNodeNoise,doRotate);
disp(['[R' int2str(whichRun) '] ' GetCurrentTime()  ' finished generating dual-mode network' ]);

nodePol_0=[intPol_0 periPol_0];   %Left-to-Right: internal nodes first, then peripheral nodes.  "_0" denotes initial position.

%% Determine node indices
%nodeXY data structure is:
%[int mob][int fix][peri mob][peri fix]
nNodes = nPeriNodes + nIntNodes; %total # nodes, =sizeall

% nMobile=nIntNodes+nPeriMobile;  %mobile # nodes
% nMobile = nIntMobile + nPeriMobile;  %13/04/06: mobile # nodes changed from assuming that all internal nodes are mobile to a
select # of internal nodes and a select # of peripheral nodes
mobileNodes.int = 1:nIntMobile; %13/06/06: don't use nMobile anymore, specifcy indices directly
mobileNodes.peri = nIntNodes+1:(nIntNodes+nPeriMobile);

[nodeXY(1,:),nodeXY(2,:)]=pol2cart(nodePol_0(1,:),nodePol_0(2,:)); %nodeXY: mobile nodes first, then fixed nodes

%% DATA I/O

%PRINT/SAVE LABELED NETWORK
if figOptions(1); figure; else figure('Visible','off'); end
TITLE=['Run',int2str(whichRun),'_Cycle0_LabeledNetwork'];
polar(pi,cellRadius+delX);
PlotLabeledNetwork(filNodeLUT, nodeXY, nodeXY(:,1:nIntNodes), nodeXY(:,nIntNodes+1:end), nIntNodes, true, TITLE); %Numerically
labeled network (doLabel=true)
if figOptions(2); print('-djpeg',[SAVE_DIR TITLE]); end

%PRINT/SAVE INITIAL NETWORK PRIOR TO STRETCHING
if figOptions(1); figure; else figure('Visible','off'); end
TITLE = ['Run',int2str(whichRun),'_Cycle0_InitialNodes'];
PrintNetwork_XY(nodeXY,[]        ,nIntNodes,cellRadius+delX,[],[],TITLE,false,nPeriMobile, [], [], nIntMobile); %FIGURE 1 - focal
adhesions/peripheral nodes ONLY (no filaments)
if figOptions(2); print('-djpeg',[SAVE_DIR TITLE]); end

if figOptions(1); figure; else figure('Visible','off'); end
TITLE =(['Run',int2str(whichRun),'_Cycle0_InitialNetwork']);
PrintNetwork_XY(nodeXY,filNodeLUT,nIntNodes,cellRadius+delX,[],[],TITLE,false,nPeriMobile, [], [], nIntMobile);  %FIGURE 2 -
entire network including both nodes & filaments
if figOptions(2); print('-djpeg',[SAVE_DIR TITLE]); end
```

```
%SAVE VARIABLES BEFORE STRETCHING
save([SAVE_DIR TITLE]);
nodeXY_0=nodeXY;    %saves original positions of nodes

breakCounter1 = zeros(1,numCycles); %tracks # filaments broken after each stretch cycle
breakCounter2 = zeros(1,numCycles); %tracks # filaments broken after each shear cycle

%Main loop
for whichCycle = 1:numCycles
    %% BEGIN STRETCH PORTION

    %Determine node elasticity
    if doElasticNodes %Kathy's original method that restores the initial positions of the interior nodes every cycle (i.e.
elastic nodes)

        %Restore nodeXY using saved nodeXY;
        nodeXY=nodeXY_0; %RESETS the locations of ALL nodes

    else %only restores fixed nodes but does not reset positions of mobile nodes

        %[nodeXY(1,nMobile+1:nNodes) nodeXY(2,nMobile+1:nNodes)] =
pol2cart(nodePol_0(1,nMobile+1:nNodes),nodePol_0(2,nMobile+1:nNodes)); %only restore "fixed" perimeter nodes

        %13/04/07 dual mode: restore fixed internal nodes
        [nodeXY(1,nIntMobile+1:nIntNodes), nodeXY(2,nIntMobile+1:nIntNodes)] =
pol2cart(nodePol_0(1,nIntMobile+1:nIntNodes),nodePol_0(2,nIntMobile+1:nIntNodes));

        %13/04/07 dual mode: restore fixed peripheral nodes
        [nodeXY(1,nIntNodes+nPeriMobile+1:nNodes), nodeXY(2,nIntNodes+nPeriMobile+1:nNodes)] =
pol2cart(nodePol_0(1,nIntNodes+nPeriMobile+1:nNodes),nodePol_0(2,nIntNodes+nPeriMobile+1:nNodes));

    end

    %For mobile nodes only: populate node->which filaments LUT and populate node->how many connected filaments
    [connectivity.nodeFilLUT, connectivity.nFilsPerNode, connectivity.nFilsPerOrgn] = PopulateNodeFilLUT_DM(mobileNodes,
filNodeLUT, nNodes);
    %"PopulateNodeFilLUT" outputs is only used for SumStrains function. SumStrains is called every "mini-cycle"

    [oldFilLen, ~] = FindFilLengthsAndAngles(nodeXY, filNodeLUT); %Find the original lengths of the filaments (e.g. after
previous cycle's relaxing) before any stretching

    %Stretch and shear loop
    currStretch = 0;
    currShear = 0;

    while currStretch < stretchMag
        %% [Stretch] Stimulation #1 - stretch fixed peripheral nodes
        currStretch = currStretch + 1;

        disp(['[R' int2str(whichRun) ' C' int2str(whichCycle) ' e' num2str(currStretch)  '% t' num2str(currShear) '%] '
GetCurrentTime() ' stretching....'])

        switch stretchMethod
            case 'p' %peripheral node stretch method (default)
                %Uniaxially stretchs the chosen nodes outwards in X-axis
                %direction by delX amount (<---->)

                stretchNodes = nIntNodes + nPeriMobile + 1:nNodes; %stretchNodes=nMobile+1:nNodes;
                nodeXY(1,stretchNodes) = nodeXY(1,stretchNodes).*(1 + delX/100); %row 1 of nodeXY is X-axis

            case 's' %Stossel method
                %Uniaxially stretchs the chosen nodes leftwards in X-axis
                %direction by delX amount (-->)

                stretchNodes=nIntNodes+FindDataSubset(periPol_0,(90-vertOffset)*pi/180,(90+vertOffset)*pi/180,1,'column data');
%upper_quadrant_nodes;
                nodeXY(1,stretchNodes)=nodeXY(1,stretchNodes)+delX/100 *cellRadius *2;  %"*2" factor because Stossel stretch is
calclated as dx/h where dx=actual stretch, h=diameter

                %ERROR CHECK
                if length(stretchNodes) ~= nPeriModes - nPeriMobile
                    disp('ERROR (cellstretch_john_execute): number of stretch nodes is not equal to number of fixed peripheral
nodes');
                    pause
                end

            otherwise
                disp(['ERROR (cellstretch_john_execute): stretchMethod ' stretchMethod ' not recognized']);
                pause
                return;
        end

        %PRINTS NETWORK AFTER INCREMENTAL STRETCH
        if mod(currStretch,1) == 0 && whichRun == 1  %only output figures when stretch and shear % is an integer for whichRun ==
1 (to save space)
            if figOptions(1); figure; else figure('Visible','off'); end
            TITLE=(['Run' int2str(whichRun) '_Cycle' int2str(whichCycle) '_e' num2str(currStretch) '_t' num2str(currShear)
'_afterStretch']);
            PrintNetwork_XY(nodeXY, filNodeLUT, nIntNodes, cellRadius+delX, [], [], TITLE, false, nPeriMobile, [], [],
nIntMobile);
            if figOptions(2); print('-djpeg',[SAVE_DIR TITLE]); end
        end

        %Make copy of network before Relax #1
        nodeXY_beforeRelax1 = nodeXY;
```

```
        filNodeLUT_beforeRelax1 = filNodeLUT;

        %% [Stretch] Relax #1 network after stretching
        disp(['[R' int2str(whichRun) ' C' int2str(whichCycle) ' e' num2str(currStretch) '% t' num2str(currShear) '%] '
GetCurrentTime() ' start relaxing #1....'])

        [nodeXY, Strain, ii_relax, strainFactor, sSquareAll] = RelaxNetwork(nodeXY, filNodeLUT, oldFilLen, connectivity,
mobileNodes, relaxThresh, iMax, nIntNodes, cellRadius, whichRun, whichCycle, currStretch, currShear, figOptions);  %relax network
by one iteration

        disp(['[R' int2str(whichRun) ' C' int2str(whichCycle) ' e' num2str(currStretch)  '% t' num2str(currShear) '%] '
GetCurrentTime() ' finished relaxing #1'])

        %PRINTS NETWORK AFTER RELAXATION #1 OF MOBILE NODES
        if mod(currStretch,1) == 0 && whichRun == 1  %only output figures when stretch and shear % is an integer (to save space)
            if figOptions(1); figure; else figure('Visible','off'); end
            TITLE=(['Run' int2str(whichRun) '_Cycle',int2str(whichCycle) '_e' num2str(currStretch) '_t' num2str(currShear)
'_postRelax1_ii' int2str(ii_relax) ]);
            PrintNetwork_XY(nodeXY, filNodeLUT, nIntNodes, cellRadius+delX, [], [], TITLE, false, nPeriMobile, [], [],
nIntMobile);
            if figOptions(2) && whichCycle==1 && whichRun==1; print('-djpeg',[SAVE_DIR TITLE]); end
        end

        disp(['[R' int2str(whichRun) ' C' int2str(whichCycle) ' e' num2str(currStretch)  '% t' num2str(currShear) '%] '
GetCurrentTime() ' relax1 term iter: ' int2str(ii_relax) ', strain factor ' num2str(strainFactor)]);

        if ii_relax >= iMax %if has not relax under iMax cycles, ...
            break   %...then abandon minicycle stretching/shearing
        end

    end %end stretch and relax

    %% [Stretch] Break and replace filaments #1 network after relaxing

    if currStretch > 0
        disp(['[R' int2str(whichRun) ' C' int2str(whichCycle) '] ' GetCurrentTime() ' breaking and replacing #1...'])

        [filNodeLUT_afterReplacement1, fBreak1, filGenCount1] = BreakReplaceFilaments(breakMethod, nodeXY, filNodeLUT, Strain,
breakFactor, nNodes, whichRun, whichCycle);

        disp(['[R' int2str(whichRun) ' C' int2str(whichCycle) '] ' GetCurrentTime() ' finished breaking and replacing #1'])

        filNodeLUT = filNodeLUT_afterReplacement1;

        %PRINTS NETWORK AFTER FILAMENT BREAKAGE/REPLACEMENT #1
        breakCounter1(whichCycle) = length(fBreak1);
        if figOptions(1); figure; else figure('Visible','off'); end
        TITLE=(['Run' int2str(whichRun) '_Cycle' int2str(whichCycle) '_e' num2str(currStretch) '_t' num2str(currShear)
'_postReplace1']);
        PrintNetwork_XY(nodeXY, filNodeLUT, nIntNodes, cellRadius+delX, [], [], [TITLE
'_w_',int2str(size(fBreak1,2)),'_fils_broken_',int2str(filGenCount1),'_fils_generated'], false, nPeriMobile, [], [], nIntMobile);

        %if whichCycles is one of the cycles in doPrint, then print
        doPrint = [1 numCycles];
        if figOptions(2) && sum(whichCycle == doPrint) && whichRun == 1 ; print('-djpeg',[SAVE_DIR TITLE]); end

        if ii_relax == iMax %if iMax hit, exit outer cycle loop and return to main function to attempt next filament network
            break
        end

    end

    %% BEGIN SHEAR PORTION

    %Determine node elasticity
    if doElasticNodes %Kathy's original method that restores the initial positions of the interior nodes every cycle (i.e.
elastic nodes)

        %Restore nodeXY using saved nodeXY;
        nodeXY=nodeXY_0; %RESETS the locations of ALL nodes

    else %only restores fixed nodes but does not reset positions of mobile nodes

        %[nodeXY(1,nMobile+1:nNodes) nodeXY(2,nMobile+1:nNodes)] =
pol2cart(nodePol_0(1,nMobile+1:nNodes),nodePol_0(2,nMobile+1:nNodes)); %only restore "fixed" perimeter nodes

        %13/04/07 dual mode: restore fixed internal nodes
        [nodeXY(1,nIntMobile+1:nIntNodes), nodeXY(2,nIntMobile+1:nIntNodes)] =
pol2cart(nodePol_0(1,nIntMobile+1:nIntNodes),nodePol_0(2,nIntMobile+1:nIntNodes));

        %13/04/07 dual mode: restore fixed peripheral nodes
        [nodeXY(1,nIntNodes+nPeriMobile+1:nNodes), nodeXY(2,nIntNodes+nPeriMobile+1:nNodes)] =
pol2cart(nodePol_0(1,nIntNodes+nPeriMobile+1:nNodes),nodePol_0(2,nIntNodes+nPeriMobile+1:nNodes));
    end

    %For mobile nodes only: populate node->which filaments LUT and populate node->how many connected filaments
    [connectivity.nodeFilLUT, connectivity.nFilsPerNode, connectivity.nFilsPerOrgn] = PopulateNodeFilLUT_DM(mobileNodes,
filNodeLUT, nNodes);
    %"PopulateNodeFilLUT" outputs is only used for SumStrains function. SumStrains is called every "mini-cycle"

    [oldFilLen, ~] = FindFilLengthsAndAngles(nodeXY, filNodeLUT); %Find the original lengths of the filaments (e.g. after
previous cycle's relaxing) before any stretching

    while currShear < shearVal
```

```
        %% [Shear] Stimulation #2 - shear fixed internal nodes

        currShear = currShear + 1;

        disp(['[R' int2str(whichRun) ' C' int2str(whichCycle) ' e' num2str(currStretch)  '% t' num2str(currShear) '%] '
GetCurrentTime() ' shearing....'])

        shearNodes = nIntMobile+1:nIntNodes;

        switch shearMethod

            case 'r' %random node shear method where Y-coordinate is simply stretched
                nodeXY(2, shearNodes) = nodeXY(2, shearNodes).*(1 + delX/100);    %row 2 of nodeXY is Y-axis

            case 'v' %random node shear method where Y-coordinates are collectively moved in one direction
                nodeXY(2, shearNodes) = nodeXY(2, shearNodes) + delX/100 * cellRadius * 2;    %row 2 of nodeXY is Y-axis

            otherwise
                disp(['ERROR (cellstretchDM_john_execute): shearMethod ' shearMethod ' not recognized']);
                return;
        end

        %PRINTS NETWORK AFTER INCREMENTAL SHEAR
        if mod(currShear,1) == 0 && whichRun == 1  %only output figures when stretch and shear % is an integer for whichRun == 1
(to save space)
            if figOptions(1); figure; else figure('Visible','off'); end
            TITLE=(['Run' int2str(whichRun) '_Cycle' int2str(whichCycle) '_e' num2str(currStretch) '_t' num2str(currShear)
'_afterShear']);
            PrintNetwork_XY(nodeXY, filNodeLUT, nIntNodes, cellRadius+delX, [], [], TITLE, false, nPeriMobile, [], [],
nIntMobile);
            if figOptions(2); print('-djpeg',[SAVE_DIR TITLE]); end
        end

        %Make copy of network before Relax #2
        nodeXY_beforeRelax2 = nodeXY;

        filNodeLUT_beforeRelax2 = filNodeLUT;

        %% [Shear] Relax network #2
        disp(['[R' int2str(whichRun) ' C' int2str(whichCycle) ' e' num2str(currStretch) '% t' num2str(currShear) '%] '
GetCurrentTime() ' start relaxing #2....'])

        [nodeXY, Strain, ii_relax, strainFactor, sSquareAll] = RelaxNetwork(nodeXY, filNodeLUT, oldFilLen, connectivity,
mobileNodes, relaxThresh, iMax, nIntNodes, cellRadius, whichRun, whichCycle, currStretch, currShear, figOptions);  %relax network
by one iteration

        disp(['[R' int2str(whichRun) ' C' int2str(whichCycle) ' e' num2str(currStretch)  '% t' num2str(currShear) '%] '
GetCurrentTime() ' finished relaxing #2'])

        %PRINTS NETWORK AFTER RELAXATION #2 OF MOBILE NODES
        if mod(currShear,1) == 0 && whichRun == 1  %only output figures when stretch and shear % is an integer (to save space)
            if figOptions(1); figure; else figure('Visible','off'); end
            TITLE=(['Run' int2str(whichRun) '_Cycle',int2str(whichCycle) '_e' num2str(currStretch) '_t' num2str(currShear)
'_postRelax2_ii' int2str(ii_relax) ]);
            PrintNetwork_XY(nodeXY, filNodeLUT, nIntNodes, cellRadius+delX, [], [], TITLE, false, nPeriMobile, [], [],
nIntMobile);
            if figOptions(2) && whichCycle==1 && whichRun==1; print('-djpeg',[SAVE_DIR TITLE]); end
        end

        disp(['[R' int2str(whichRun) ' C' int2str(whichCycle) ' e' num2str(currStretch)  '% t' num2str(currShear) '%] '
GetCurrentTime() ' relax2 term iter: ' int2str(ii_relax) ', strain factor ' num2str(strainFactor)]);

        if ii_relax >= iMax %if has not relax under iMax cycles, ...
            break   %...then abandon minicycle stretching/shearing
        end

    end %end shear and relax

    if currShear > 0
        %% [Shear] Break and replace filaments #2 network after shearing
        disp(['[R' int2str(whichRun) ' C' int2str(whichCycle) '] ' GetCurrentTime() ' breaking and replacing #2...'])

        [filNodeLUT_afterReplacement2, fBreak2, filGenCount2] = BreakReplaceFilaments(breakMethod, nodeXY, filNodeLUT, Strain,
breakFactor, nNodes, whichRun, whichCycle);

        filNodeLUT = filNodeLUT_afterReplacement2;

        disp(['[R' int2str(whichRun) ' C' int2str(whichCycle) '] ' GetCurrentTime() ' finished breaking and replacing #2'])

        %PRINTS NETWORK AFTER FILAMENT BREAKAGE/REPLACEMENT #2
        breakCounter2(whichCycle) = length(fBreak2);
        if figOptions(1); figure; else figure('Visible','off'); end
        TITLE=(['Run' int2str(whichRun) '_Cycle' int2str(whichCycle) '_e' num2str(currStretch) '_t' num2str(currShear)
'_postReplace2']);
        PrintNetwork_XY(nodeXY, filNodeLUT, nIntNodes, cellRadius+delX, [], [], [TITLE
'_w_',int2str(size(fBreak2,2)),'_fils_broken_',int2str(filGenCount2),'_fils_generated'], false, nPeriMobile, [], [], nIntMobile);

        %if whichCycles is one of the cycles in doPrint, then print
        doPrint = [1 numCycles];
        if figOptions(2) && sum(whichCycle == doPrint) && whichRun == 1 ; print('-djpeg',[SAVE_DIR TITLE]); end

        if ii_relax == iMax %if iMax hit, exit outer cycle loop and return to main function to attempt next filament network
            break
        end
    end
```

```
    %% Save completed network after complted cycles of stretch and shear
    name =['Run',int2str(whichRun),'_Cycle',int2str(whichCycle),'_complete'];

    save([SAVE_DIR name]);

end %/end outer cycle loop

lastCycle=whichCycle;
save([SAVE_DIR 'last_cycle'],'lastCycle'); %saves only the last_cycle variable
clear variables;

disp('CellstretchDM_john_execute finished');
end

function [filNodeLUT_break,fBreak]=BreakFilamentsByStrain(filNodeLUT,Strain,breakFactor)
%BreakFilamentsByStrain: breaks filaments probabilistically such that
%filaments with heaviest strain are more likely to break
%-Note: if breakFactor is larger (i.e., >1), then it is less likely
%filaments will break

nFilaments=size(Strain,2);
normStrain = abs(Strain)./max(abs(Strain));
fBreak = find(normStrain>breakFactor*rand(1,nFilaments)); %determine which filaments break and store indices in filamentsToBreak

filNodeLUT_break=filNodeLUT;
filNodeLUT_break(:,fBreak)=[];
end

%Relaxes network and returns relaxed node coordinates, as well as squared
%strains, and how many iterations were required to relax
function [nodeXY, Strain, ii, strainFactor, sSquareAll] = RelaxNetwork(nodeXY, filNodeLUT, oldFilLen, connectivity, mobileNodes,
relaxThresh, iMax, nIntNodes, cellRadius, whichRun, whichCycle, currStretch, currShear, figOptions)

sSquare= intmax;    %represents summed squared strains (sum(strain^2)) of all filaments
sSquareAll = zeros(iMax,1);  %stored sSquare values for each iteration

ii=1;                           %iteration counter, must be < iMax
strainFactor = 1;               %strainFactor is the factor that strain is multiplied by to convert it to step size

while (sSquare >= relaxThresh)               %ii++ every loop. Escape condition if ii > iMax

    [strcFilLen, strcFilAng] = FindFilLengthsAndAngles(nodeXY,filNodeLUT);   %find new filament lengths and angles

    %"Strain" is a vector of magnitudes for all filaments
    Strain = double((strcFilLen-oldFilLen)./oldFilLen);     %strcFilLen contains the "new" filament lengths. oldFilLen is the
lengths before any stretch this cycle.

    %sum strains over indices indicated in "mobileNodes"
    %Note: nodeStrainXY contains only strains for only mobile nodes
    %by has size nNodes-by-nNodes.  Fixed nodes have NaN for
    %strain values
    nodeStrainXY = SumStrainsDM(Strain,strcFilAng,connectivity,mobileNodes);

    %adjust node positions (nodeXY) based on Strains
    nodeXY(:,[mobileNodes.int mobileNodes.peri]) = nodeXY(:,[mobileNodes.int mobileNodes.peri]) + strainFactor.*nodeStrainXY(:,
[mobileNodes.int mobileNodes.peri]);  %13/06/06: supports dual mode stimulation

    %sum squared strains for the mobile nodes in current iteration
    sSquare = sum(sqrt(nodeStrainXY(1,[mobileNodes.int mobileNodes.peri]).^2 + nodeStrainXY(2,[mobileNodes.int
mobileNodes.peri]).^2));
    sSquareAll(ii)=sSquare; %stores sum squared strain for the current iteration of relaxation

    if ii >= iMax
        break
    elseif ii > 1
        strainFactor=AdjustStrainFactor(strainFactor,sSquareAll(ii-1),sSquareAll(ii));
    end
    ii = ii+1;  %iteration counter

    %Outputs certain figures during relaxation.  Frequency
    %controlled by "mod" function
    if mod(ii,iMax*0.05)==0 %print network when at certain iterations
        STATUS=['[R' int2str(whichRun) ' C' int2str(whichCycle) ' e' num2str(currStretch)  '% t' num2str(currShear) '%] '
GetCurrentTime() ' ii=' int2str(ii) ' max abs strain=' num2str(max(max(abs(nodeStrainXY)))) ' sSquare=' num2str(sSquare)];
        disp(STATUS);

        %PRINT NETWORK WITH STRAINS OF FILAMENTS AND NODES
        if figOptions(1); figure; else figure('Visible','off'); end

        TITLE=['Run' int2str(whichRun) '_Cycle' int2str(whichCycle) '_StPct' num2str(currStretch) '_ShPct' num2str(currShear)
'_ii' int2str(ii) '_maxAbsStrain' num2str(max(max(abs(nodeStrainXY)))) '_sSquare' num2str(sSquare) '.tif'];
        PrintNetwork_XY(nodeXY, filNodeLUT, nIntNodes, cellRadius+1, [], [], TITLE, false, length(mobileNodes.peri),
nodeStrainXY, Strain, length(mobileNodes.int));

        if figOptions(2) && whichCycle==1 && whichRun==1; print('-djpeg',[SAVE_DIR TITLE]); end

        %PRINT STRAINS COLUMN-INDEXED BY NODES
        if figOptions(1); figure; else figure('Visible','off'); end
    end
end


end
```

```
function [filNodeLUT_afterReplacement, fBreak, filGenCount] = BreakReplaceFilaments(breakMethod, nodeXY, filNodeLUT, Strain,
breakFactor, nNodes, whichRun, whichCycle)

switch breakMethod

    case 'k' %Kathy
        [filNodeLUT_break,fBreak] = BreakFilamentsByStrain(filNodeLUT,Strain,breakFactor);

        filNodeLUT_afterReplacement = GenerateRandomFilaments(length(fBreak),nNodes,filNodeLUT_break);

        filGenCount = size(fBreak,2);

    case 'c' %Critical concentration
        %Critical concentration=sum of the lengths of all filaments in
        %the fully stretched network
        conc_crit = sum(FindFilLengthsAndAngles(nodeXY,filNodeLUT))*breakFactor;

        disp(['R[' int2str(whichRun) ' C' int2str(whichCycle) '] critical conc: ',num2str(conc_crit)]);

        %Proposed network after breakage/reform
        [filNodeLUT_break,fBreak] = BreakFilamentsByStrain(filNodeLUT, Strain, breakFactor);
        currentSum = -1;

        %Iteratively reform filaments
        filGenCount = 0;
        while currentSum < conc_crit

            filNodeLUT_break = GenerateRandomFilaments(1, nNodes, filNodeLUT_break);

            currentSum = sum(FindFilLengthsAndAngles(nodeXY, filNodeLUT_break));

            filGenCount = filGenCount + 1;
        end
        disp(['R',int2str(whichRun),' C',int2str(whichCycle),' filaments broken: ',int2str(size(fBreak,2)),', filaments
generated: ' int2str(filGenCount)]);

        filNodeLUT_afterReplacement = filNodeLUT_break;

    otherwise
        disp(['ERROR (cellstretch_john_execute/BreakReplaceFilaments): break method ' breakMethod ' not recognized'])
end

end
```

7.2 Strain summation

```
function [nodeStrainXY] = SumStrainsDM(Strain, strcFilAng, connectivity, mobileNodes)

%SumStrains: adds strains on nodes (all internal nodes and certain peripheral nodes)
%Sum the strains on all mobile nodes (internal node and mobile peripheral node).  Strain proportional force by Hooke's Law
%Part of the iterative relaxation procedure (Gauss Seidel)

%Inputs:
%1. Strain: 1D vector of strain magnitude
%2. strcFilAng: angle of this strain
%3. connectivity: class containing different attributes for node-filament connectivity.  See code for details.
%4. mobileNodes: contains fields "int" and "peri" containing indices of
%mobile nodes in both internal and peripheral nodes

%Outputs:
%1. nodeStrainXY, 2D matrix for strains in X and Y directions for
%each column-delineated node

%Note: nodeStrainXY sign "points" from origin node to destination node

%13/05/20: Dual Mode version initiated

if nargin==0
    disp('Start SumStrainsDM');

    %5 nodes, 3 filaments
    mobileNodes.int = [2 3];
    mobileNodes.peri = [4 5];
    filNodeLUT=[1 3; 1 2; 4 5]';
    nNodes = 5;
    [connectivity.nodeFilLUT, connectivity.nFilsPerNode, connectivity.nFilsPerOrgn] = PopulateNodeFilLUT_DM(mobileNodes,
filNodeLUT, nNodes);
    Strain = [0.1 0.15 0.2];
    strcFilAng = [0.2 0.3 0.4];
end

nodeFilLUT = connectivity.nodeFilLUT; %for each mobile node, what filaments are connected
nFilsPerNode = connectivity.nFilsPerNode; %for each mobile node, how many filaments are connected
nFilsPerOrgn = connectivity.nFilsPerOrgn; %for each mobile node, how many filaments are connected to it at the "origin" as
opposed to destination (must be <nFilsPerNode)
% nMobile = length(nFilsPerNode);   %the number of mobile nodes is equal to the length of parameter nFilsPerNode, which is row-
indexed mobile nodes
nNodes = size(nodeFilLUT,2);

%ERROR CHECKS
```

```
if length(nFilsPerNode)~=length(nFilsPerOrgn)
    disp(['ERROR (SumStrains): nFilsPerNode (length ' int2str(nFilsPerNode) ') and nFilsPerOrgn length(' length(nFilsPerOrgn) ')
not consistent']);
end

nodeStrainXY = NaN(2,nNodes);

%calculate node strain for mobile internal nodes
nodeStrainXY = CalcNodeStrain(nodeStrainXY, mobileNodes.int, nodeFilLUT,nFilsPerNode, nFilsPerOrgn, Strain, strcFilAng);

%calculate node strain for mobile peripheral nodes
nodeStrainXY = CalcNodeStrain(nodeStrainXY, mobileNodes.peri, nodeFilLUT,nFilsPerNode, nFilsPerOrgn, Strain, strcFilAng);

end

function [nodeStrainXY] = CalcNodeStrain( nodeStrainXY, mobileNodes, nodeFilLUT,nFilsPerNode, nFilsPerOrgn, Strain, strcFilAng)

for jj = mobileNodes               %iterates through mobile nodes
    n1 = nFilsPerOrgn(jj,1);       %# filaments with node jj as origin
    n12 = n1+1;                    %divider between origin node and rest of nodes
    n2 = nFilsPerNode(jj,1);       %total # filaments w/ node jj

    %Sum strain of filaments with node jj as "origin" first, then...
    nodeStrainXY(1,jj) = sum(Strain(nodeFilLUT(1:n1,jj)).*cos(strcFilAng(1,nodeFilLUT(1:n1,jj))));
    nodeStrainXY(2,jj) = sum(Strain(nodeFilLUT(1:n1,jj)).*sin(strcFilAng(1,nodeFilLUT(1:n1,jj))));

    %...sum total strain of filaments with node jj as "destination".
    %NOTE: This part is separate due to needing to add "pi"
    nodeStrainXY(1,jj) = nodeStrainXY(1,jj) + sum(Strain(nodeFilLUT(n12:n2,jj)).*cos(strcFilAng(1,nodeFilLUT(n12:n2,jj))+pi));
%"pi" makes up for offset due to axis origin at "origin" node
    nodeStrainXY(2,jj) = nodeStrainXY(2,jj) + sum(Strain(nodeFilLUT(n12:n2,jj)).*sin(strcFilAng(1,nodeFilLUT(n12:n2,jj))+pi));
end

end
```

7.3 Angle calculation

```
function [ filLens, filAng ] = FindFilLengthsAndAngles(nodeXY,filNodeLUT)
%FindFilLengthsAndAngles:
%   Find the lengths and angles (using atan2) of filaments using node XY coords and the lookup
%   table for nodes and filaments

%11/09/16:

if nargin==0
    nodeXY=[0 0; sqrt(pi)/2 sqrt(pi)/2; sqrt(pi)/2 -sqrt(pi)/2]';   %3 nodes: #1 at (0,0), #2 at (0.89, 0.89), #3 at (0.89. -
0.89)
    filNodeLUT=[1 2; 1 3]';  %2 filaments
end

filX(1,:)=nodeXY(1,filNodeLUT(1,:));    %x-coord of origin nodes
filX(2,:)=nodeXY(1,filNodeLUT(2,:));    %x-coord of destination nodes
filY(1,:)=nodeXY(2,filNodeLUT(1,:));    %y-coord of origin nodes
filY(2,:)=nodeXY(2,filNodeLUT(2,:));    %y-coord of destination node

dX = double(filX(2,:)-filX(1,:));       %change in x-coordinates for filament
dY = double(filY(2,:)-filY(1,:));       %change in y-coordinates for filament

filLens = double(sqrt(dX.^2 + dY.^2));  %length of filament

filAng = double(atan2(dY,dX));           %<1,nFilaments> find new filaments angle

end
```

Bibliography

1. Discher, D., et al., *Biomechanics: Cell Research and Applications for the Next Decade.* Annals of Biomedical Engineering, 2009. **37**(5): p. 847-859.
2. Wang, J.H. and B.P. Thampatty, *An introductory review of cell mechanobiology.* Biomech Model Mechanobiol, 2006. **5**(1): p. 1-16.
3. Hahn, C. and M.A. Schwartz, *Mechanotransduction in vascular physiology and atherogenesis.* Nat Rev Mol Cell Biol, 2009. **10**(1): p. 53-62.
4. Sato, M. and T. Ohashi, *Biorheological views of endothelial cell responses to mechanical stimuli.* Biorheology, 2005. **42**(6): p. 421-41.
5. Franke, R.P., et al., *Induction of human vascular endothelial stress fibres by fluid shear stress.* Nature, 1984. **307**(5952): p. 648-9.
6. Wong, A.J., T.D. Pollard, and I.M. Herman, *Actin filament stress fibers in vascular endothelial cells in vivo.* Science, 1983. **219**(4586): p. 867-9.
7. Danciu, T.E., et al., *Mechanical strain delivers anti-apoptotic and proliferative signals to gingival fibroblasts.* J Dent Res, 2004. **83**(8): p. 596-601.
8. Joshi, S.D. and K. Webb, *Variation of cyclic strain parameters regulates development of elastic modulus in fibroblast/substrate constructs.* J Orthop Res, 2008. **26**(8): p. 1105-13.
9. Pender, N. and C.A. McCulloch, *Quantification of actin polymerization in two human fibroblast sub-types responding to mechanical stretching.* J Cell Sci, 1991. **100 (Pt 1)**: p. 187-93.
10. Boccafoschi, F., et al., *Dynamic fibroblast cultures: response to mechanical stretching.* Cell Adh Migr, 2007. **1**(3): p. 124-8.
11. Wang, J.H., et al., *Specificity of endothelial cell reorientation in response to cyclic mechanical stretching.* J Biomech, 2001. **34**(12): p. 1563-72.
12. Sipkema, P., et al., *Effect of cyclic axial stretch of rat arteries on endothelial cytoskeletal morphology and vascular reactivity.* J Biomech, 2003. **36**(5): p. 653-9.
13. Chu, J.W. and G.A. Voth, *Coarse-grained modeling of the actin filament derived from atomistic-scale simulations.* Biophys J, 2006. **90**(5): p. 1572-82.
14. Ming, D., et al., *Simulation of F-actin filaments of several microns.* Biophys J, 2003. **85**(1): p. 27-35.
15. Satcher, R.L., Jr. and C.F. Dewey, Jr., *Theoretical estimates of mechanical properties of the endothelial cell cytoskeleton.* Biophys J, 1996. **71**(1): p. 109-18.
16. Stamenovic, D. and M.F. Coughlin, *A quantitative model of cellular elasticity based on tensegrity.* J Biomech Eng, 2000. **122**(1): p. 39-43.
17. Stamenovic, D. and D.E. Ingber, *Models of cytoskeletal mechanics of adherent cells.* Biomech Model Mechanobiol, 2002. **1**(1): p. 95-108.
18. Stamenovic, D. and N. Wang, *Invited review: engineering approaches to cytoskeletal mechanics.* J Appl Physiol, 2000. **89**(5): p. 2085-90.
19. Wilhelm, J. and E. Frey, *Elasticity of stiff polymer networks.* Phys Rev Lett, 2003. **91**(10): p. 108103.
20. Bausch, A.R. and K. Kroy, *A bottom-up approach to cell mechanics.* Nat Phys, 2006. **2**(4): p. 231-238.
21. Chen, C.S., J. Tan, and J. Tien, *Mechanotransduction at cell-matrix and cell-cell contacts.* Annual Review of Biomedical Engineering, 2004. **6**(1): p. 275-302.
22. Georges, P.C. and P.A. Janmey, *Cell type-specific response to growth on soft materials.* J Appl Physiol, 2005. **98**(4): p. 1547-53.

23. Gudi, S.R., et al., *Equibiaxial strain and strain rate stimulate early activation of G proteins in cardiac fibroblasts.* Am J Physiol Cell Physiol, 1998. **274**(5): p. C1424-1428.
24. Wang, N. and D.E. Ingber, *Control of cytoskeletal mechanics by extracellular matrix, cell shape, and mechanical tension.* Biophys J, 1994. **66**(6): p. 2181-9.
25. Guilak, F., et al., *Control of stem cell fate by physical interactions with the extracellular matrix.* Cell Stem Cell, 2009. **5**(1): p. 17-26.
26. Mirsky, I., *Left Ventricular Stresses in the Intact Human Heart.* Biophysical Journal, 1969. **9**(2): p. 189-208.
27. Owatverot, T.B., et al., *Effect of combined cyclic stretch and fluid shear stress on endothelial cell morphological responses.* J Biomech Eng, 2005. **127**(3): p. 374-82.
28. Zhao, S., et al., *Synergistic effects of fluid shear stress and cyclic circumferential stretch on vascular endothelial cell morphology and cytoskeleton.* Arterioscler Thromb Vasc Biol, 1995. **15**(10): p. 1781-6.
29. Kaunas, R., et al., *Cooperative effects of Rho and mechanical stretch on stress fiber organization.* Proc Natl Acad Sci U S A, 2005. **102**(44): p. 15895-900.
30. Kanda, K. and T. Matsuda, *Mechanical stress-induced orientation and ultrastructural change of smooth muscle cells cultured in three-dimensional collagen lattices.* Cell Transplant, 1994. **3**(6): p. 481-92.
31. Raeber, G.P., M.P. Lutolf, and J.A. Hubbell, *Part II: Fibroblasts preferentially migrate in the direction of principal strain.* Biomech Model Mechanobiol, 2008. **7**(3): p. 215-25.
32. Takakuda, K. and H. Miyairi, *Tensile behaviour of fibroblasts cultured in collagen gel.* Biomaterials, 1996. **17**(14): p. 1393-7.
33. Cunningham, K.S. and A.I. Gotlieb, *The role of shear stress in the pathogenesis of atherosclerosis.* Lab Invest, 2005. **85**(1): p. 9-23.
34. Hoffman, B.D., C. Grashoff, and M.A. Schwartz, *Dynamic molecular processes mediate cellular mechanotransduction.* Nature, 2011. **475**(7356): p. 316-23.
35. Kanchanawong, P., et al., *Nanoscale architecture of integrin-based cell adhesions.* Nature, 2010. **468**(7323): p. 580-4.
36. del Rio, A., et al., *Stretching single talin rod molecules activates vinculin binding.* Science, 2009. **323**(5914): p. 638-41.
37. Ehrlicher, A.J., et al., *Mechanical strain in actin networks regulates FilGAP and integrin binding to filamin A.* Nature, 2011. **478**(7368): p. 260-3.
38. Eastwood, M., D.A. McGrouther, and R.A. Brown, *Fibroblast responses to mechanical forces.* Proc Inst Mech Eng H, 1998. **212**(2): p. 85-92.
39. Loesberg, W.A., et al., *The effect of combined cyclic mechanical stretching and microgrooved surface topography on the behavior of fibroblasts.* J Biomed Mater Res A, 2005. **75**(3): p. 723-32.
40. Park, S.A., et al., *Biological responses of ligament fibroblasts and gene expression profiling on micropatterned silicone substrates subjected to mechanical stimuli.* J Biosci Bioeng, 2006. **102**(5): p. 402-12.
41. Steward, R.L., Jr., et al., *Probing cell structure responses through a shear and stretching mechanical stimulation technique.* Cell Biochem Biophys, 2010. **56**(2-3): p. 115-24.
42. Kubicek, J.D., et al., *Integrated lithographic membranes and surface adhesion chemistry for three-dimensional cellular stimulation.* Langmuir, 2004. **20**(26): p. 11552-6.
43. Bellin, R.M., et al., *Defining the role of syndecan-4 in mechanotransduction using surface-modification approaches.* Proc Natl Acad Sci U S A, 2009. **106**(52): p. 22102-7.
44. Gov, N.S., *Dynamics and morphology of microvilli driven by actin polymerization.* Phys Rev Lett, 2006. **97**(1): p. 018101.

45. Satyanarayana, S.V. and A. Baumgaertner, *Shape and motility of a model cell: a computational study.* J Chem Phys, 2004. **121**(9): p. 4255-65.
46. Stephanou, A., M.A. Chaplain, and P. Tracqui, *A mathematical model for the dynamics of large membrane deformations of isolated fibroblasts.* Bull Math Biol, 2004. **66**(5): p. 1119-54.
47. Lee, K.C. and A.J. Liu, *New proposed mechanism of actin-polymerization-driven motility.* Biophys J, 2008. **95**(10): p. 4529-39.
48. Lee, K.C. and A.J. Liu, *Force-velocity relation for actin-polymerization-driven motility from brownian dynamics simulations.* Biophys J, 2009. **97**(5): p. 1295-304.
49. Lin, Y., *Mechanics model for actin-based motility.* Phys Rev E Stat Nonlin Soft Matter Phys, 2009. **79**(2 Pt 1): p. 021916.
50. Mogilner, A. and G. Oster, *Force generation by actin polymerization II: the elastic ratchet and tethered filaments.* Biophys J, 2003. **84**(3): p. 1591-605.
51. Hsu, H.J., C.F. Lee, and R. Kaunas, *A dynamic stochastic model of frequency-dependent stress fiber alignment induced by cyclic stretch.* PLoS One, 2009. **4**(3): p. e4853.
52. Kang, J., et al., *Response of an actin filament network model under cyclic stretching through a coarse grained Monte Carlo approach.* Journal of theoretical biology, 2011. **274**(1): p. 109-19.
53. Na, S., G.A. Meininger, and J.D. Humphrey, *A theoretical model for F-actin remodeling in vascular smooth muscle cells subjected to cyclic stretch.* J Theor Biol, 2007. **246**(1): p. 87-99.
54. Palmer, J.S. and M.C. Boyce, *Constitutive modeling of the stress-strain behavior of F-actin filament networks.* Acta Biomater, 2008. **4**(3): p. 597-612.
55. Civelekoglu, G., Y. Tardy, and J.J. Meister, *Modeling actin filament reorganization in endothelial cells subjected to cyclic stretch.* Bull Math Biol, 1998. **60**(6): p. 1017-37.
56. Silveira, P.S., J.P. Butler, and J.J. Fredberg, *Length adaptation of airway smooth muscle: a stochastic model of cytoskeletal dynamics.* J Appl Physiol, 2005. **99**(6): p. 2087-98.
57. Silveira, P.S. and J.J. Fredberg, *Smooth muscle length adaptation and actin filament length: a network model of the cytoskeletal dysregulation.* Can J Physiol Pharmacol, 2005. **83**(10): p. 923-31.
58. DiDonna, B.A. and A.J. Levine, *Filamin cross-linked semiflexible networks: fragility under strain.* Phys Rev Lett, 2006. **97**(6): p. 068104.
59. Cano, M.L., D.A. Lauffenburger, and S.H. Zigmond, *Kinetic analysis of F-actin depolymerization in polymorphonuclear leukocyte lysates indicates that chemoattractant stimulation increases actin filament number without altering the filament length distribution.* J Cell Biol, 1991. **115**(3): p. 677-87.
60. Xu, J., J.F. Casella, and T.D. Pollard, *Effect of capping protein, CapZ, on the length of actin filaments and mechanical properties of actin filament networks.* Cell Motil Cytoskeleton, 1999. **42**(1): p. 73-81.
61. Xu, J., D. Wirtz, and T.D. Pollard, *Dynamic cross-linking by alpha-actinin determines the mechanical properties of actin filament networks.* J Biol Chem, 1998. **273**(16): p. 9570-6.
62. Isambert, H., et al., *Flexibility of actin filaments derived from thermal fluctuations. Effect of bound nucleotide, phalloidin, and muscle regulatory proteins.* J Biol Chem, 1995. **270**(19): p. 11437-44.
63. Lu, L., et al., *Mechanical properties of actin stress fibers in living cells.* Biophys J, 2008. **95**(12): p. 6060-71.
64. Deng, L., et al., *Fast and slow dynamics of the cytoskeleton.* Nat Mater, 2006. **5**(8): p. 636-40.
65. Chen, C.S., et al., *Cell shape provides global control of focal adhesion assembly.* Biochem Biophys Res Commun, 2003. **307**(2): p. 355-61.
66. Kubicek, J.D., et al., *Integrated Lithographic Membranes and Surface Adhesion Chemistry for Three-Dimensional Cellular Stimulation.* Langmuir, 2004. **20**(26): p. 11552-11556.

67. Kim, Y., et al., *Modulation of fluidic resistance and capacitance for long-term, high-speed feedback control of a microfluidic interface.* Lab Chip, 2009. **9**(17): p. 2603-9.
68. Suciu, A., et al., *Model for the alignment of actin filaments in endothelial cells subjected to fluid shear stress.* Bull Math Biol, 1997. **59**(6): p. 1029-46.
69. Swailes, N.T., P.J. Knight, and M. Peckham, *Actin filament organization in aligned prefusion myoblasts.* Journal of Anatomy, 2004. **205**(5): p. 381-391.
70. Alberts, B., *Molecular biology of the cell*. 4th ed. 2002, New York: Garland Science. xxxiv, 1463, [86] p.
71. Lee, H., et al., *Passive and active microrheology for cross-linked F-actin networks in vitro.* Acta Biomater, 2010. **6**(4): p. 1207-18.
72. Mitsui, Y. and E.L. Schneider, *Relationship between cell replication and volume in senescent human diploid fibroblasts.* Mech Ageing Dev, 1976. **5**(1): p. 45-56.
73. Mitchison, T.J. and L.P. Cramer, *Actin-based cell motility and cell locomotion.* Cell, 1996. **84**(3): p. 371-9.
74. Ono, S., *Regulation of actin filament dynamics by actin depolymerizing factor/cofilin and actin-interacting protein 1: new blades for twisted filaments.* Biochemistry, 2003. **42**(46): p. 13363-70.
75. Janmey, P.A., et al., *Viscoelastic properties of vimentin compared with other filamentous biopolymer networks.* J Cell Biol, 1991. **113**(1): p. 155-60.
76. Tsuda, Y., et al., *Torsional rigidity of single actin filaments and actin-actin bond breaking force under torsion measured directly by in vitro micromanipulation.* Proc Natl Acad Sci U S A, 1996. **93**(23): p. 12937-42.
77. Krendel, M., G. Sgourdas, and E.M. Bonder, *Disassembly of actin filaments leads to increased rate and frequency of mitochondrial movement along microtubules.* Cell Motil Cytoskeleton, 1998. **40**(4): p. 368-78.
78. Slepoy, A., A.P. Thompson, and S.J. Plimpton, *A constant-time kinetic Monte Carlo algorithm for simulation of large biochemical reaction networks.* J Chem Phys, 2008. **128**(20): p. 205101.
79. Rathinam, M., et al., *Stiffness in stochastic chemically reacting systems: The implicit tau-leaping method.* The Journal of Chemical Physics, 2003. **119**(24): p. 12784-12794.
80. Pirentis, A.P., et al., *A Model for Stress Fiber Realignment Caused by Cytoskeletal Fluidization During Cyclic Stretching.* Cell Mol Bioeng, 2011. **4**(1): p. 67-80.
81. Takemasa, T., et al., *Oblique alignment of stress fibers in cells reduces the mechanical stress in cyclically deforming fields.* Eur J Cell Biol, 1998. **77**(2): p. 91-9.
82. Luchsinger, P.C., M. Sachs, and D.J. Patel, *Pressure-radius relationship in large blood vessels of man.* Circ Res, 1962. **11**: p. 885-8.
83. Nakajima, H., *[Measurement of the normal and hypertensive heart and great vessels based on cardiosynchronous angiocardiography].* Jpn Circ J, 1968. **32**(1): p. 79-98.
84. Patel, D.J., F.M. De Freitas, and A.J. Mallos, *Mechanical function of the main pulmonary artery.* J Appl Physiol, 1962. **17**: p. 205-8.
85. Dobrin, P.B., *Mechanical properties of arterises.* Physiol Rev, 1978. **58**(2): p. 397-460.
86. Trepat, X., et al., *Universal physical responses to stretch in the living cell.* Nature, 2007. **447**(7144): p. 592-+.
87. Civelekoglu-Scholey, G., et al., *Model of coupled transient changes of Rac, Rho, adhesions and stress fibers alignment in endothelial cells responding to shear stress.* J Theor Biol, 2005. **232**(4): p. 569-85.
88. Noria, S., et al., *Assembly and reorientation of stress fibers drives morphological changes to endothelial cells exposed to shear stress.* Am J Pathol, 2004. **164**(4): p. 1211-23.
89. Haviv, L., et al., *A cytoskeletal demolition worker: myosin II acts as an actin depolymerization agent.* J Mol Biol, 2008. **375**(2): p. 325-30.

90. Ngu, H., et al., *Effect of focal adhesion proteins on endothelial cell adhesion, motility and orientation response to cyclic strain.* Ann Biomed Eng, 2010. **38**(1): p. 208-22.
91. Ziegler, W.H., et al., *Integrin connections to the cytoskeleton through talin and vinculin.* Biochem Soc Trans, 2008. **36**(Pt 2): p. 235-9.
92. Pesen, D. and J.H. Hoh, *Micromechanical architecture of the endothelial cell cortex.* Biophys J, 2005. **88**(1): p. 670-9.
93. McClatchey, A.I. and R.G. Fehon, *Merlin and the ERM proteins--regulators of receptor distribution and signaling at the cell cortex.* Trends Cell Biol, 2009. **19**(5): p. 198-206.
94. Gu, Y., et al., *Images of apoptotic cells produce and transmit the bioactive lipid sphingosine-1-phosphate (S1P) during extrusion*, in *The Cell: An Image Library, www.cellimagelibrary.org*. 2011, ASCB.
95. Diz-Munoz, A., et al., *Control of directed cell migration in vivo by membrane-to-cortex attachment.* PLoS Biol, 2010. **8**(11): p. e1000544.
96. Ingber, D.E., *Mechanobiology and diseases of mechanotransduction.* Ann Med, 2003. **35**(8): p. 564-77.
97. Engler, A.J., et al., *Matrix elasticity directs stem cell lineage specification.* Cell, 2006. **126**(4): p. 677-89.
98. Gilbert, P.M., et al., *Substrate elasticity regulates skeletal muscle stem cell self-renewal in culture.* Science, 2010. **329**(5995): p. 1078-81.
99. Samuel, M.S., et al., *Actomyosin-mediated cellular tension drives increased tissue stiffness and beta-catenin activation to induce epidermal hyperplasia and tumor growth.* Cancer Cell, 2011. **19**(6): p. 776-91.
100. Kilarski, W.W., et al., *Biomechanical regulation of blood vessel growth during tissue vascularization.* Nat Med, 2009. **15**(6): p. 657-64.
101. Pedersen, J.A. and M.A. Swartz, *Mechanobiology in the third dimension.* Ann Biomed Eng, 2005. **33**(11): p. 1469-90.
102. Burridge, K. and R. Doughman, *Front and back by Rho and Rac.* Nat Cell Biol, 2006. **8**(8): p. 781-2.
103. Ohta, Y., J.H. Hartwig, and T.P. Stossel, *FilGAP, a Rho- and ROCK-regulated GAP for Rac binds filamin A to control actin remodelling.* Nat Cell Biol, 2006. **8**(8): p. 803-14.
104. Johnson, C.P., et al., *Forced unfolding of proteins within cells.* Science, 2007. **317**(5838): p. 663-6.
105. Ferrer, J.M., et al., *Measuring molecular rupture forces between single actin filaments and actin-binding proteins.* Proc Natl Acad Sci U S A, 2008. **105**(27): p. 9221-6.
106. Chen, H., et al., *Differential mechanical stability of filamin A rod segments.* Biophys J, 2011. **101**(5): p. 1231-7.
107. Thomas, W.E., V. Vogel, and E. Sokurenko, *Biophysics of catch bonds.* Annu Rev Biophys, 2008. **37**: p. 399-416.
108. Hertig, S. and V. Vogel, *Catch bonds.* Curr Biol, 2012. **22**(19): p. R823-5.
109. Nakamura, F., T.P. Stossel, and J.H. Hartwig, *The filamins: organizers of cell structure and function.* Cell Adh Migr, 2011. **5**(2): p. 160-9.
110. Nakamura, F., et al., *Molecular basis of filamin A-FilGAP interaction and its impairment in congenital disorders associated with filamin A mutations.* PLoS One, 2009. **4**(3): p. e4928.
111. Ohta, Y., et al., *The small GTPase RalA targets filamin to induce filopodia.* Proc Natl Acad Sci U S A, 1999. **96**(5): p. 2122-8.
112. Ueda, K., Y. Ohta, and H. Hosoya, *The carboxy-terminal pleckstrin homology domain of ROCK interacts with filamin-A.* Biochem Biophys Res Commun, 2003. **301**(4): p. 886-90.
113. Kanters, E., et al., *Filamin B mediates ICAM-1-driven leukocyte transendothelial migration.* J Biol Chem, 2008. **283**(46): p. 31830-9.

114. Kiema, T., et al., *The molecular basis of filamin binding to integrins and competition with talin.* Mol Cell, 2006. **21**(3): p. 337-47.
115. Calderwood, D.A., et al., *Increased filamin binding to beta-integrin cytoplasmic domains inhibits cell migration.* Nat Cell Biol, 2001. **3**(12): p. 1060-8.
116. Razinia, Z., et al., *Filamins in mechanosensing and signaling.* Annu Rev Biophys, 2012. **41**: p. 227-46.
117. MacPherson, M. and S.C. Fagerholm, *Filamin and filamin-binding proteins in integrin-regulation and adhesion. Focus on: "FilaminA is required for vimentin-mediated cell adhesion and spreading".* Am J Physiol Cell Physiol, 2010. **298**(2): p. C206-8.
118. Kang, J., et al., *Response of an actin filament network model under cyclic stretching through a coarse grained Monte Carlo approach.* J Theor Biol, 2011. **274**(1): p. 109-19.
119. Nakamura, F., et al., *Structural basis of filamin A functions.* J Cell Biol, 2007. **179**(5): p. 1011-25.
120. Puklin-Faucher, E. and V. Vogel, *Integrin activation dynamics between the RGD-binding site and the headpiece hinge.* J Biol Chem, 2009. **284**(52): p. 36557-68.
121. Dancu, M.B. and J.M. Tarbell, *Large Negative Stress Phase Angle (SPA) attenuates nitric oxide production in bovine aortic endothelial cells.* J Biomech Eng, 2006. **128**(3): p. 329-34.
122. Califano, J.P. and C.A. Reinhart-King, *Exogenous and endogenous force regulation of endothelial cell behavior.* Journal of Biomechanics, 2010. **43**(1): p. 79-86.
123. Chen, C., et al., *Fluidization and resolidification of the human bladder smooth muscle cell in response to transient stretch.* PLoS One, 2010. **5**(8).
124. Chiu, J.J., S. Usami, and S. Chien, *Vascular endothelial responses to altered shear stress: pathologic implications for atherosclerosis.* Ann Med, 2009. **41**(1): p. 19-28.
125. Fedosov, D.A., B. Caswell, and G.E. Karniadakis, *A multiscale red blood cell model with accurate mechanics, rheology, and dynamics.* Biophys J, 2010. **98**(10): p. 2215-25.
126. Crowl, L.M. and A.L. Fogelson, *Computational model of whole blood exhibiting lateral platelet motion induced by red blood cells.* Int j numer method biomed eng, 2010. **26**(3-4): p. 471-487.
127. Then, K.L. and J.A. Rankin, *Hypertension: a review for clinicians.* Nurs Clin North Am, 2004. **39**(4): p. 793-814.
128. Lehoux, S., Y. Castier, and A. Tedgui, *Molecular mechanisms of the vascular responses to haemodynamic forces.* J Intern Med, 2006. **259**(4): p. 381-92.
129. Thodeti, C.K., et al., *TRPV4 channels mediate cyclic strain-induced endothelial cell reorientation through integrin-to-integrin signaling.* Circ Res, 2009. **104**(9): p. 1123-30.
130. Shukla, A., et al., *Endothelial cells as mechanical transducers: enzymatic activity and network formation under cyclic strain.* Mech Chem Biosyst, 2004. **1**(4): p. 279-90.
131. Ueda, A., et al., *Effect of shear stress on microvessel network formation of endothelial cells with in vitro three-dimensional model.* Am J Physiol Heart Circ Physiol, 2004. **287**(3): p. H994-1002.
132. Krishnan, L., et al., *Effect of mechanical boundary conditions on orientation of angiogenic microvessels.* Cardiovasc Res, 2008. **78**(2): p. 324-32.
133. Huang, S. and D.E. Ingber, *The structural and mechanical complexity of cell-growth control.* Nature Cell Biology, 1999. **1**(5): p. E131-E138.
134. Pietramaggiori, G., et al., *Tensile forces stimulate vascular remodeling and epidermal cell proliferation in living skin.* Annals of Surgery, 2007. **246**(5): p. 896-902.
135. Kilarski, W.W., et al., *Biomechanical regulation of blood vessel growth during tissue vascularization.* Nature Medicine, 2009. **15**(6): p. 657-U145.
136. Thoumine, O., et al., *ELONGATION OF CONFLUENT ENDOTHELIAL-CELLS IN CULTURE - THE IMPORTANCE OF FIELDS OF FORCE IN THE ASSOCIATED ALTERATIONS OF THEIR CYTOSKELETAL STRUCTURE.* Experimental Cell Research, 1995. **219**(2): p. 427-441.

137. Sato, M., M.J. Levesque, and R.M. Nerem, *Micropipette aspiration of cultured bovine aortic endothelial cells exposed to shear stress.* Arteriosclerosis, 1987. **7**(3): p. 276-86.